

Alma Mater Studiorum – Università di Bologna

DOTTORATO DI RICERCA IN

Scienze Chimiche

Ciclo XXVII

Settore Concorsuale di afferenza: 03/C1

Settore Scientifico disciplinare: CHIM/06

**SYNTHESIS AND CONFORMATIONAL ANALYSIS OF HETEROAROMATIC
ATROPISOMERIC SYSTEMS**

Presentata da: Silvia Ranieri

Coordinatore Dottorato

Prof. Aldo Roda

Relatore

Prof. Andrea Mazzanti

Correlatore

Dr. Michele Mancinelli

Esame finale anno 2015

Summary

Introduction	3
Atropisomerism and axial chirality	3
Axial chirality in drug discovery	7
Atropisomerism in catalysis and atroposelective synthesis.....	15
Conformational analysis and methodologies.....	23
Dynamic NMR	24
Optical techniques	31
Dynamic HPLC	31
Theoretical approach	33
Application of conformational analysis to the absolute configuration determination.....	41
Electronic Circular Dichroism (ECD).....	41
Vibrational Circular Dichroism (VCD).....	43
Research objectives	47
Results and discussion.....	49
Synthesis and conformational analysis of atropisomeric systems.....	49
Atropisomers of arylmaleimides	49
Atropisomers of 4-arylpyrazolo[3,4- <i>b</i>]pyridines.....	65
Study of the intramolecular NO ₂ /CO interaction in solution	89
Long range bonding/non-bonding interactions: study on 2- arylpyridines.....	103
Application of conformational analysis to the absolute configuration determination.....	113
Absolute configuration of substituted 1,2,3,4-tetrahydroquinolines	113

Absolute configuration of compounds from enantioselective Friedel-Crafts alkylation-acetalization cascade of naphthols with α,β -unsaturated cyclic ketones	127
Absolute configuration of substituted 3,4-annulated indoles	145
Experimental section	163
Atropisomers of arylmaleimides	163
Atropisomers of 4-arylpyrazolo[3,4- <i>b</i>]pyridines.....	171
Study of the intramolecular NO ₂ /CO interaction in solution.....	177
Long range bonding/non-bonding interactions: study on 2-arylpyridines	186

Introduction

Atropisomerism and axial chirality

Chirality is defined as the property of a molecule which can exist in two forms non-superimposable, mirror image one another. This kind of molecules lack of symmetry elements of the second kind: a mirror plane ($\sigma = S_1$), a centre of inversion ($i = S_2$), a rotation-reflexion axis (S_{2n}).

The elements of asymmetry that can generate a chiral compound can be chiral centers, chiral axes or helix. All pairs of chiral molecules have same chemical properties, but opposite optical properties. For what concerns axial chirality, it can be found in molecules containing bonds around which the rotation could be hindered, generating conformers that are stable at ambient temperature.

The most general definition of conformation is the following: “the conformations of a molecule (of defined constitution and configuration) are those arrangements in space of the atoms of the molecule which are not superimposable upon each other”. This definition of conformation was coined by Barton¹ in the middle of the 20th century. In 1922, Christie and Kenner² demonstrated that 2,2-dinitrodiphenyl-6,6-dicarboxylic acid could be separated into the two enantiomers due to the hindered rotation about the aryl-aryl single bond. Some years later, the term “atropisomerism” was proposed by Kuhn³ to define the stereoisomerism due to the hindered rotation about a single bond. This terminology comes from the greek *tropos* (i.e., “it turns”) with the negative prefix *a*, indicating something that “does not turn”.

Finally in 1983, with the Oki definition,⁴ a pair of conformers which can interconvert with an half-life time greater then 1000s at 25 °C, has been

defined as “atropisomers”. A pair of atropisomers can be separated as stable compounds at ambient temperature and their racemization can be obtained by heating the single atropisomer.

The configuration of these molecules is related to the dihedral angle generated by the chiral axis, as reported in Figure 1.⁵

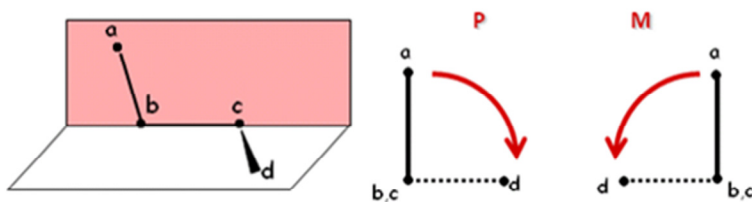


Figure 1. Dihedral angle and its nomenclature.

In a chain of atoms **a-b-c-d**, the torsion angle is the dihedral between the plane containing the atoms **a, b, c** and that containing **b, c, d**. This system has two extreme conformations called *anti* and *eclipsed*. The torsion angle between groups **a** and **d** is then considered to be positive (absolute configuration is *P* or Δ) if the bond **a-b** is rotated in a clockwise direction in order to eclipse the bond **c-d** moving away from the observer. A negative torsion angle requires rotation in the opposite sense (absolute configuration is *M* or Λ).⁶ The Cahn-Ingold-Prelog priority rules to the substituents bonded to atoms **b** and **c** to find atoms **a** and **d** allow the assignment of the dihedral angle sign.

It is important to note that the slow axial rotation along the chirality axis can be due not only to steric hindrance, but also to electronic factors (weak interactions) and that conformational stability of the stereogenic axis under the reaction conditions is the key requirement to obtain enantio-enriched products. This implies that the rotational barrier must be

greater than 25–26 kcal/mol or, more conveniently, greater than 30 kcal/mol.

The concept of axial chirality as a stereogenic source in a rotationally hindered compound was for many years relegated to the academic field. However this situation changed with the discovery of many bioactive natural compounds containing stereogenic chiral axes⁷ and with the discovery of many catalysts useful for asymmetric synthesis.⁸

References

¹ Barton, D. H. R. *Principles of Conformational Analysis. Nobel Lectures, Chemistry 1963 – 1970*. Amsterdam: Elsevier Publishing Company; **1972**.

² Christie, G. H.; Kenner, J. *J. Chem. Soc. Trans.* **1922**, 121, 614 – 620.

³ Kuhn R. *Molekulare asymmetrie*. In: Freuberg H., ed. *Stereochemie*. Leipzig-Wien: Franz Deutike; **1933**, 803–824.

⁴ Oki, M. *Topics in stereochemistry* **1983**, 14, 1 – 81.

⁵ Kenner, J.; Stubbings, W. V. *J. Chem. Soc.* **1921**, 119, 593 – 602.

⁶ Compendium of Chemical Terminology, Goldbook- International Union of Pure and Applied Chemistry, version 2.3.1 **2012**.

⁷ a) Clayden, J.; Moran, W. J.; Edwards, P. J.; LaPlante, S. R. *Angew. Chem. Int. Ed.* **2009**, 48, 6398 – 6401. b) LaPlante, S. R.; Fader, L. D.; Fandrick, K. R.; Fandrick, D. R.; Hucke, O.; Kemper, R.; Miller, S. P. F.; Edwards, P. J. *J. Med. Chem.* **2011**, 54, 7005 – 7022. c) LaPlante, S. R.; Edwards, P. J.; Fader, L. D.; Jakalian, A.; Hucke, O. *ChemMedChem* **2011**, 6, 505 – 513.

⁸ Bringmann, G.; Price Mortimer, A. J.; Keller, P. A.; Gresser, M. J.; Garner, J.; Breuning, M. *Angew. Chem. Int. Ed.* **2005**, 44, 5384 – 5427.

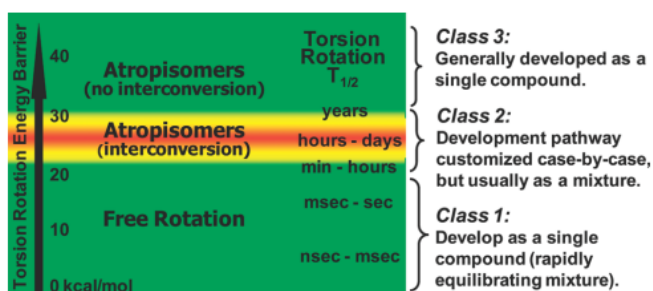
Axial chirality in drug discovery¹

Many biomolecular interactions are based on the ligand-receptor chirality and this feature becomes of main importance in drug discovery. The biological effects of enantiomers can result not only in the curative effects, but also in pharmacokinetics and toxicity.² The well-known cases of thalidomide³ and perhexiline,⁴ whose enantiomers led to unexpected effects in humans, emphasized the importance of addressing chirality. In pharmaceutical industry stereoisomers are most frequently observed as a result of chiral centers, but atropisomerism can be another, yet overlooked, source of chirality.

The U.S. Food and Drug Administration (FDA) Policy Statement for the Development of New Stereogenic Drugs,⁵ gives precise outlines about the development of chiral drugs as single enantiomers or racemic mixture, given the technical advances in chiral separation and stereochemically controlled synthesis. Anyway, these statements are referred to classical chiral centered molecules, whereas there are no direct guidelines for atropisomers.

Atropisomerism may give rise to geometrical isomers, diastereoisomers, or enantiomers, all with the feature that they can be thermally equilibrated, involving an intramolecular dynamic process that is bond rotation. Moreover, bond rotation is time-dependent and half-life for atropisomers can vary between minutes to years, depending on the steric hindrance, electronic interactions, temperature and solvent. Because of this time-dependent feature, drug discovery campaigns can become more complex.

In order to give some guidelines to manage this time-dependent feature in the development of atropisomeric drugs, LaPlante, Edwards and co-workers proposed a classification^{1b,c} of compounds, based on barriers and rotation rates, reported in the following Scheme 1.



Scheme 1. Qualitative, cross-discipline guide to help correlate axial (torsion) rotation energy barriers, $t_{1/2}$, and compound classes for predicting development strategies.

Class 1 compounds possess fast axial rotation rates, in the order of seconds or lower, with $\Delta E_{\text{rot}} < 20$ kcal/mol. They display no axial chirality and are developed as single compounds, without any analytical strategy implemented. On the other hand, compounds with $\Delta E_{\text{rot}} > 20$ kcal/mol can generate atropisomers.

Class 3 compounds have $\Delta E_{\text{rot}} \gg 30$ kcal/mol, so they have very slow rotation rates, in the order of years. These compounds are stable over time and can be isolated as optically pure and have an acceptable shelf life. Development can proceed similarly to conventional stereoisomers that results from chiral centers.

Class 2 compounds show axial interconversion with values in the range of minutes, days or months. Their development can be challenging, because stereochemical integrity can be compromised not only during drug production, but also in administration to patients and shelf life. In

some cases it may be possible to modify the structure to obtain a more suitable analogue for development, designing related compounds that have slower or faster axial rotation rates. When this is not practical, information on the activity of the separate atropisomer in an appropriate *in vitro* or *in vivo* model may help support the proposed development pathway.

The decision to develop a drug candidate as a purified enantiomer or a racemate should be made as early as possible during the optimization stage. If possible, options for dealing with the atropisomeric phenomenon should be developed and implemented at this early drug design stage.

For example, if the barrier to atropisomerization is high (Class 3), one should aim to develop the drug as a single, pure and stereochemically stable atropisomer. This is the case of Telenzepine **1**, a selective muscarinic antagonist, that has found use in the treatment of peptic ulcers⁶.

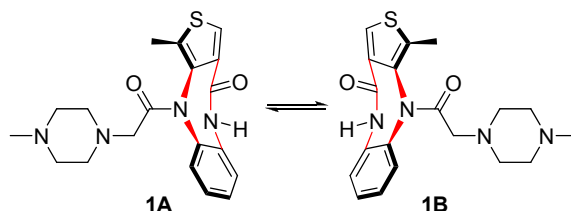


Figure 2. Slow interconversion between the atropisomers of Telenzepine 1A and 1B.

If the barrier to atropisomerization of a compound is low (Class 2), then one should consider developing the drug as a consistent and reproducible interconverting mixture.⁷ This is the case of Sch40120 (**2**), which is an inhibitor of 5-lipoxygenase. This compound has found use in treating acute inflammatory diseases such as psoriasis.⁸ The enantiomers of **2** can be observed by chiral HPLC, but they readily interconvert with a half-life

of only 1.6 min at physiological temperatures (37 °C). The short racemization rate justifies the development of this compound as a racemic mixture.

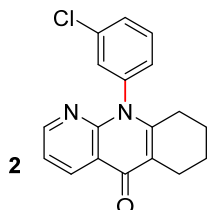


Figure 3. Compound 2 has a fast racemization, of 1.6 min at 37 °C. The rotation axis is colored in red.

In some cases compounds with atropisomeric interconversion properties can be too challenging to be developed as drugs, then for this purpose some practical options can be used to simplify the structure. For example, compound 3 in Figure 4 exists as a mixture of four stereoisomers, which have half-life of interconversion of ~5h at 37 °C. To obviate this potential problem, symmetrical amide analogues (4) were prepared, where symmetry around Ar-CO bond eliminates diastereoisomerism.⁹

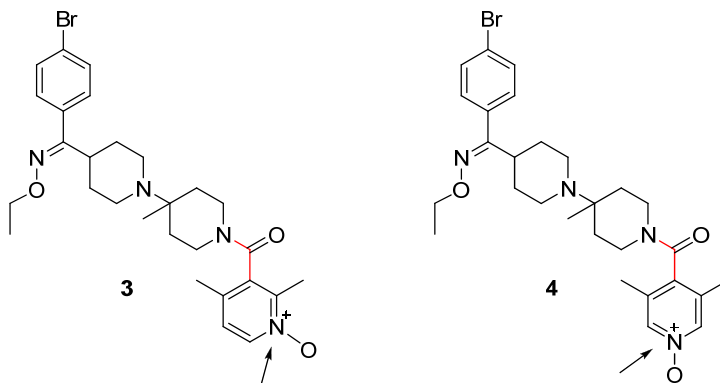


Figure 4. (Left) compound 3 existing as four diastereoisomers. (Right) symmetrical analogue 4.

A related approach to simplification is to modulate the rate of axial bond rotation through engineering faster bond rotation such as atropisomers no longer exist. In this case compounds switch from class 2 to class 1, as the reported example of compound **5** in Figure 5 where the removal of the methyl from the central ring lowers the steric hindrance enough to remove atropisomerism from the molecule (**6**).⁷

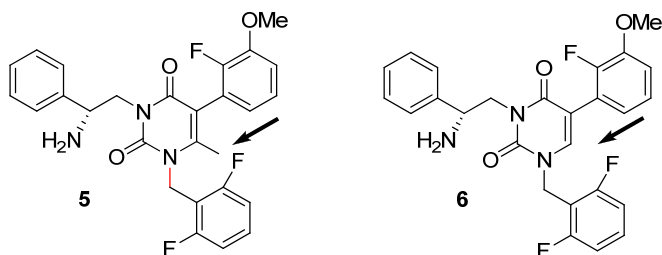


Figure 5. Example of reduced steric hindrance from compound 5 to compound 6.

Foreseeing the existence of atropisomerism in compounds of interest is critical at all stages of drug discovery and development. Recently, LaPlante and co-workers showed that a computational approach is suitable for this purpose.^{1c} In this approach, a relaxed torsion scan simulates rotation along a sterically hindered bond and the energy is recorded at each increment of rotation. The method used is quantum mechanics, for the calculation of energy values that consider steric and electronic properties and will be discussed more extensively along the Introduction.

The computational tool becomes useful during the drug discovery pathway, especially when used in combination with the compounds classification in Scheme 1, determining whether to develop the drug as a racemic mixture or as an isolated single isomer. Another application of the computational tool is to flag potential atropisomeric compounds from

drug databases. In fact this study, not only identified known atropisomeric drugs, but also revealed compounds with previously unreported atropisomeric properties. Some examples are Dicoumarol (**7**, Figure 6), used as anticoagulant,¹⁰ for which the calculated barrier resulted 25.5 kcal/mol. Another example is Iomeprol (**8**, Figure 6), belonging to the family of X-ray contrast reagents,¹¹ that exists as a mixture of diastereoisomer, based on chiral centers and a class 3 chiral axis.

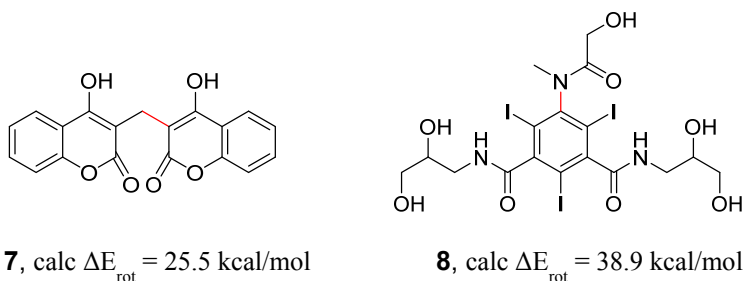


Figure 6. Examples of drugs candidates identified from search of a drug database that employed the quantum mechanics prediction strategy.

In conclusion atropisomer chirality could have a significant impact on drug discovery and so must be managed appropriately. The first step in dealing with this phenomenon would be to recognize its existence for compounds of interest. Strategies for detecting and computationally revealing atropisomers are discussed above. Once identified, there are multiple options that range from avoiding atropisomerism to design compounds that rotate more quickly or more slowly. A categorization scheme is proposed as a guide to help the early drug discovery stages.

References

- ¹ a) Clayden, J.; Moran, W. J.; Edwards, P. J.; LaPlante, S. R. *Angew. Chem. Int. Ed.* **2009**, 48, 6398 – 6401. b) LaPlante, S. R.; Fader, L. D.; Fandrick, K. R.; Fandrick, D. R.; Hucke, O.; Kemper, R.; Miller, S. P. F.; Edwards, P. J. *J. Med. Chem.* **2011**, 54, 7005 – 7022. c) LaPlante, S. R.; Edwards, P. J.; Fader, L. D.; Jakalian, A.; Hucke, O. *ChemMedChem* **2011**, 6, 505 – 513.
- ² a) Eichelbaum, M.; Gross, A. S. *Adv. Drug Res.* **1996**, 28, 1 – 64. b) Crossley, R. J. *Chirality and the Biological Activity of Drugs*, CRC Press, Boca Raton, **1995**. c) Shah, R. R.; Midgley, J. M.; Branch, S. K. *Adverse Drug React. Toxicol. Rev.* **1998**, 17, 145 – 190.
- ³ a) Blaschke, G.; Kraft, H. P.; Fickentscher, K.; Köhler, F. *Arzneim.-Forsch.* **1979**, 29, 1640 – 1642. b) Fabro, S.; Smith, R. L.; Williams, R. T. *Nature* **1967**, 215, 296 – 297. c) Reist, M.; Carrupt, P.-A.; Francotte, E.; Testa, B. *Chem. Res. Toxicol.* **1998**, 11, 1521 – 1528. d) Eriksson, T.; Bjorkman, S.; Roth, B.; Fyge, A.; Hoglund, P. *Chirality* **1995**, 7, 44 – 52.
- ⁴ a) Agranat, I.; Caner, H.; Caldwell, J. *Nat. Rev. Drug Discovery* **2002**, 1, 753 – 768. b) Rouhi, A. M. *Chem. Eng. News* **2003**, 81, 18, 56 – 61.
- ⁵ a) FDA's Policy Statement for the Development of New Stereo-isomeric Drugs; Department of Health and Human Services, Food and Drug Administration: Washington, DC, **1992**; www.fda.gov/downloads/AboutFDA/CentersOffices/CDER/ucm103532.pdf. b) Miller, S. P. F. Presented at the 18th International Symposium on Chirality, Busan, Korea, June 26, **2006**.
- ⁶ Eveleigh, P.; Hulme, E. C.; Schudt, C.; Birdsall, N. J. M. *Mol. Pharmacol.* **1989**, 35, 477 – 483.
- ⁷ Tucci, F. C.; Hu, T.; Mesleh, M. F.; Bokser, A.; Allsopp, E.; Gross, T. D.; Guo, Z.; Zhu, Y.-F.; Struthers, R. S.; Ling, N.; Chen, C. *Chirality* **2005**, 17, 559 – 564.
- ⁸ Friary, R. F.; Spangler, M.; Osterman, R.; Schulman, L.; Schwerdt, J. H. *Chirality* **1996**, 8, 364 – 371.
- ⁹ a) Palani, A.; Shapiro, S.; Clader, J. W.; Greenlee, W. J.; Blythin, D.; Cox, K.; Wagner, N. E.; Strizki, J.; Baroudy, B. M.; Dan, N. *Bioorg. Med. Chem. Lett.*

-
- 2003**, 13, 705 – 708. b) Palani, A.; Shapiro, S.; Clader, J. W.; Greenlee, W. J.; Vice, S.; McCombie, S.; Cox, K.; Strizki, J.; Baroudy, B. M. *Bioorg. Med. Chem. Lett.* **2003**, 13, 709 – 712.
- ¹⁰ Fitos, I.; Visy, J.; Zsila, F.; Bikádi, Z.; Mády, G.; Simonyi, M. *Biochem. Pharmacol.* **2004**, 67, 679 – 688.
- ¹¹ a) Dooley, M.; Jarvis, B. *Drugs* **2000**, 59, 1169 – 1186. b) Arbughi, T.; Bertani, F.; Celeste, R.; Piero, T. *J. Chromatogr., B* **1999**, 729, 323 – 332.

Atropisomerism in catalysis and atroposelective synthesis

Natural products bearing a rotationally hindered biaryl axis are far more widespread and structurally diverse than initially assumed. The configuration at a biarylaxis can be a decisive factor in governing the pharmacological properties of a bioactive compound and axial chirality is the fundamental basis for useful reagents and catalysts in asymmetric synthesis.¹

Axially chiral biaryl auxiliaries and catalysts exhibit excellent chirality transfer properties. The most known example of an axially chiral ligand is the diphosphine 2,2'-bis(diphenylphosphino)-1,1'-binaphthyl (BINAP) **1** (Figure 7), a C_2 -symmetric triaryldiphosphine,² which synthesis and first applications were reported by Noyori and Takaya in 1980.³ BINAP is the ligand of choice in Ru(II) and Rh(I) catalyzed asymmetric hydrogenations of C=C or C=O bonds as α,β -unsaturated carboxylic acids,⁴ *N*-acylaminoacrylic acids,⁵ allylic alcohols⁶ (see Scheme 2) and more examples. The reported examples, and many others, reveal the high level success of BINAP in inducing asymmetry, so that the design of other atropisomeric diphosphines have become an active area of research since 1980. Some other examples, as well reported in Figure 7, are a series of BINAP analogues, containing the bis-arylphosphine group (**15**)⁷ and a series of biphenyl phosphines (**16**)⁸.

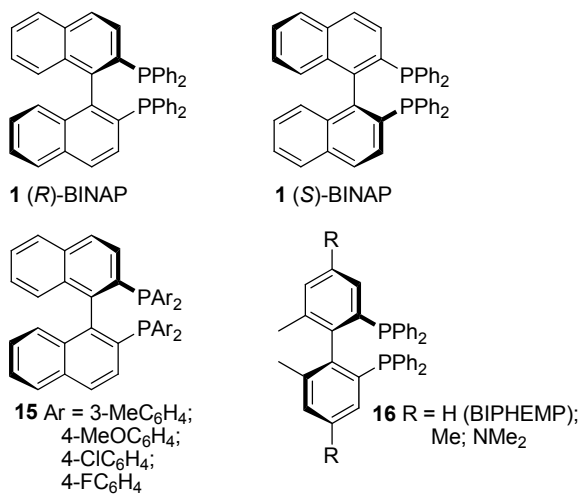
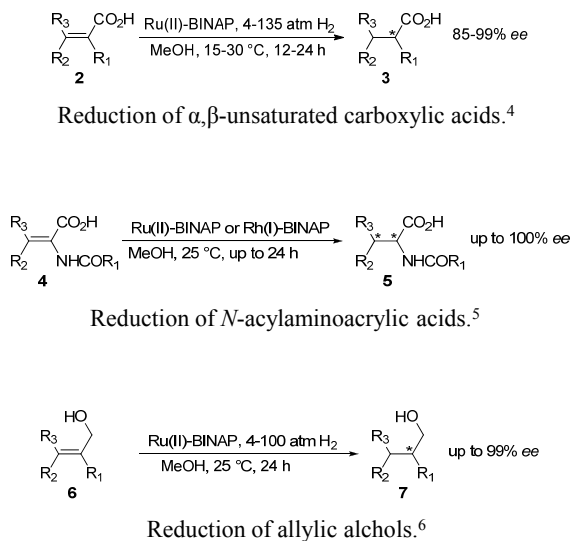


Figure 7. BINAP and modified analogues used as asymmetric catalysts.



Scheme 2. Example reactions with Ru(II)-BINAP as ligand.

Some other examples of more complex biaryl systems are reported in Figure 8. The epoxidation catalyst **17** possesses two axially chiral binaphthyl subunits embedded in a sterically demanding backbone.⁹ More recently, attention has been focused on non- C_2 -symmetric biaryl compounds such as the tertiary aminophenol **18**, which catalyzes the enantioselective addition of diethylzinc to aldehydes.¹⁰ The isoquinoline-containing phosphine quinap (**19**) is an example of an axially chiral heteroaromatic biaryl; it has been used as a ligand in Pd-catalyzed asymmetric allylic alkylation reactions.¹¹

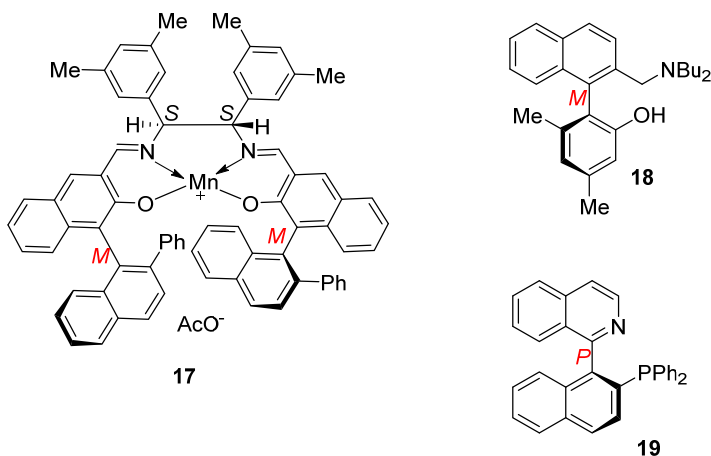


Figure 8. Examples of axially chiral ligands and catalysts.

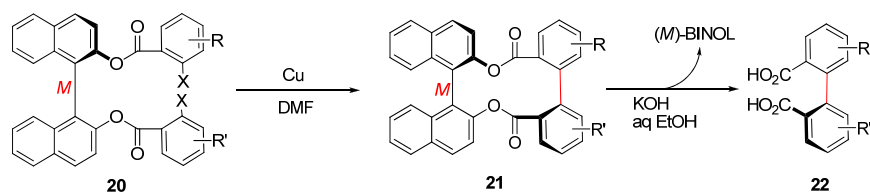
Given the importance of axially chiral biaryl compounds, a variety of excellent methods for their atroposelective synthesis have been developed. Three fundamental strategies can be outlined:¹²

1. Biaryl formation in a single step by C-C coupling, with simultaneous asymmetric induction.¹³
2. Atroposelective transformation of an existing, but stereochemically not yet defined, biaryl system.¹⁴ Within this

two-step approach, a non-stereoselective coupling step precedes the introduction of the stereochemical information at the axis.

3. A C-C bond formation between an arene and a precursor substituent, followed by the transformation into a chiral biaryl axis by construction of an aromatic ring, usually with a central-to-axial chirality transfer.

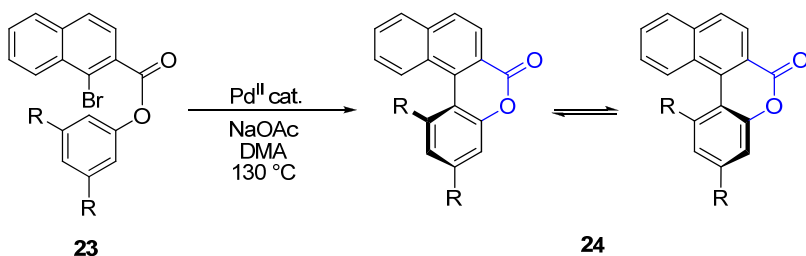
The first approach is a direct, atroposelective aryl-aryl coupling step, as in the case of two aryl units pre-fixed through a chiral bridge. The pioneering work is done by Myano et al., employing diester-bridged systems, as the example reported in Scheme 3.¹⁵ This reported approach is of the kind in which the chiral inductive part is an artificial auxiliary, that has to be eliminated at the end. There are other approaches in which the chiral moieties are part of the intended product.¹²



Scheme 3. Atroposelective preparation of biaryl diacids 22, by Ullmann coupling.

The second kind of approach is based on the desymmetrization of an existing biaryl system. Many examples of this strategy are based on stereochemically labile lactone-bridged biaryls, as key intermediates.¹⁴ This approach separates the aryl-aryl bond formation from the introduction of the stereochemical information at the biaryl axis, thus avoiding a direct asymmetric biaryl-coupling step. As reported by Bringmann et al.^{14a,b} the first step is the pre-fixation of *ortho*-bromobenzoic acids and phenols to obtain bromoesters **23**, which give the

configurationally unstable biaryl lactones **24**, by Pd^{II} catalyzed aryl–aryl coupling (see Scheme 4). The second step requires the atroposelective transformation of the lactones **24** into configurationally stable biaryl compounds, which can be achieved simply by cleavage of the bridge with chiral O, N, or H nucleophiles.^{14b}

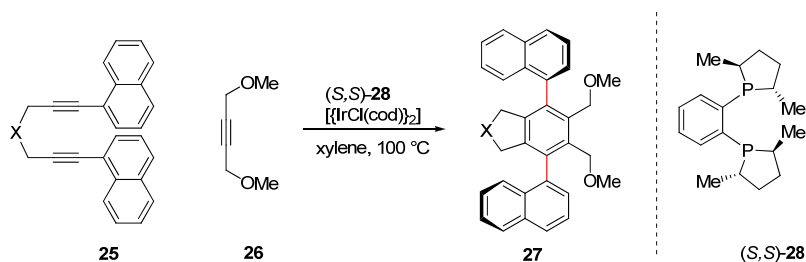


Scheme 4. Preparation of the biaryl lactones **24**.

Examples of nucleophiles reported are potassium (*S*)-1-phenylethylamide and sodium (*R*)-menthoxide,¹⁶ (*R*)-8-phenylmenth-oxide,¹⁷ (*P*)-binal-H or with borane in the presence of the (*S*)-CBS.¹⁸ From a stereochemical point of view, the transformation of the lactones into axially chiral biaryl compounds can be considered as a dynamic kinetic resolution.¹⁹ The chiral nucleophile selectively attacks only one of the two conformational enantiomers of **24**, say (*M*)-**24**, which is steadily resupplied with the remaining enantiomer (*P*)-**24** through the rapid (*M*)-**24** ↔ (*P*)-**24** equilibrium, thus allowing conversion of the entire racemic material of **24** into a stereochemically homogeneous product of either configurations.

The third concept for the preparation of asymmetric biaryl compounds is based on a preformed aryl–C single bond, then transformed atroposelectively into the aryl axis. The chirality transfer to the axis results from a stereogenic center of by enantioselective catalysis. An example for this strategy is given by Gutnov, Heller and co-workers who

synthesized chiral aryl pyridines by catalytic asymmetric [2+2+2] cycloaddition.²⁰ Independently, Shibata et al. reported iridium-catalyzed [2+2+2] cycloadditions of dyines **25** and alkyne **26** to construct the two-fold axially chiral teraryls **27**.²¹



Scheme 5. Construction of teraryls **27, by iridium catalyzed [2+2+2] cycloaddition.**

There are more examples of the conversion of C centrochirality approach, like the Lewis-acid promoted benzanellation²², diastereoselective addition of a naphthyl Grignard, followed by oxidation with DDQ²³. This synthetic strategy for the construction of chiral biaryl compounds is highly innovative. At this time is still at the beginning, and not much has been done yet, so that the scope is largely limited in terms of functional-group compatibility and substitution patterns accessible.²⁴

References

¹ a) Rosini, C.; Franzini, L.; Raffaelli, A.; Salvadori, P. *Synthesis* **1992**, 503 – 517. b) McCarthy, M.; Guiry, P. J. *Tetrahedron* **2001**, 57, 3809 – 3844.
² Miyashita, A.; Yasuda, A.; Takaya, H.; Toriumi, K.; Ito, T.; Souchi, T.; Noyori, R. *J. Am. Chem. Soc.* **1980**, 102, 7932 – 7934.
³ a) Noyori, R.; Takaya, H. *Acc. Chem. Res.* **1990**, 23, 345 – 350. b) Noyori, R. *Acta Chem. Scand.* **1996**, 50, 380 – 390.
⁴ Ohta, T; Takaya, H.; Kitamura, M.; Nagia, K.; Noyori, R. *J. Org. Chem.* **1987**, 52, 3174 – 3176.

-
- ⁵ Noyori, R.; Ikeda, T.; Ohkuma, T.; Widhalm, M.; Kitamura, M.; Takaya, H.; Akutagawa, S.; Sayo, N.; Saito, T.; Taketomi, T.; Kumobayashi, H. *J. Am. Chem. Soc.* **1989**, 111, 9134 – 9135.
- ⁶ Noyori, R.; Ohta, M.; Hsiao, Y.; Kitamura, M.; Ohta, T.; Takaya, H. *J. Am. Chem. Soc.* **1986**, 108, 7117 – 7119.
- ⁷ a) Takaya, H.; Mashima, K.; Koyano, K.; Yagi, M.; Kumobayashi, H.; Taketomi, T.; Akutagawa, S.; Noyori, R. *J. Org. Chem.* **1986**, 51, 629 – 635. b) Mashima, K.; Kusano, K.; Sato, N.; Matsumura, Y.; Nozaki, K.; Kumobayashi, H.; Sayo, N.; Hori, T.; Ishizaki, T.; Akutagawa, S.; Takaya, H. *J. Org. Chem.* **1994**, 59, 3064 – 3076.
- ⁸ a) Schmid, R.; Cereghetti, M.; Heiser, B.; Schönholzer, P.; Hansen, H. –J. *Helv. Chim. Acta* **1988**, 71, 897 – 929. b) Svensson, G.; Albertsson, J.; Frejd, T.; Klingsedt, T.; *Acta Crystallogr. C* **1986**, 42, 1324 – 1327.
- ⁹ Sasaki, H.; Irie, R.; Hamada, T.; Suzuki, K.; Katsuki, T. *Tetrahedron* **1994**, 50, 11827 – 11838.
- ¹⁰ Bringmann, G.; Breuning, M.; *Tetrahedron: Asymmetry* **1998**, 9, 667 – 679.
- ¹¹ a) Brown, J. M.; Hulme, D. I.; Guiry, P. J., *Tetrahedron* **1994**, 50, 4493 – 4506.
- ¹² Bringmann, G.; Price Mortimer, A. J.; Keller, P. A.; Gresser, M. J.; Garner, J.; Breuning M. *Angew. Chem Int. Ed.* **2005**, 44, 5384 – 5427.
- ¹³ a) For a review on planar-chirality-induced asymmetric biaryl syntheses, see: Kamikawa, K.; Uemura, M. *Synlett* **2000**, 938 – 949. b) For a review on selected asymmetric biaryl couplings, see: Lloyd-Williams, P.; Giralt, E. *Chem. Soc. Rev.* **2001**, 30, 145 – 157.
- ¹⁴ For reviews on the lactone method, see: a) Bringmann, G.; Breuning, M.; Pfeifer, R.-M.; Schenk, W. A.; Kamikawa, K.; Uemura, M. *J. Organomet. Chem.* **2002**, 661, 31 – 47. b) Bringmann, G.; Tasler, S.; Pfeifer, R.-M.; Breuning, M.; *J. Organomet. Chem.* **2002**, 661, 49 – 65. c) For a review on the desymmetrization of achiral biaryl compounds and the dynamic kinetic

resolution of configurationally unstable biaryl products, see: Khanbabaee, K.; *Nachr. Chem.* **2003**, 51, 163 – 166.

¹⁵ a) Miyano, S.; Tobita, M.; Hashimoto, H. *Bull. Chem. Soc. Jpn.* **1981**, 54, 3522 – 3526. b) Miyano, S.; Handa, S.; Shimizu, K.; Tagami, K.; Hashimoto, H. *Bull. Chem. Soc. Jpn.* **1984**, 57, 1943 – 1947. c) Miyano, S.; Fukushima, H.; Handa, S.; Ito, H.; Hashimoto, H. *Bull. Chem. Soc. Jpn.* **1988**, 61, 3249 – 3254.

¹⁶ a) Bringmann, G.; Breuning, M.; Tasler, S.; Endress, H.; Ewers, C. L. J.; Göbel, L.; Peters, K.; Peters, E.-M.; *Chem. Eur. J.* **1999**, 5, 3029 – 3038. b) Seebach, D.; Jaeschke, G.; Gottwald, K.; Matsuda, K.; Formisano, R.; Chaplin, D. A.; Breuning, M.; Bringmann, G. *Tetrahedron* **1997**, 53, 7539 – 7556.

¹⁷ Bringmann, G.; Breuning, M.; Walter, R.; Wuzik, A.; Peters, K.; Peters, E.-M. *Eur. J. Org. Chem.* **1999**, 11, 3047 – 3055.

¹⁸ Bringmann, G.; Breuning, M.; Henschel, P.; Hinrichs, J. *Org. Synth.* **2002**, 79, 72 – 83

¹⁹ Pellissier, H. *Tetrahedron* **2003**, 59, 8291 – 8327.

²⁰ Gutnov, A.; Heller, B.; Fischer, C.; Drexler, H.-J.; Spannenberg, A.; Sundermann, B.; Sundermann, C. *Angew. Chem. Int. Ed.* **2004**, 43, 3795 – 3797.

²¹ Shibata, T.; Fujimoto, T.; Yokota, K.; Takagi, K. *J. Am. Chem. Soc.* **2004**, 126, 8382 – 8383.

²² Nishii, Y.; Wakasugi, K.; Koga, K.; Tanabe, Y. *J. Am. Chem. Soc.* **2004**, 126, 5358 – 5359.

²³ Hattori, T.; Date, M.; Sakurai, K.; Morohashi, N.; Kosugi, H.; Miyano, S.; *Tetrahedron Lett.* **2001**, 42, 8035 – 8038.

²⁴ For a central-to-axial chirality transfer in the field of naturally occurring biaryl compounds, see: Wanjohi, J. M.; Yenesew, A.; Midiwo, J. O.; Heydenreich, M.; Peter, M. G.; Dreyer, M.; Reichert, M.; Bringmann, G. *Tetrahedron* **2005**, 61, 2667 – 2674.

Conformational analysis and methodologies

Stereochemistry embraces a broad variety of static and dynamic aspects that are all related to the three-dimensional structure of molecules. While static stereochemistry deals with the spatial arrangement of atoms in molecules and the corresponding chemical and physical properties, **dynamic stereochemistry** emphasizes structural change and comprises asymmetric reactions as well as interconversion of configurational and conformational isomers. The dynamic stereochemistry plays a fundamental role in modern chemistry, spanning multiple disciplines from asymmetric synthesis and drug discovery to material sciences.

In the middle of the 1930s, Kemp and Pitzer¹ came to the fundamental conclusion that the discrepancy in the measurements of ethane entropy could be interpreted considering the restricted rotation about the carbon-carbon single bond, and that the ground state of ethane corresponded to a staggered conformation instead of an eclipsed one,² with a rotational barrier of about 3 kcal/mol. The concept of staggered conformation of an alkyl chain was finally confirmed by Hassel et al.,³ who established that the chair conformation of cyclohexane is normally the preferred one, where all the carbon-carbon bonds have a dihedral angle of 60°. Finally, in the middle of the 1950s, Winstein and Holness⁴ and Eliel *et al*⁵ laid the foundations for the modern conformational analysis. Subsequently, Barton and Hassel were awarded the 1969 Nobel Prize in chemistry.

With the advent of sophisticated analytical techniques and with the support of the raising power of computational chemistry, the research field of conformational analysis grew in importance and gained reliability.⁶

The main methodologies used in the dynamic stereochemistry studies are listed below, and further explained within this section:

- Dynamic NMR
- Optical techniques (ECD, VCD)
- Dynamic HPLC
- Theoretical conformational analysis (MM, DFT)

Dynamic NMR

Variable-temperature NMR spectroscopy, often called dynamic NMR (DNMR), is a powerful tool for investigating stereodynamic processes.⁷ As a first example we can consider the molecule in Figure 9: dimethylformamide (DMF).⁸



Figure 9. DMF is a two-site exchange example.

When the rotation about the C-N bond is frozen the two methyl groups are different (A and B), and they have distinct NMR signals.

The resonance frequency of a nucleus is given by its specific magnetic environment. If nuclei change quickly the magnetic environment, on NMR timescale, only an averaged NMR spectrum is visible, on the other hand when nuclei exchange slowly, individual environments can be seen.

This is the case when:

$$k = \frac{1}{t} \ll \pi \frac{\Delta\nu}{\sqrt{2}}$$

Where:

k = the interconversion rate constant (s^{-1})

t = interconversion time (s)

$\Delta\nu$ = NMR shift separation of the signal (Hz) at low temperature at which exchange does not occur.

This equation indicates that different positions of the same nucleus can show distinct signals when the chemical shift difference ($\Delta\nu$) corresponds to a time spent by the nuclei in different positions longer than the interconversion time t .

As the difference of the signals, in Hz, is proportional to the strength of the applied magnetic field, a higher magnetic field NMR spectrometer can distinguish two conformations that are not distinguishable by a low field NMR spectrometer at the same temperature. This is important when the shift separations are very small or when it is necessary to perform spectra at very low temperatures, where the solvent viscosity broadens the signals or the products are not very soluble.

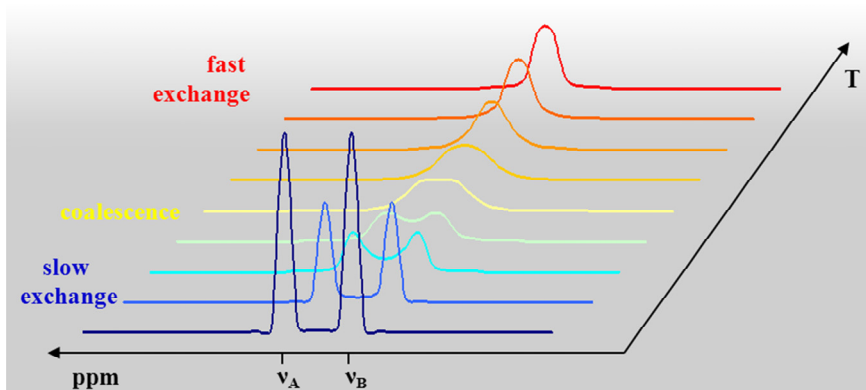


Figure 10. Variable-temperature NMR spectra of an uncoupled dynamic two-site system.

The blue line in Figure 10, taken at relatively low temperature, shows this splitting. However, the two methyl groups can exchange themselves by rotation about the bond between the nitrogen and the aldehyde group. As the temperature of the sample is raised, the methyl signals broaden as the exchange rate becomes faster in the the NMR timescale. The two signals reach coalescence (yellow line in Figure 10) and eventually merge to yield a single averaged sharp line when the rotation is very fast (red line in Figure 10).

Variable-temperature NMR spectroscopy has been applied extensively in the conformational analyses and kinetic studies of stereodynamic processes with energy barriers between 4.5 and 31 kcal/mol. The energy range covered by DNMR is limited by the NMR timescale, spectral resolution and the practical NMR temperature range, from -180 °C to +160 °C, limits determined by the solvents and by the probe design. For the high-temperature range, DMSO-d₆ (b.p. +210 °C) or C₂D₂Cl₄ (b.p. +146 °C) are usually employed. Solvents without any hydrogen atom, such as tetrachloroethylene (b.p. +121 °C), hexachloroacetone (b.p. +70 °C/6 mm Hg) or hexachlorobutadiene (b.p. +210 °C) can also be used.

Variable-temperature experiments down to -100 °C are usually recorded in CD₂Cl₂ (m.p. -97 °C), THF-d₈ (m.p. -118 °C) or CD₃OD (m.p. -95 °C). Quite a wide temperature range is accessible with toluene-d₈ (from -95 °C to +110 °C).^{6b} If the temperature has to be decreased well below -100 °C, the samples have to be prepared in a more sophisticated way, with use of liquefied gases such as Me₂O,⁹ vinyl chloride,¹⁰ propane,¹¹ propene,¹² Freons® or mixture of these.

Coalescence Method

In the absence of any coupling, the first-order interconversion rate constant at the coalescence temperature can be calculated as:

$$k_{TC} = \pi \frac{\Delta\nu}{\sqrt{2}}$$

k_{TC} = rate constant (s^{-1});

T_C = coalescence temperature (K);

$\Delta\nu$ = difference in the chemical shifts (Hz) of the two signals without exchange.

Further increasing the temperature, the exchange rate is too fast and only a single averaged signal is observed (red line in Figure 10). By weighted average the chemical shift can be calculated:

$$\nu_{A,B} = \nu_A \chi_A + \nu_B \chi_B$$

$\nu_{A,B}$ = chemical shift (Hz) of the signal with exchange

ν_A = chemical shift (Hz) of the signal at low field without exchange

ν_B = chemical shift (Hz) of the signal at high field without exchange

χ_A = molecular fraction of the signal at low field without exchange

χ_B = molecular fraction of the signal at high field without exchange.

From the k values, the free energy of activation (ΔG^\ddagger in kcal/mol) can be extracted by application of the Eyring equation,¹³ where T is the absolute temperature and k is the rate constant in s^{-1} :

$$k = \kappa \frac{k_B \cdot T}{h} e^{-\frac{\Delta G^\ddagger}{RT}}$$

h = Planck's constant ($1.584 \cdot 10^{-34}$ cal·s)

k_B = Boltzmann constant ($3.2998 \cdot 10^{-24}$ cal/K)

R = universal gas constant (1.9872 cal/K·mol)

κ = transmission coefficient (can be considered equal to 1)

Solving for ΔG^\ddagger (in kcal/mol):

$$\Delta G^\ddagger = 4.574 \cdot 10^{-3} \cdot T \cdot \left(\log \frac{T}{k} + 10.318 \right)$$

The determination of the exact temperature inside the sample is crucial for the determination of the thermodynamic parameters. An error of ± 2 °C in the temperature causes an error in ΔG^\ddagger of 0.15 to 0.2 kcal/mol, and this is usually the main source of errors in the DNMR technique.

The NMR spectrometer always shows a “dial temperature” determined by a thermocouple underneath the NMR tube. The temperature of the sample giving rise to the observed NMR signals (i.e., in the region of the RF coils) is usually different, and can be correlated to the “dial temperature” by a calibration curve.

The most common samples used for temperature calibration are isopentane or methanol (for low temperature range) and DMSO-d₆ or ethylene glycol (for high temperature range). The real temperature inside the sample in the coil region is determined by a tiny Cu-Ni thermocouple connected to an high precision digital thermometer. From the experimentally measured temperatures and dial temperatures, a calibration curve can be derived. The uncertainty in subsequent temperature measurements with such a calibration curve can be estimated as ± 1 °C or less.

The simplicity of the coalescence method, for the simple two-site case, has certainly contributed to its widespread use. However, this method is not applicable neither to interconversion of species with different thermodynamic stability, nor to compounds that show complicated NMR spectra with multiple coupling patterns. In these cases, the rate constants, at the different temperatures, are better obtained by NMR line shape analysis with customized programs.

Line Shape Simulation

The rate constants involved in conformation processes detectable by dynamic NMR cover approximately the range from 10^2 to 10^6 s⁻¹.

When two nuclei A and B are exchanged in a dynamic process with a kinetic constant k , the corresponding lines broaden, reach the coalescence point and eventually yield an average signal when the exchange rate constant becomes large. The presence of more than two signals and more than a single rate constant can complicate this situation; nevertheless the whole system can be mathematically simulated. With the use of increasing calculation power it is possible to handle mathematical models that can simulate second-order spectra and quite complex spin systems (up to 11 nuclei).¹⁴ Once a good spectral simulation is obtained at the temperature where all the dynamic processes are frozen (i.e. $k = 0$), the line shape at higher temperatures can be simulated by changing the values of the rate constants. Corrections are needed if chemical shifts, J couplings and conformer ratios are also temperature-dependent. Through the matching of simulated and experimentally measured spectra, the kinetic constant (k value) is obtained at each given temperature and the free energy of activation (ΔG^\ddagger) can then be derived by means of Eyring equation.

An example of how a complex spectral pattern can be reproduced is displayed in Figure 11.

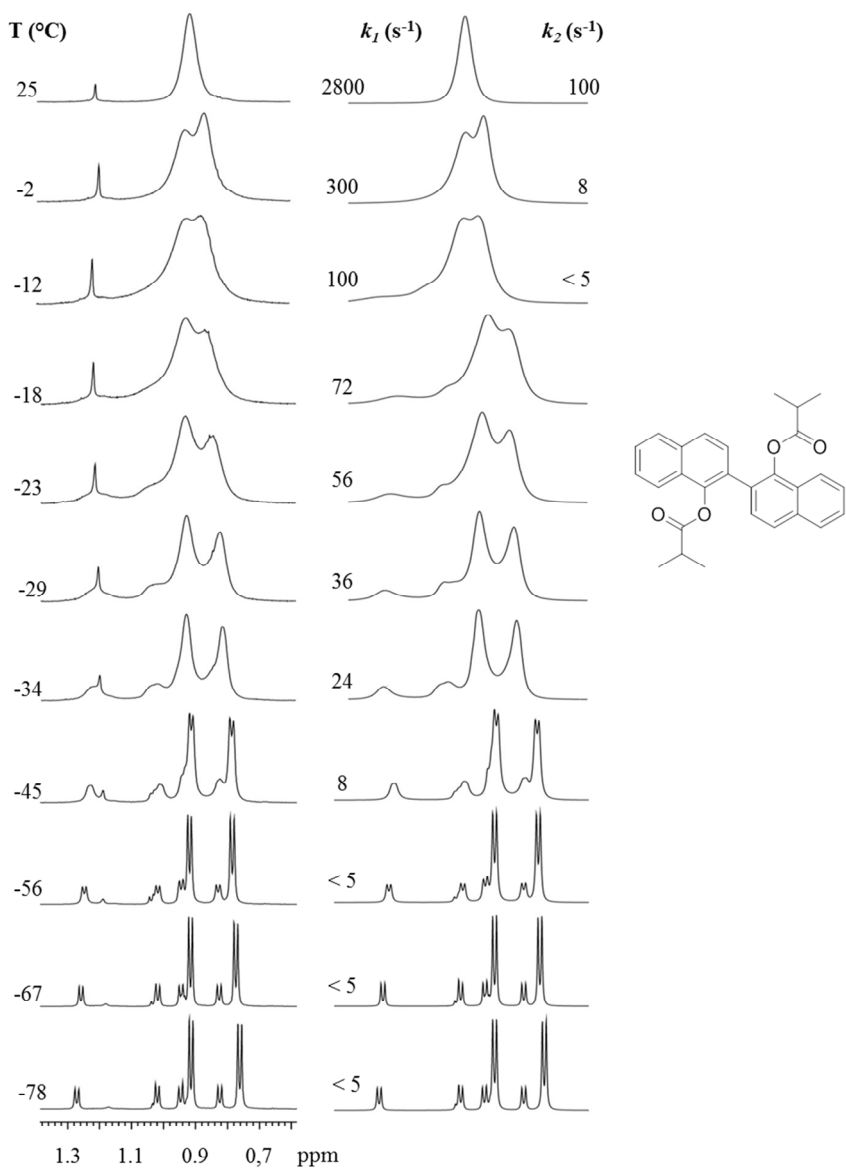


Figure 11. Example of line-shape simulation. (Left) experimental spectra. (Right) line shape simulation obtained with the rate constants indicated.

Optical techniques

Chiroptical techniques such as electronic circular dichroism (ECD) have been used for many years for the conformational analysis of organic molecules, following the landmark observations of Djerassi and co-workers¹⁵ in the early 1960s. By this technique, the conformational preference of a variety of cyclohexanones, bicyclic and polycyclic ketones, and biaryls and helicenes have been studied. This topic has been summarized by Lightner and Gurst¹⁶ and more recently reviewed by Pescitelli et al.¹⁷ ECD can be successfully used in conformational analysis when the conformations are different in the relative disposition of the chromophoric parts because this implies either different patterns of the ECD spectra or a very different $\Delta\varepsilon$ at the same wavelengths. For example, ECD spectra have been widely used to analyze the conformations of many binaphthyl derivatives, where the splitting of the exciton coupling is strongly related to the dihedral angle between the two aryl rings.¹⁸

The infrared counterpart of ECD, the vibrational circular dichroism (VCD) technique works in the same way of ECD. The main advantages of the VCD technique, with respect to ECD, are the large number of infrared (IR) bands that are more sensitive to any conformational change and the availability of these information regardless the lack of any UV chromophoric group. VCD spectroscopy has been recently applied to the conformational analysis of some complex molecules such as baccatine III¹⁹ and (*R*)-thalidomide.²⁰

Dynamic HPLC

In recent years enantioselective HPLC has been extended to the investigation of stereolabile compounds. Dynamic HPLC (DHPLC) can

be applied in the form of variable temperature, or variable flow chromatography and is employed to determine the enantiomerization barrier of chiral stereolabile species, when their interconversion takes place at the time scale of this technique.²¹ The HPLC time scale extends from seconds, in the case of fast HPLC on short columns, to hours, when long columns and low flow rates of the columns are used. Peak shape characteristic of an on-column interconversion are usually observed as a profile between the two resolved peaks, that don't reach the baseline (Figure 12).

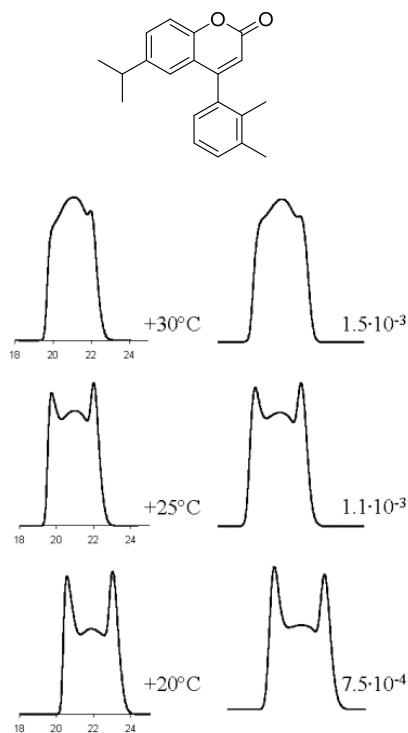


Figure 12. Temperature-dependent chromatograms of an aryl coumarin on an enantioselective HPLC column. (Left) Experimental profiles with the time scale in minutes. (Right) profiles calculated on the basis of the best fit rate constants (k , in s^{-1}) for enantiomerization.

The resulting peak shapes contain the necessary information to extract kinetic parameters related to the exchange process between the two species. Several methods have been used to extract kinetic data from experimental elution profiles, such as the theoretical plate model,²² the stochastic model,²³ the continuous flow model,²⁴ peak deconvolution methods,^{23b} approximation functions^{23b} and unified equation.^{21b}

Considering the time scale of these experiments, DHPLC is complementary to DNMR in that it can reveal the existence of the exchange phenomena, and yield the corresponding exchange rates. Moreover, the physical separation of the interconverting species can be exploited to proceed with their characterization by chiroptical methods.

Theoretical approach

Up to the end of the 1990s, conformational calculations of organic molecules were mainly performed by molecular mechanics (MM3,²⁵ MMX,²⁶ MMFF,²⁷ Amber²⁸ etc.). These calculations were reasonably simple and could be completed in short times on standard desktop PCs without the need for super-computers. The results obtained were often quite accurate, at least for the calculation of the ground-state conformations. For the calculation of transition states, these methods have intrinsic limitations. Usually the interconversion barriers were calculated by moving the relative parts of the molecule in fixed steps and optimizing the remaining parts. Otherwise, a “handmade” transition state was assumed, and the geometry was optimized within certain constraints. As a result of these approximations, the computed barriers were prone to relatively large errors, and there was no guarantee that a real transition state had been located.

The development of computing hardware allowed the theoretical chemists to find solutions of the wave equations for complex atomic systems. The first Hartree–Fock (HF) calculations were performed in the middle of the 1950s. Since the HF methods suffered from low power of calculation of the first digital computers, a semi-empirical approach was developed to partially solve this problem.²⁹

Finally, in the middle of the 1960s, Hohenberg and Kohn³⁰ demonstrated that the molecular energy can be calculated from the electron density, given the knowledge of the correct functional. It was also demonstrated that the electron density follows the variational theorem, and some years later the mathematical approach to the calculation of the energy was proposed.³¹ That was the beginning of the Density Functional Theory (DFT). The ability to manage large molecules at an affordable computational cost, and the possibility to calculate a variety of chemical and physical properties focused the attention of a huge number of researchers and justified the 1998 Nobel Prize in Chemistry to Pople and Kohn.³² DFT has the great advantage of taking account of electronic correlation at a reasonable computational cost.³³ In recent years, the availability of inexpensive high-performance servers and manageable software (Gaussian 09,³⁴ Turbomole,³⁵ Spartan³⁶ and NWChem³⁷) has allowed high-level calculations to be performed in a reasonable amount of time for molecules containing up to 50 – 60 atoms.

DFT calculations are very interesting for dynamic NMR because they can be applied both to obtain the conformations of ground states and to find the correct geometries and energies of transition states. The confirmation that the correct transition state has been unambiguously identified is done by vibrational analysis.

Ground States

There is some uncertainty in determining the relative energy of possible ground states and in recent times many papers addressing performance of various functionals have appeared.³⁸ In our experience, the popular B3LYP functional,³⁹ together with 6-31G(d) or the larger 6-311++G(2d,p) basis sets, is usually a good compromise between accuracy and computational cost. Geometries obtained by calculations can in many cases be checked by X-ray diffraction data, and the relative energies of conformations can be compared with the results of variable-temperature NMR spectroscopy. Although such a calculation usually refers to an isolated molecule, DFT structures compare very well with experimental observations and the relative energies of possible conformations are correctly calculated.

Transition States

As addressed by D. Young,⁴⁰ a transition state (or saddle point) structure is mathematically defined as “the geometry that has zero derivative of energy with respect to moving every one of the nuclei, and has positive second derivative energy for all but one geometric movement”. There are several algorithms that can be used to find a transition structure and the optimization procedure can find the saddle point only if the starting geometry is sufficiently close (Figure 13). Once the stationary point is found, the first way to verify whether it corresponds to a transition state is to compute the vibrational frequencies. A transition state must have only one negative (imaginary) frequency, and the vibrational motion associated with this frequency corresponds to the motion going towards reagents in one direction, and toward the products in the other, being “reagents” and “products” two different conformations.

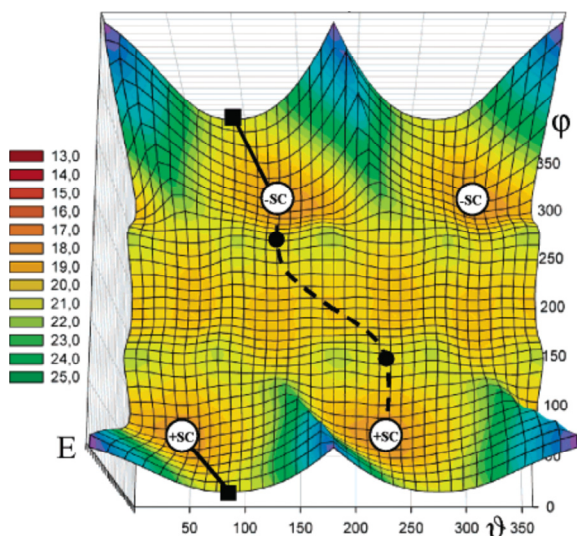


Figure 13. MM computed energy surface for a conformational exchange.⁴¹

Many modelling packages can visualize an animation of the molecular displacements corresponding to the calculated frequencies, clarifying whether the correct transition state has been found.⁴² The reliability and performance of the DFT calculations to predict the energy barrier of a conformational process can be checked by comparison with the experimental activation energies obtained by spectroscopic methods such as DNMR or by dynamic high performance liquid chromatography⁴³ and standard kinetic measurements.

References

- ¹ Kemp, J. D.; Pitzer, K. S. *J. Chem. Phys.* **1936**, 4, 749.
- ² Kemp, J. D.; Pitzer, K. S. *J. Am. Chem. Soc.* **1937**, 59, 276 – 279.
- ³ a) Hassel, O.; Viervoll, H. *Acta Chem. Scand.* **1947**, 1, 149 – 168. b) Hassel, O.; Ottar, B. *Acta Chem. Scand.* **1947**, 1, 929 – 943. c) Hassel, O. *Structural*

Aspects of Interatomic Charge-Transfer Bonding. Nobel Lectures, Chemistry 1963–1970. Amsterdam: Elsevier Publishing Company; **1972**.

⁴ Winstein, S.; Holness, N. J. *J. Am. Chem. Soc.* **1955**, *77*, 5562 – 5578.

⁵ Eliel, E. L.; Allinger, N. L.; Angyal, S. J.; Morrison, G. A. *Conformational Analysis.* New York: Interscience; **1965**.

⁶ a) Mazzanti, A.; Casarini, D. *WIREs Comput. Mol. Sci.* **2012**, *2*, 613 – 641. b) Casarini, D.; Lunazzi, L.; Mazzanti, A. *Eur. J. Org. Chem.* **2010**, *11*, 2035 – 2056.

⁷ Oki, M. *Applications of Dynamic NMR Spectroscopy to Organic Chemistry*, VCH Publishers, Inc. **1985**.

⁸ Gutowsky, H. S.; Holm, C. H. *J. Chem. Phys.* **1956**, *25*, 1228.

⁹ a) Lunazzi, L.; Macciantelli, D.; Boicelli, A. *Tetrahedron Lett.* **1975**, *16*, 1205 – 1206. b) Lunazzi, L.; Magagnoli, D.; Guerra, M.; Macciantelli, D. *Tetrahedron Lett.* **1979**, *20*, 3031 – 3032. c) Lunazzi, L.; Macciantelli, D.; Placucci, G. *Tetrahedron Lett.* **1980**, *21*, 975 – 976.

¹⁰ Bushweller, C. H.; O’Neil, J. W. *J. Am. Chem. Soc.* **1970**, *92*, 2159 – 2160.

¹¹ a) Ritter, R.; Hull, W.; Cantow, H.-J. *Tetrahedron Lett.* **1978**, *19*, 3093 – 3096. b) Pawar, D. M.; Brown II, J.; Chen, K.-H.; Allinger, N. L.; Noe, E. A. *J. Org. Chem.* **2006**, *71*, 6512 – 6515. c) Brown II, J.; Pawar, D. M.; Noe, E. A. *J. Org. Chem.* **2003**, *68*, 3420 – 3424. d) Pawar, D. M.; Miggins, S. D.; Smith, S. V.; Noe, E. A. *J. Org. Chem.* **1999**, *64*, 2418 – 2421.

¹² Pawar, D. M.; Noe, E. A. *J. Am. Chem. Soc.* **1998**, *120*, 5312 – 5314.

¹³ Eyring, H. *Chem. Revs.* **1935**, *17*, 65 – 77.

¹⁴ Brown, J. H.; Bushweller, C. H. *DNMR6: Calculation of NMR spectra subject to the effects of chemical exchange*, (Program 633) QCPE Bulletin, Bloomington, Indiana, **1983**, *3*, 103.

¹⁵ Wellman, K. M.; Briggs, W. S.; Djerassi, C. *J. Am. Chem. Soc.* **1965**, *87*, 73 – 81.

-
- ¹⁶ Lightner, D. A.; Gurst J. E. *Organic Conformational Analysis and Stereochemistry from Circular Dichroism Spectroscopy*. Wiley-VCH: New York, **2000**.
- ¹⁷ Pescitelli, G.; Di Bari, L.; Berova, N. *Chem. Soc. Rev.* **2011**, 40, 4603 – 4625.
- ¹⁸ Di Bari, L.; Pescitelli, G.; Salvadori, P. *J. Am. Chem. Soc.* **1999**, 121, 7998 – 8004.
- ¹⁹ Izumi, H.; Ogata, A.; Nafie, L. A.; Dukor, R. K.; *J. Org. Chem.* **2008**, 73, 2367 – 2372.
- ²⁰ Izumi, H.; Futamura, S.; Tokita, N.; Hamada, Y. *J. Org. Chem.* **2007**, 72, 277 – 279.
- ²¹ a) Mannschreck, A.; Zinner, H.; Pustet, N. *Chimia* **1989**, 43, 165 – 166. b) Trapp, O. *Anal. Chem.* **2006**, 78, 189 – 198.
- ²² Jung, M.; Schurig, V.; *J. Am. Chem. Soc.* **1992**, 114, 529 – 534.
- ²³ a) Veciana, J.; Crespo, M. I. *Angew. Chem. Int. Ed.* **1991**, 30, 74 – 77. b) Krupcik, J.; Oswald, P.; Majek, P.; Sandra, P.; Armstrong, D. W. *J. Chromatogr. A* **2003**, 1000, 779 – 800.
- ²⁴ Pirkle, W. H.; Schreiner, J. L. *J. Org. Chem.* **1981**, 46, 4988 – 4991.
- ²⁵ Allinger, N. L.; Yuh, Y. H.; Lii, J.-H. *J. Am. Chem. Soc.* **1989**, 111, 8551–8566.
- ²⁶ PCMODEL, v9, Serena Software, Bloomington, IN (USA)
- ²⁷ Halgren, T. A. *J. Comput. Chem.* **1996**, 17, 520 – 552.
- ²⁸ Weiner, S. J.; Kollman, P. A.; Case, D. A.; Singh, U. C.; Ghio, C.; Alagona, G.; Profeta, S.; Weiner, P. *J. Am. Chem. Soc.* **1984**, 106, 765 – 784.
- ²⁹ The first successful semiempirical MO programs: CNDO and INDO: a) Pople, J. A.; Segal, G. A. *J. Chem. Phys.* **1966**, 44, 3289 – 3297. b) Pople, J. A.; Beveridge, D. L.; Dobosh, P. A. *J. Chem. Phys.* **1967**, 47, 2026 – 2033. Then the MNDO, AM1, and PM3 packages have been developed: c) Dewar, M. J. S.; Thiel, W. *J. Am. Chem. Soc.* **1977**, 99, 4907 – 4917. d) Dewar, M. J. S.;

-
- Zoebisch, E. J.; Healy, E. F.; Stewart, J. J. P. *J. Am. Chem. Soc.* **1985**, 107, 3902 – 3909. e) Stewart, J. J. P. *J. Comput. Chem.* **1989**, 10, 221 – 264.
- ³⁰ Hohenberg, P.; Kohn, W. *Phys. Rev.* **1964**, 136, B864 – B871.
- ³¹ Kohn, W.; Sham, L. J. *Phys. Rev.* **1965**, 140, A1133 – A1138.
- ³² a) Pople, J. A. *Angew. Chem. Int. Ed.* **1999**, 38, 1894 – 1902. b) Kohn, W.; *Rev. Mod. Phys.* **1999**, 71, 1253 – 1267.
- ³³ a) Koch, W.; Holthausen, M. C.; *A Chemist's Guide to Density Functional Theory*, Wiley-VCH: Weinheim, 2nd ed., **2002**; b) *A Primer in Density Functional Theory* (Eds.: C. Fiolhais, F. Nogueira, M. Marques), Springer-Verlag, Heidelberg, **2003**.
- ³⁴ *Gaussian 09*, Frisch, M. J.; Trucks, G. W.; Schlegel, H. B.; Scuseria, G. E.; Robb, M. A.; Cheeseman, J. R.; Scalmani, G.; Barone, V.; Mennucci, B.; Petersson, G. A.; et al. Gaussian, Inc., Wallingford, Connecticut; **2009**.
- ³⁵ Ahlrichs, R.; Bär, M.; Häser, M.; Horn, H.; Kölmel, C. *Chem. Phys. Lett.* **1989**, 162, 165 – 169. See also: <http://www.turbomole.com/>
- ³⁶ *Spartan 08*, Wavefunction Inc., Irvine, CA (USA).
- ³⁷ Kendall, R. A.; Apra, E.; Bernholdt, D. E.; Bylaska, E. J.; Dupuis, M.; Fann, G. I.; Harrison, R. J.; Ju, J.; Nichols, J. A.; Nieplocha, J.; Straatsma, T. P.; Windus, T. L.; Wong, A. T. *Computer Phys. Commun.* **2000**, 128, 260 – 283. See also: <http://www.emsl.pnl.gov/capabilities/computing/nwchem/>.
- ³⁸ a) Check, C. E.; Gilbert, T. M. *J. Org. Chem.* **2005**, 70, 9828 – 9834. b) Wodrich, M. D.; Corminbouef, C.; Schleyer, P. v. R. *Org. Lett.* **2006**, 8, 3631 – 3634. c) Shreiner, P. R.; Fokin, A. A.; Pascal, R. A.; De Mejere, A. *Org. Lett.* **2006**, 8, 3635 – 3638. d) Grimme, S.; *Angew. Chem. Int. Ed.* **2006**, 45, 4460 – 4464. e) Zhao, Y.; Truhlar, D. G. *Org. Lett.* **2006**, 8, 5753 – 5755. f) Rokob, T. A.; Hamza, A.; Pápai, I. *Org. Lett.* **2007**, 9, 4279 – 4282. g) Shreiner, P. R. *Angew. Chem. Int. Ed.* **2007**, 46, 4217 – 4219. h) Wodrich, M. D.; Wannere, C. S.; Mo, Y.; Jarowski, P. D.; Houk, K. N.; Schleyer, P. v. R. *Chem. Eur. J.* **2007**, 13, 7731 – 7744. i) Zhao, Y.; Truhlar, D. G. *Acc. Chem. Res.* **2008**, 41, 157 –

-
167. j) Schwabe, T.; Grimme, S. *Acc. Chem. Res.* **2008**, 41, 569 – 579. k) Wodrich, M. D.; Jana, D. F.; Schleyer, P. v. R.; Corminbouef, C. *J. Phys. Chem. A*, **2008**, 112, 11495 – 11500.
- ³⁹ a) Becke, A. D.; *J. Chem. Phys.* **1993**, 98, 5648 – 5652. b) Lee, C.; Yang, W.; Parr, R. G. *Phys. Rev. B* **1988**, 37, 785 – 789. c) Stephens, P. J.; Devlin, F. J.; Chabalowski, C. F.; Frisch, M. J. *J. Phys. Chem.* **1994**, 98, 11623 – 11627.
- ⁴⁰ Young, D. *Computational Chemistry*, chapter 17, pp. 147–158, Wiley Interscience: New York, **2001**.
- ⁴¹ Casarini, D.; Lunazzi, L.; Mancinelli, M.; Mazzanti, A. *J. Org. Chem.* **2007**, 72, 998 – 1004.
- ⁴² a) *Gaussview 4.1.2*, Gaussian Inc., Wallingford CT, USA. b) *MOLDEN 4.6*, available at <http://www.cmbi.ru.nl/molden/>. See: Schaftenaar, G.; Noordik, J. H. *J. Cold Reg. Eng. J. Comput. Aided Mol. Design* **2000**, 14, 123 – 134; *Chem. Abstr.* **2000**, 132, 321509.
- ⁴³ a) Wolf, C. *Chem. Soc. Rev.* **2005**, 34, 595 – 608. b) D'Acquarica, I.; Gasparri, F.; Pierini, M.; Villani, C.; Zappia, G. *J. Sep. Sci.* **2006**, 29, 1508 – 1516.

Application of conformational analysis to the absolute configuration determination

In recent years an increasing number of papers describing the Absolute Configuration (AC) assignment by chiroptical methods have been presented.¹ This approach is particularly important in the cases that the anomalous dispersion X-ray diffraction technique can't be used.² This can happen when a compound does not contain a suitable heavy atom ($Z > \text{Si}$) or, even if containing, it can't be crystallized. Thus the simulation of one or more chiroptical properties represents a good alternative for the AC assignment. The theoretical background for the calculation of the optical properties such as optical rotation (OR),³ optical rotatory dispersion, VCD,⁴ and ECD methods has been coded and refined between 1970s and 1990s. With the implementation of DFT and TD-DFT⁵ methods into affordable software, all optical properties have become relatively simple to calculate.

Electronic Circular Dichroism (ECD)⁶

Many theoretical models have been applied to the calculations of the ECD spectra with the TD-DFT method. Simulations can be performed with the hybrid functionals BH&HLYP⁷ and M06-2X,⁸ ω B97XD that includes empirical dispersion,⁹ and CAM-B3LYP that includes long range correction using the Coulomb Attenuating Method.¹⁰ The calculations employed the 6-311++G(2d,p) basis set that proved to be sufficiently accurate at a reasonable computational cost.¹¹

Although the theoretical simulations have shown to be highly reliable when dealing with rigid molecules selected to validate the methodology,¹² the critic point of this technique is due to the conformational freedom of the major part of the organic molecules, and the main risk is to overlook a

populated conformation. For this reason, before calculating any optical property or spectra, an accurate conformational analysis must be always performed because the experimental spectrum is the average of the spectra corresponding to all the populated conformations weighted by Boltzmann distribution. In this case, the resulting spectrum is not averaged on the timescale, as in NMR spectra, because the optical techniques have a temporal resolution of picoseconds.

The conformational search starts from a simple calculation based on an MM force field and a systematic or a Monte Carlo approach for the determination of the starting geometries of all the possible conformations. This step usually provides a large number of MM minimized geometries and an energy cutoff of 5–10 kcal/mol is usually applied to reduce the number of energy minima to be subsequently refined. After this step the structures are subjected to a more sophisticated minimization, based on DFT with a moderate basis set. The simulation of the chiroptical property of each populated conformation is then obtained by the appropriate method (DFT or TD-DFT) using a larger basis set, as 6-311++G(2d,p), or Dunning-type orbitals (aug-cc-PVDZ and aug-cc-PVTZ).¹³ The simulated ECD spectrum, weighted on the Boltzmann population distribution is then superimposed with the experimental one, and the matching of the peaks validates the AC.

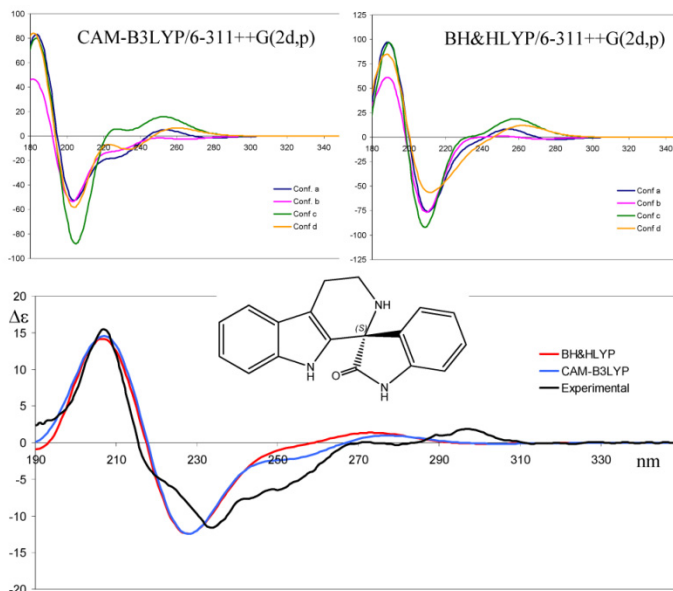


Figure 14. (Top) calculated ECD spectra for the four conformations of the reported compound (*S* absolute configuration) using the geometries obtained by gas-phase calculations. TD-DFT calculations were performed at the CAM-B3LYP/6-311++G(2d,p) and BH&HLYP/6-311++G(2d,p) level. (Bottom), superimposition between the experimental trace (black) and the two simulated spectra.^{11c}

Vibrational Circular Dichroism (VCD)

The assignment of the AC of organic molecules by VCD has been very recently reviewed in its different aspects.¹⁴ The prediction of the Absolute Configuration of a chiral molecule from its experimental VCD spectrum requires a methodology analogue to the determination via ECD. As first step the experimental spectrum of the solution of an enantiomer is acquired, in the mid-IR spectral region. Then the simulation of the spectrum is performed via DFT calculations, by means of prediction of the harmonic vibrational frequencies, dipole strength and rotational strength of the fundamental transitions of all populated conformations. The predicted VCD spectrum, weighted on the population distribution of

the conformations is compared with the experimental spectrum to define the Absolute Configuration.

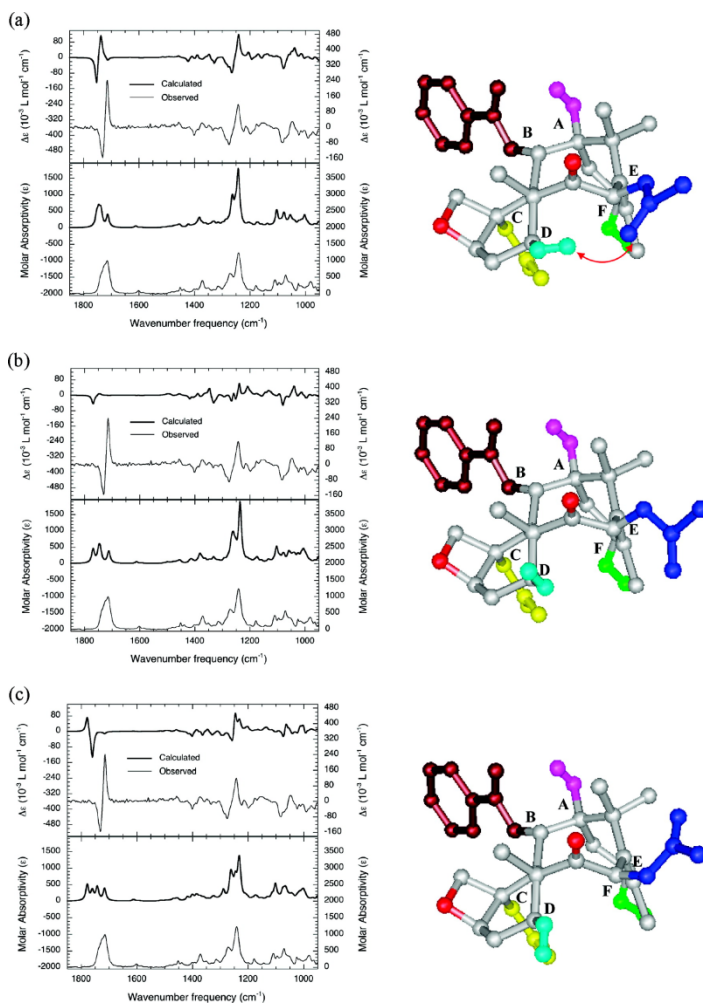


Figure 15. (Left) comparison of the measured VCD and IR spectra of baccatin III with the predicted spectra. (Right) the optimized geometries of the three conformations [B3LYP/6-31G(d)].¹

References

- ¹ a) Izumi, H.; Ogata, A.; Nafie, L. A.; Dukor, R. K. *J. Org. Chem.* **2008**, 73, 2367 – 2372. b) Izumi, H.; Futamura, S.; Tokita, N.; Hamada, Y. *J. Org. Chem.* **2007**, 72, 277 – 279.
- ² Peerdeman, A. F.; van Bommel, A. J.; Bijvoet, J. M. *Nature* **1951**, 168; 271 – 271.
- ³ Stephens, P. J.; Devlin, F. J.; Cheeseman, J. R.; Frisch, M. J. *J. Phys. Chem. A* **2001**, 105, 5356 – 5371.
- ⁴ a) Nafie, L. A.; Keiderling, T. A.; Stephens, P. J. *J. Am. Chem. Soc.* **1976**, 98, 2715 – 2723. b) Stephens, P. J. *J. Phys. Chem.* **1987**, 91, 1712 – 1715.
- ⁵ Runge, E.; Gross, E. K. U. *Phys. Rev. Lett.* **1984**, 52, 997 – 1000.
- ⁶ Berova, N.; Nakanishi, K.; Woody, R. W. *Circular Dichroism, Principle and Applications*. 2nd ed. John Wiley & Sons: New York, **2000**.
- ⁷ In Gaussian 09 the BH&HLYP functional has the form: $0.5 * E_X^{HF} + 0.5 * E_X^{LSDA} + 0.5 * \Delta E_X^{Becke88} + E_C^{LYP}$
- ⁸ Zhao, Y.; Truhlar, D. G. *Theor. Chem. Acc.*, **2008**, 120, 215 – 241.
- ⁹ Chai, J-D.; Head-Gordon, M. *Phys. Chem. Chem. Phys.*, **2008**, 10, 6615 – 6620.
- ¹⁰ Yanai, T.; Tewand D.; Handy, N. *Chem. Phys. Lett.*, **2004**, 393, 51 – 57.
- ¹¹ a) Cera, G.; Chiarucci, M.; Mazzanti, A.; Mancinelli M.; Bandini, M. *Org. Lett.*, **2012**, 14, 1350 – 1353. b) Pesciaioli, F.; Righi, P.; Mazzanti, A.; Bartoli, G.; Bencivenni, G. *Chem. Eur. J.*, **2011**, 17, 2842 – 2845. c) Duce, S.; Pesciaioli, F.; Gramigna, L.; Bernardi, L.; Mazzanti, A.; Ricci, A.; Bartoli, G.; Bencivenni, G. *Adv. Synt. Catal.*, **2011**, 353, 860 – 864. d) Bernardi, L.; Comes-Franchini, M.; Fochi, M.; Leo, V.; Mazzanti, A.; Ricci, A. *Adv. Synt. Catal.*, **2010**, 352, 3399 – 3406.
- ¹² a) Crawford, T. D.; Stephens, P. J. *J. Phys. Chem. A* **2008**, 112, 1339 – 1345. b) McCann, D. M.; Stephens, P. J.; Cheeseman, J. R. *J. Org. Chem.* **2004**, 69, 8709 – 8717.

¹³ Kendall, R. A.; Dunning, T. H.; Harrison, R. J. *J. Chem. Phys.* **1992**, *96*, 6796 – 6806.

¹⁴ a) Nafie, L. A. *Vibrational Optical Activity: Principles and Applications*, Wiley: Chichester, **2011**. b) Magyarfalvi, G.; Tarczay, G.; Vass, E. *WIREs Comp. Mol.* **2011**, *1*, 403 – 425. c) Stephens, P. J.; Devlin, F. J.; Pan, J. J. *Chirality* **2008**, *20*, 643 – 663.

Research objectives

The research work reported in this Thesis was held along two main lines of research. The first and main line of research is about the synthesis of heteroaromatic compounds with increasing steric hindrance, with the aim of preparing stable atropisomers. The main tools used for the study of these dynamic systems, as described in the Introduction, are DNMR, coupled with line shape simulation and DFT calculations, aimed to the conformational analysis for the prediction of the geometries and energy barriers to the transition states. This techniques have been applied to the research projects about:

- atropisomers of arylmaleimides;
- atropisomers of 4-arylpyrazolo[3,4-*b*]pyridines;
- study of the intramolecular NO₂/CO interaction in solution;
- study on 2-arylpyridines.

Parallel to the main project, in collaboration with other groups, the research line about determination of the absolute configuration was followed. The products, deriving from organocatalytic reactions, in many cases couldn't be analyzed by means of X-Ray diffraction, making necessary the development of a protocol based on spectroscopic methodologies: NMR, circular dichroism and computational tools (DFT, TD-DFT) have been implemented in this scope. In this Thesis are reported the determination of the absolute configuration of:

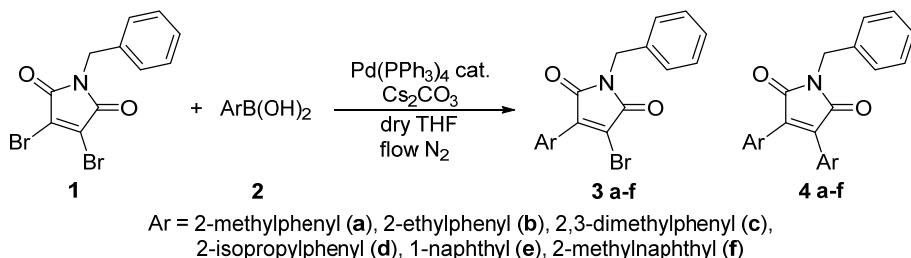
- substituted 1,2,3,4-tetrahydroquinolines;
- compounds from enantioselective Friedel-Crafts alkylation-acetalization cascade of naphthols with α,β -unsaturated cyclic ketones;
- substituted 3,4-annulated indoles.

Results and discussion

Synthesis and conformational analysis of atropisomeric systems

Atropisomers of arylmaleimides¹

Molecules containing stereogenic axes usually have a planar framework with one or more substituents linked in the key sites. Depending on the hindrance of the substituents and the geometry of the planar scaffold, the resulting conformational enantiomers can be stereolabile or configurationally stable, generating atropisomers. In this work we synthesized a series of benzyl maleimides bearing in position 3,4 variously *ortho*-substituted aromatic groups which adopt tilted conformations relative to the planar scaffold. The compounds have been prepared with a modified Suzuki coupling, under milder conditions, as reported in Scheme 6.



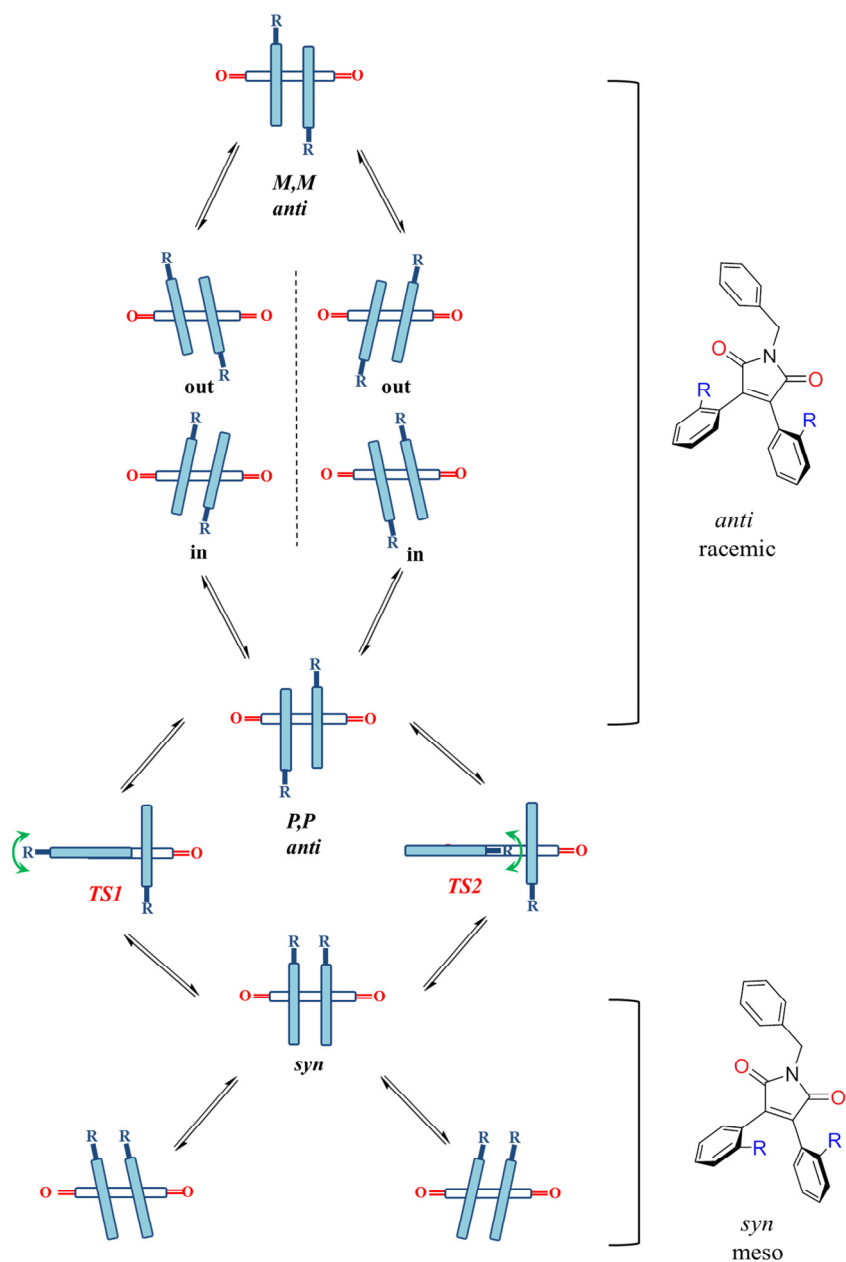
Scheme 6. Preparation of compounds 3a-f, 4a-f.

3,4-bisaryl *N*-benzyl maleimide

When equal aryl substituents are linked in position 3,4 of the maleimide (4), *syn/anti* conformers are formed. The substituents on the aryl ring can stay either on the same (*syn*) or on the opposite side (*anti*). As showed in Scheme 7, their interconversion corresponds to a 180° rotation and requires a passage through a transition state in which one ring is coplanar

to the scaffold, individuating a steric barrier.² The second process pointed out in Scheme 7 correspond to a flipping process, in which the two rings adopt a twisted disposition, originating a pair of enantiomers that interconvert through a transition state where the rings are orthogonal to the scaffold (π -barrier)². However the π -barrier is very low and its value decreases with the increasing of the steric barrier, so in this case is not possible to detect it by dynamic NMR.

We theoretically analyzed the stereodynamic pathway performing DFT optimization of the ground states and the available transition states, at the B3LYP/6-31G(d) level of theory. For compound **4a** calculated energy value of the π -barrier resulted 3.8 kcal/mol, thus the *syn* and the *anti* conformations can be considered as the average of the limiting structures. When *ortho* substituents of the aryl rings are on the same side of the maleimide scaffold the conformation has an average C_s symmetry and corresponds to a *meso* form. If the *ortho* substituents are arranged in the *anti* configuration the resulting symmetry is C_2 and implies a pair of conformational enantiomers. The interconversion between *syn* and *anti* conformations can be reached through two transition states: TS1 in which the *o*-aryl substituent crosses on the carbonyl group, TS2 corresponds to the internal crossing on the second aryl ring.



Scheme 7. Stereodynamic network for 3,4-bisaryl-*N*-benzylmaleimide.

In order to detect these conformations the hindrance caused by the *ortho* substituents must generate rotational energy barrier detectable within the dynamic NMR range (4.5 – 22 kcal/mol). Moreover when the interconversion is frozen on the NMR timescale the conformational diastereoisomers can be observed, but the assignment to the *meso* or racemic form can be performed only in presence of a chirality probe.³ For this reason the benzyl moiety was linked to the nitrogen of maleimide. It contains an uncoupled CH₂ group that displays different multiplicity depending on molecular symmetry, acting as chirality probe.

In the left part of Figure 16 is reported the variable-temperature NMR spectra for the CH₂ signal in compound **4d** (Ar = 2-isopropylphenyl). At room temperature the signal of CH₂ is very broad and unresolved, at 0°C the signals of *syn* and *anti* conformers can be distinguished, as the process becomes slow on the NMR timescale. The singlet at 4.826 ppm (cyan) corresponds to the *syn* conformation, with 49% of population, the AB system (red) corresponds to the *anti* conformers (51%), as the CH₂ becomes diastereotopic. On the right in Figure 16 the line shape simulation is reported, considering the coupling constant of the AB spin system and the exchange of the AB lines with the singlet of the *syn* form. It's important to point out that the racemization of the *anti* conformers corresponds to a two-step mechanism with the *syn* conformation as intermediate, thus the experimental free energy measured by dynamic NMR corresponds to the transition state *anti*-to-*syn* process. The experimental energy barrier obtained by line shape simulation for **4d** was 15.5 ± 0.1 kcal/mol and the ΔG^\ddagger values are almost invariant with the temperature, implying that the activation entropy is very small or negligible. This is quite usual for rotational processes.⁴

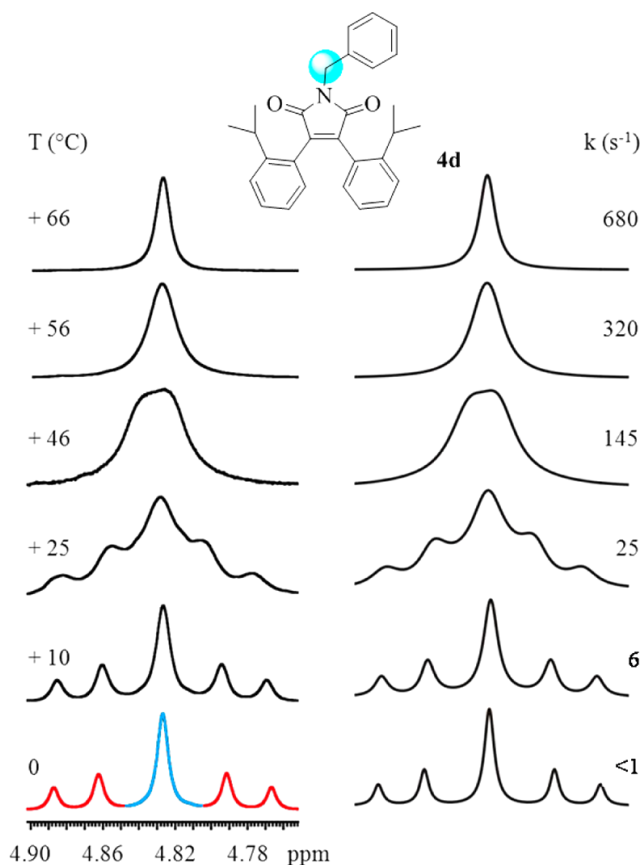


Figure 16. (Left) Temperature dependence of the ^1H benzylic CH_2 signal of **4d (600 MHz in $\text{C}_2\text{D}_2\text{Cl}_4$). (Right) Line shape simulation obtained with the rate constants reported.**

The energy barriers obtained for compounds **4a–f**, reported in Table 1, suggest that the barrier is controlled only by steric factors and the DFT computed energies matched well the relative stability of the two conformational diastereoisomers, as well as the energy barriers for their interconversion.

In the case of compound **4f** (Ar = 2-methylnaphthyl) DFT calculation for TS1 and TS2 yielded 23.5 and 25.1 kcal/mol respectively, implying the presence of thermally stable atropisomeric forms. This has been validated

by experimental results: the ^1H NMR recorded at room temperature showed two sets of signals, supporting the existence of stable diastereomeric forms and on heating the sample up to 120°C in $\text{C}_2\text{D}_2\text{Cl}_4$ no evidence of dynamic exchange has been detected.

Table 1. DFT-Computed and experimental energies of 3,4-bisaryl-*N*-benzylmaleimides 4a–f^a

Entry	GS1 (<i>syn</i>)	GS2 (<i>anti</i>)	TS1 (ext)	TS2 (int)	$\Delta G_{\text{exp}}^{\neq b}$	<i>syn/anti</i> _c
4a	0.28	0.00	11.55	12.43	12.9	55/45
4b	0.47	0.00	12.86	13.44	13.9	54/46
4c	0.16	0.00	13.93	14.56	14.9	55/45
4d	1.33	0.00	14.43	15.93	15.5	49/51
4e	0.00	0.00	12.88	12.98	14.0	45/55
4f	0.00	0.21	23.52	25.12	24.5	51/49

^a All energy barriers are reported in kcal/mol. ^b This value corresponds to the *syn/anti* interconversion, derived from line shape simulations. ^c Determined by NMR integration at appropriate temperature.

The three stereoisomers have been then resolved with enantioselective HPLC (Figure 17), cellulose based enantioselective column, eluent 90:10 hexane:isopropanol) and ^1H NMR spectra of the collected fractions confirmed the assignment of the chromatographic peaks.

The experimental energy barrier for the interconversion in compound **4f** has been determined by a kinetic study. A sample of the *syn* diastereoisomer in CDCl_3 was kept at 46°C and a set of spectra were recorded at fixed intervals (180 s) until the equilibrium composition was reached. At equilibrium a *syn/anti* ratio of 51/49 was observed. The kinetic process was analyzed at three different temperatures (46 , 51 and 61°C , Figure 18) and from the equilibrium ratio and the slope of the

regression lines a $\Delta G^\ddagger = 24.5$ kcal/mol was derived. This energy barrier corresponds to a half-life time of 128 h at 25 °C.

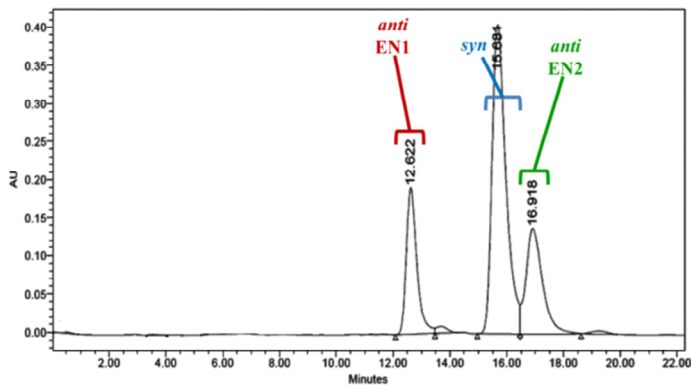


Figure 17. Chromatogram of 4f on enantioselective HPLC column.

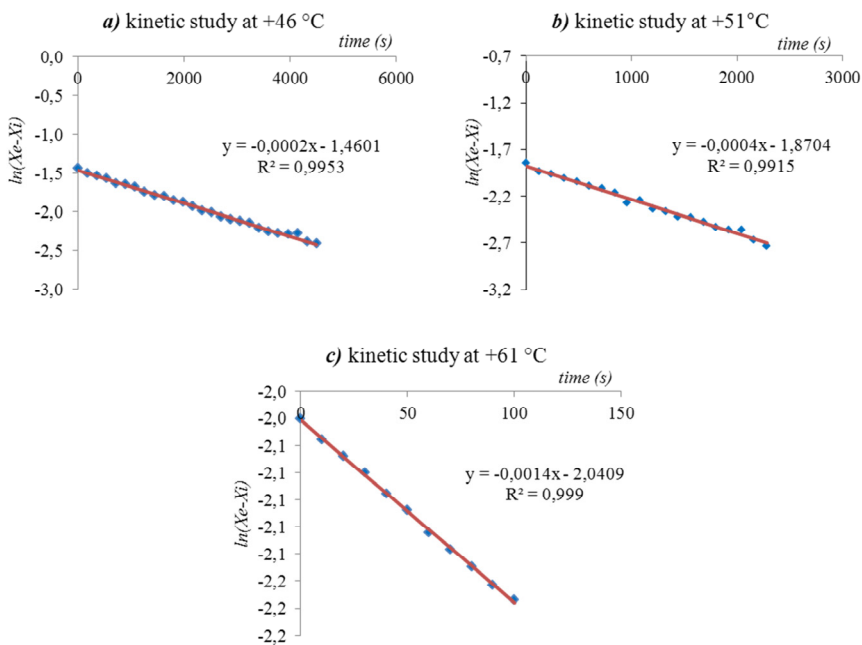
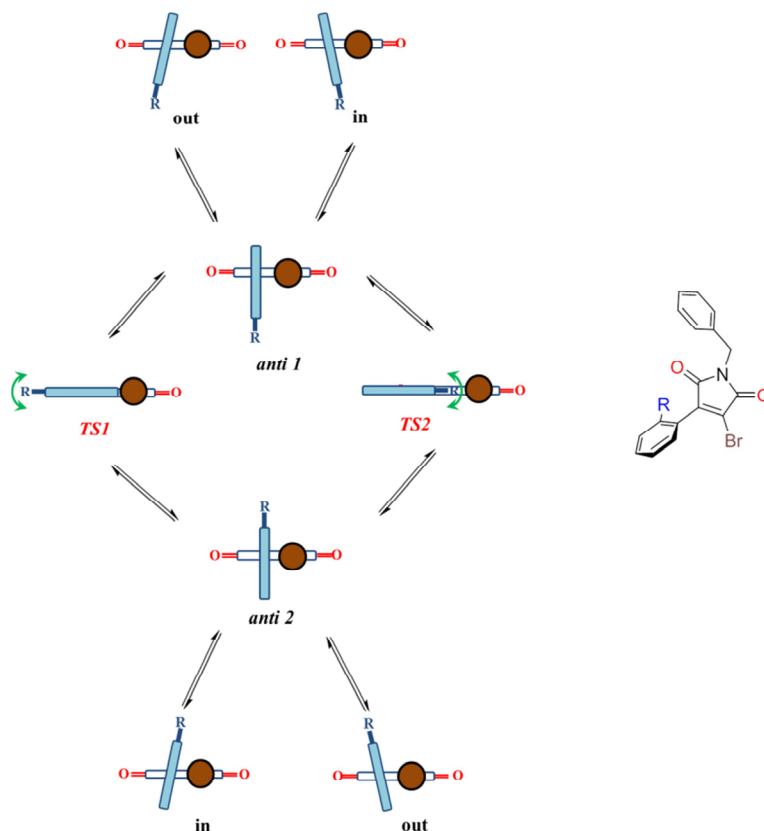


Figure 18. Kinetic data for the *syn/anti* interconversion of 4f.

3-Bromo-4-arylmaleimides

In this work 3-Bromo-4-arylmaleimides have been studied as well (compounds **3a-f**, Scheme 8). This compounds have a single stereogenic axis, so it can generate only enantiomeric conformations, due to the skewed disposition of the *o*-substituted aryl ring. As for compounds **4**, there are two available transitions states: TS1 in which the *o*-aryl substituent crosses on the carbonyl group, TS2 corresponds to the internal crossing towards the bromine.



Scheme 8. Stereodynamic network for 3-Bromo-4-aryl-*N*-benzylmaleimide.

As reported in Table 2, DFT calculations suggest that the preferred transition state pathway is TS1 and the experimental energy barriers, determined by dynamic-NMR, for compounds **3** are higher than those of compounds **4** ($\Delta\Delta G^\ddagger$ in Table 2). This difference can be related to the steric hindrance caused by the spherical bromine in the transition state, while in the ground state its effect is negligible.⁵ The difference in experimental free energy of activation is similar for each entry, with values is between 1 and 2 kcal/mol, except for compounds **3f** and **4f**, where it's about 4 kcal/mol. This can be related to the steric hindrance on both sides of the rotating aryl ring.

Table 2. DFT-Computed and experimental energy barriers of 3-Aryl-4-bromo-*N*-benzylmaleimides 3a–f^a

Entry	TS1 (ext)	TS2 (int)	$\Delta G_{\text{exp}}^\ddagger$	$\Delta\Delta G^\ddagger$ ^b
3a	11.23	12.65	14.3	1.4
3b	13.63	14.55	15.3	1.4
3c	14.21	15.24	16.6	1.7
3d	15.01	15.58	17.3	1.8
3e	13.16	14.83	15.7	1.7
3f	25.88	28.19	28.6 ^c	4.1

^a All energy barriers are reported in kcal/mol, as the difference with the corresponding 3,4-bisaryl-*N*-benzylmaleimide energy barrier ($\Delta\Delta G^\ddagger$ in kcal/mol) are also reported. ^b This value was obtained by considering the racemization barrier of the corresponding compound **4**. ^c Derived from HPLC analysis.

Compound **3f** resulted having free energy of activation up to 28.6 kcal/mol and the atropisomers were separation by AD-H enantioselective HPLC column (90:10 hexane:isopropanol).

Absolute configuration of 4f

The reference method to assign the absolute configuration relies on the X-ray anomalous scattering (the “Bijovet method”). However, this approach requires the preparation of enantiopure single crystals and the presence of a heavy atom in the molecule (usually $Z > \text{Si}$). In this case compound **4f** does not contain any heavy atom and the assignment by X-ray crystallography is unfeasible. In the present case the determination of the absolute configuration of atropisomers has been performed with the chiroptical technique of electronic circular dichroism (ECD) coupled with the theoretical calculation of the spectra, performed via TD-DFT. In order to correctly simulate the experimental ECD spectrum all the possible conformations of the *anti* diastereoisomer should be considered, the experimental spectrum resulting from the weighted sum of the populated conformations.

The conformational search performed on the *M,M* atropisomer suggested that two conformations are available for the two naphthyl rings: one with the methyl groups pointing toward the five-membered ring (*anti-in*) and the other in which they are directed toward the two carbonyl oxygens (*anti-out*). The theoretical ECD spectrum of both conformations was obtained with the TD-DFT method at CAM-B3LYP/6-311+G(d,p) level. The electronic excitation energies and rotational strengths were calculated in the gas phase using TD-DFT with four different functionals to explore whether different types of calculations provide different shapes of the simulated spectra. Simulations were performed on the previously optimized geometries using four different functionals: the hybrid functionals BH&HLYP⁶ and M06-2X,⁷ the long-range correlated

ω B97XD that includes empirical dispersion,⁸ and CAM-B3LYP that includes long-range correction using the Coulomb Attenuating Method.⁹

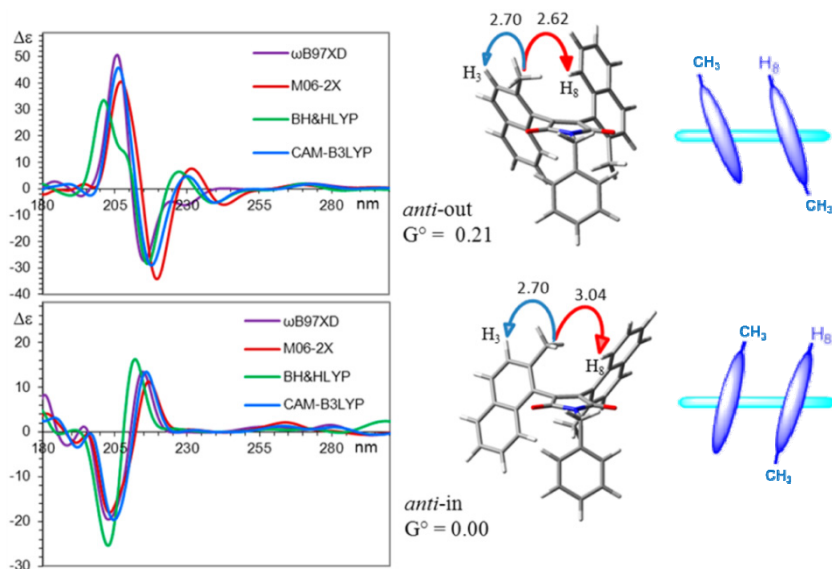


Figure 19. (Left) Theoretical ECD spectra of the two conformations of *M,M*-4f obtained with the TD-DFT method with four different theoretical methods and the 6-311+G(d,p) basis set. All the spectra were obtained by applying Gaussian shapes (line width = 0.25 eV) to the discrete transitions. The vertical scale has been reduced by a factor of 20 with respect to the calculated value. **(Right)** are reported the two optimized structures (relative ZPE-corrected free energies in kcal/mol, distances in Å).

As shown in Figure 19 the simulations obtained for the two conformations have nearly opposite spectrum. For this reason the correct population ratio of the two conformations is required to obtain a correct ECD spectrum simulation. Direct method to the determination of the population can't be used, being the π -barrrier inaccessible for dynamic-NMR technique, for this reason NOE spectrum (in CD₃CN) of the second eluted atropisomer (Figure 17) was used. In both conformations, the methyl group of each naphthyl ring is spatially close to the hydrogen in

position 3 of the same ring and to the H-8 of the other naphthyl ring. The distances from the 2-methyl to H-3 and H-8 are different, depending on the conformation considered. In the *anti-in* conformation this ratio is calculated as 0.89, while in *anti-out* conformation this ratio is 1.03 (Figure 19). The observed NOE corresponds to a 60:40 ratio of the two conformations (*anti-in:anti-out*). This result is in agreement with the 59:41 ratio based on the computed free energies of the two conformations (0.00 and 0.21 kcal/mol for the *anti-in* and *anti-out*, respectively). The second eluted atropisomer (EN2) resulted having *M,M* absolute configuration.

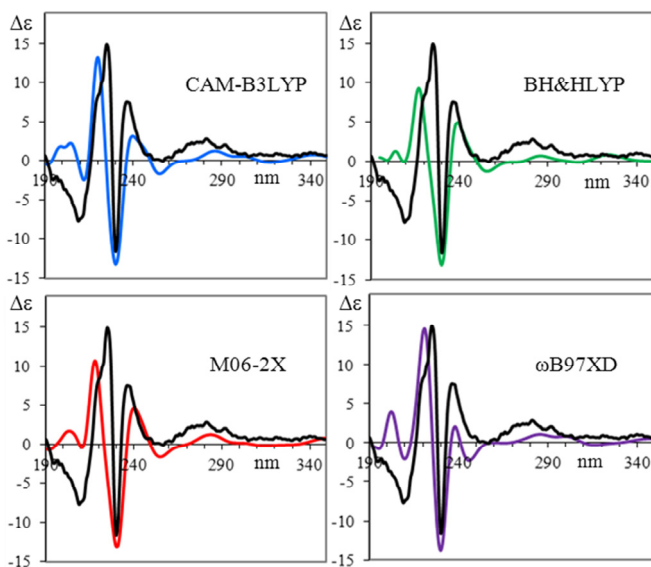


Figure 20. Computed ECD spectra of 4f considering a ratio of 59:41 of the two conformations, using four different functionals. All the calculations employed the 6-311+G(d,p) basis set. Black line: experimental ECD spectrum of the second eluted atropisomer of 4f.

Absolute configuration of 3f

In the case of compound **3f**, atropisomers separation was obtained by AD-H enantioselective HPLC column (90:10 hexane:iso-propanol as 60

eluent) as reported in Figure 21). Using the same approach of compound **4f** the absolute conformations of the enantiomers have been obtained by ECD spectra. From the preliminary conformational search by MM four different conformations were found to be populated, which correspond to the two dispositions of the naphthyl ring, combined with the two available dispositions of the benzyl ring. Simulation of the ECD spectrum is obtained assuming Boltzmann population distribution of the four conformations (30:26:24:21 ratio, using ZPE corrected free energies). The first eluted atropisomer (EN1) resulted having *M* absolute configuration.

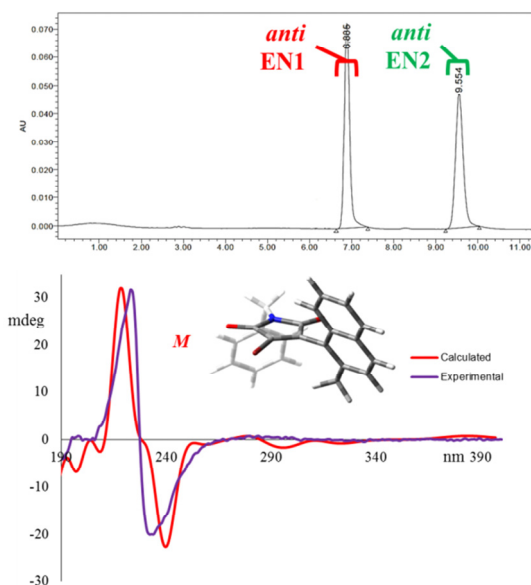


Figure 21. (Top) Chromatogram, with retention times, in AD-H enantioselective HPLC column, 90:10 hexane/isopropanol. (Bottom) 9 nm shifted finally computed *M* spectrum (purple line) and experimental ECD spectrum of EN1 (red line)

Conclusions

Stable atropisomers can be generated when hindered aryl rings occupy the 3,4 positions of the benzyl maleimide. DFT calculation, at B3LYP/6-31G(d) level, were able to well predict the energy barrier of the racemization in the case of compound **4f**, which have been confirmed with experimental data. 3-bromo-4aryl maleimides can generate atropisomers as well, as in the case of compound **3f**. Absolute configuration of the atropisomers obtained has been determined by theoretical simulation of the ECD spectrum, by means of TD-DFT calculation, supported by NMR conformational analysis.

References

- ¹ Ambroggi, M.; Ciogli, A.; Mancinelli, M.; Ranieri, S.; Mazzanti, A. *J. Org. Chem.*, **2013**, 78, 3709 – 3719.
- ² a) Wolf, C. *Chem. Soc. Rev.* **2005**, 34, 595 – 608. b) D'Acquarica, I.; Gasparrini, F.; Pierini, M.; Villani, C.; Zappia, G. *J. Sep. Sci.* **2006**, 29, 1508 – 1516. c) Piron, F.; Vanthuyne, N.; Joulin, B.; Naubron, J. -V.; Cismaş, C.; Terec, A.; Varga, R. A.; Roussel, C.; Roncali, J.; Grosu, I. *J. Org. Chem.* **2009**, 74, 9062 – 9070.
- ³ a) Jennings, W. B. *Chem. Rev.* **1975**, 75, 307 – 322. b) Mislow, K.; Raban, M. *Top. Stereochem.* **1967**, 1, 1 – 38.
- ⁴ a) Casarini, D.; Lunazzi, L.; Mazzanti, A. *Eur. J. Org. Chem.* **2010**, 11, 2035 – 2056. b) Bogdan, N.; Grosu, I.; Benoît, G.; Toupet, L.; Ramondenc, Y.; Condamine, E.; Dumitrescu, I. S.; Plé, G. *Org. Lett.* **2006**, 8, 2619 – 2622.
- ⁵ Lunazzi, L.; Mazzanti, A.; Muñoz Álvarez, A. *J. Org. Chem.* **2000**, 65, 3200 – 3206.
- ⁶ In Gaussian 09 the BH&HLYP functional has the form: $0.5 * E_X^{HF} + 0.5 * E_X^{LSDA} + 0.5 * \Delta E_X^{Becke88} + E_C^{LYP}$.
- ⁷ Zhao, Y.; Truhlar, D. G. *Theor. Chem. Acc.* **2008**, 120, 215 – 241.

⁸ Chai, J.-D.; Head-Gordon, M. *Phys. Chem. Chem. Phys.* **2008**, 10, 6615 – 6620.

⁹ Iikura, H.; Tsuneda, T.; Yanai, T.; Hirao, K. *J. Chem. Phys.* **2001**, 115, 3540 – 3544.

Atropisomers of 4-arylpyrazolo[3,4-*b*]pyridines¹

The pyrazolo[3,4-*b*]pyridine ring system has emerged as a privileged substructure in the pharmaceutical industry because of its occurrence in various biologically active compounds exhibiting medicinal properties,^{2,3} among which as HIV reverse transcriptase inhibitors⁴ and as effective candidate in the treatment of Alzheimer's disease (BAY 41-2272)⁵. Furthermore, pyrazolo[3,4-*b*]pyridines cartazolate, etazolate, and tracazolate (Figure 22), are well-established anxiolytic drugs.⁶ In addition to their pharmacological importance this scaffold possess a high structural resemblance to purine bases, essential constituents of DNA and RNA nucleosides,⁷ which adds further significance to the synthesis and study of this moiety.

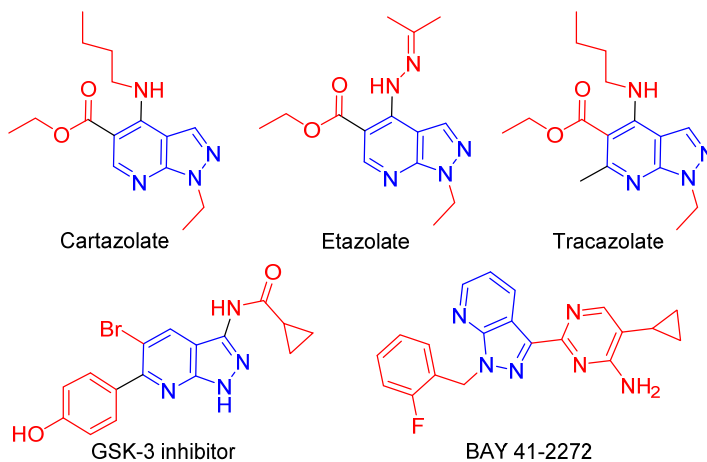


Figure 22. Pyrazolopyridine-embedded drugs and bioactive compounds.

The aim of this section is a thorough investigation of the stereodynamics of a class of pyrazolo[3,4-*b*]pyridines (Figure 23) and an evaluation of the steric requirements needed to produce stable heteroaromatic

atropisomers. Many bioactive natural compounds contain stereogenic axes, thus Clayden, LaPlante and co-workers have recently begun to address pharmaceutical implications of atropisomerism in drug discovery.⁸ As an additional feature of interest these compounds bear a fluorinated substituent on the heterocyclic scaffold. Over the years, great attention has been focused on the design and synthesis of fluorinated organic compounds because of their chemical and biological properties.⁹

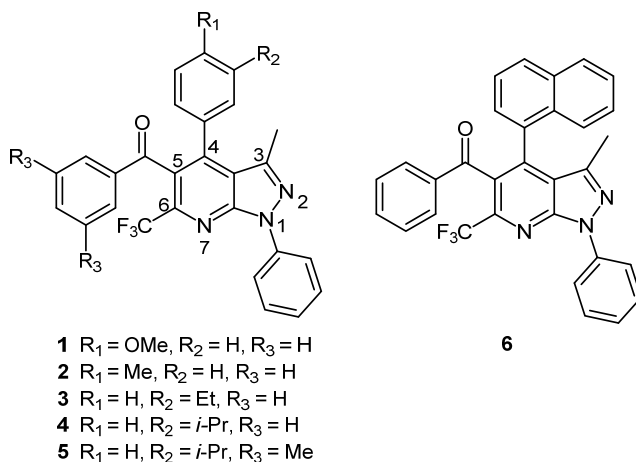
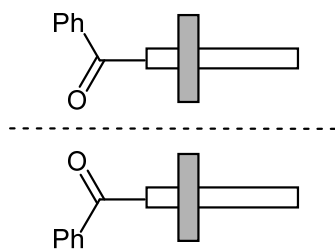


Figure 23. Chemical structure of compounds 1 – 6.

The pyrazolo[3,4-*b*]pyridine scaffold of compounds **1** – **6** (Figure 23) bears a methyl group in position 3 and a trifluoromethyl group in position 6. Because of the presence of these sterically demanding substituents, these compounds bear two single bonds around which the rotation could be hindered: the aryl group in position 4 and the benzoyl group in position 5. From a stereochemical point of view, compounds **1** and **2** bear a single stereogenic axis corresponding to the bond in position 5 and when in this rotation is frozen in the NMR timescale a pair of conformational enantiomers is generated. (Scheme 9).



Scheme 9. The two enantiomeric conformations of **1** and **2** (the grey rectangle stands for the *p*-substituted phenyl moiety, the white stands for the heterocyclic scaffold)

Whereas the *p*-anisole (**1**) and the *p*-tolyl (**2**) aryl in position 4 is symmetrically substituted thus is not generating a stereogenic axis. When optimized at the B3LYP/6-31G(d) level, the ground-state structures showed that the *p*-substituted ring was almost perpendicular to the pyrazolo[3,4-*b*]pyridine ring and the benzoyl moiety was disposed in a skewed conformation, too. In its ground-state geometry, compounds **1** and **2** belong to the C_1 symmetry point group. These calculated structures fully agree with the known X-ray structure of compound **2**.¹⁰

In compound **1** two transition states (TS1 and TS2 in Figure 24) should be considered to achieve racemization by the 180° rotation of the benzoyl moiety. In TS1 the carbonyl oxygen crosses the pyrazolo pyridine plane on CF₃ group side, while in TS2 the oxygen is close to the *p*-anisole group. According to DFT calculations, the transition state with the lower energy is TS1, with a ΔH^\ddagger of 15.1 kcal/mol, while TS2 has a ΔH^\ddagger of 15.6 kcal/mol. The computed transition state for anisole rotation corresponds to a coplanar conformation (TS3 in Figure 24) and its energy was calculated as 17.1 kcal/mol.

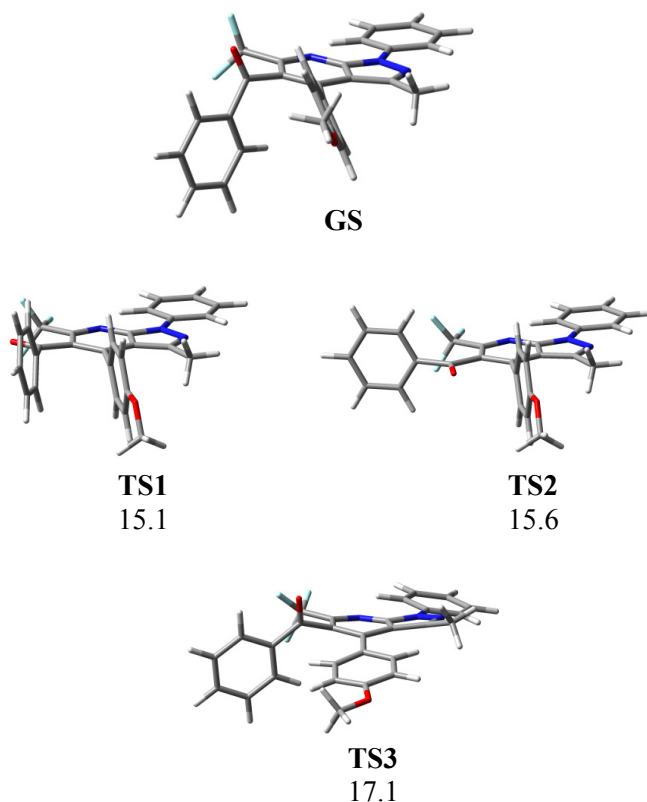
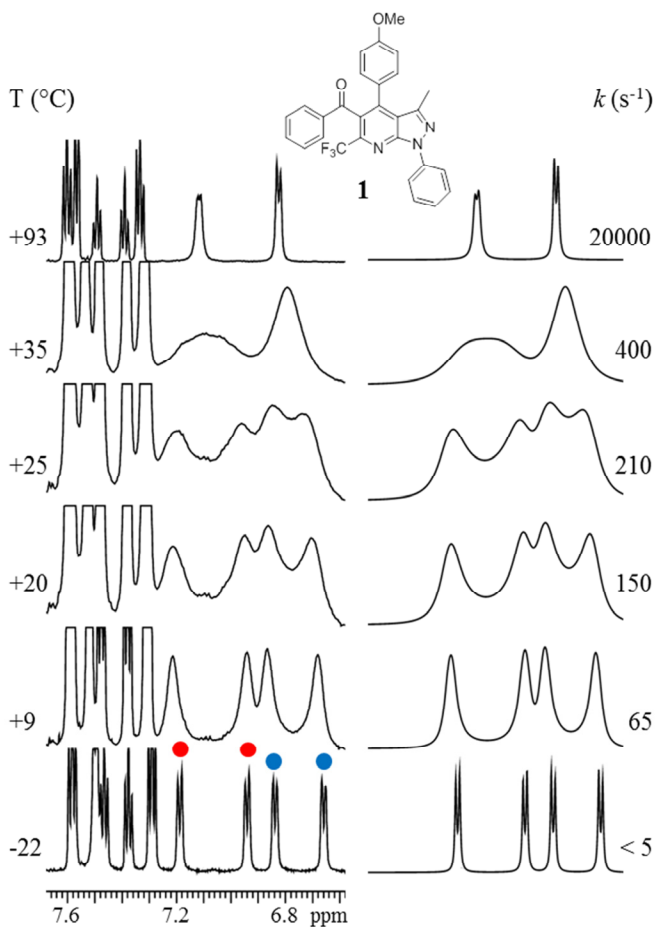


Figure 24. Calculated transition states for compound **1** at the B3LYP/6-31G(d) level. The reported energy values (relative to the ground state) are thermal corrected enthalpies, in kcal/mol.

The room temperature NMR spectrum of **1** showed broad peaks in the aromatic region, corresponding to the signals of the *p*-anisole ring. On raising the temperature above +25 °C, broad signals sharpened at +93 °C into the expected AA'BB' spectrum. On lowering the temperature these signals sharpened and eventually split at -22 °C into two sets of signals in a 50:50 ratio (see Figure 25). The same behavior was observed in the case of compound **2**. The experimental energy barriers were determined by line-shape simulations as 14.3 ± 0.2 kcal/mol and 14.1 ± 0.2 for **1** and

2, respectively. If the rotation of anisole is frozen and the benzoyl rotation is still fast in the NMR time scale, the two sides of anisole are enantiotopic, thus their hydrogens are not anisochronous. If the benzoyl rotation is frozen and the anisole rotation is fast, the two sides of anisole are exchanged by rotation (homomerization) and again no splitting is observed in the NMR spectrum. When both rotations are frozen, nevertheless, the two sides of the aromatic ring belong to different magnetic environments, giving the observed splitting. For these reasons, the experimental energy barrier must be assigned to the lower calculated barrier for the two stereodynamic pathways, i.e., that for the benzoyl group rotation (15.1 kcal/mol). The barrier for the anisole (tosyl) rotation can't be determined.

To get information about the stereodynamics of the aryl ring in position 4 we prepared compounds **3** and **4**, bearing a *m*-ethylphenyl and a *m*-isopropylphenyl ring, respectively. The presence of a substituent in the *meta* position does not alter to a great extent the heteroaryl–aryl rotational barrier, nevertheless, the aromatic ring loses its local C_2 symmetry and a new stereogenic axis is generated when its rotation is frozen. For these compounds when both barriers are frozen we should take into consideration four possible conformations, as reported in Figure 26.



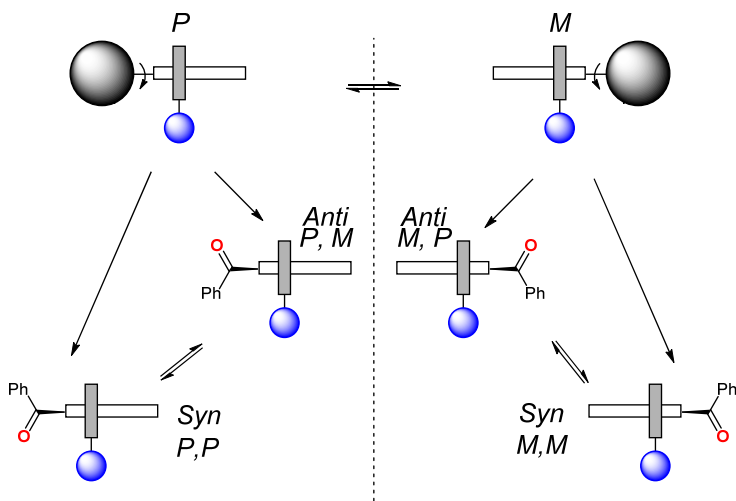


Figure 26. Stereochemical pathways for compounds 3 – 6. The black spheres correspond to the benzoyl moiety. The blue spheres correspond to the meta substituent on the aryl ring in position 4 of the pyrazolopyridine ring.

When the dynamic process with the higher barrier is frozen, a pair of conformational enantiomers is generated, whereas when rotation around the second stereogenic axis is restricted, two pairs of conformational diastereoisomers are formed. Using *M*, *P* descriptors,¹¹ the *syn* diastereoisomer corresponds to $4M^*,5M^*$ and the *anti* to the $4M^*,5P^*$ relative configuration. The ethyl and isopropyl groups were chosen because they act as stereochemical probes by showing diastereotopic signals in the NMR spectra.¹²

Compound **3** crystals were obtained from a hexane/ethyl acetate 4:1 v:v solution, as a racemate of the *P*-1 point group. X-ray structure showed that the *m*-ethylphenyl and the CO moieties are skewed with respect to the pyrazolo[3,4-*b*]pyridine ring, with 61.7° and 71.6° angles, respectively. Moreover in the solid state the two groups adopt the *syn* disposition, see Figure 27.

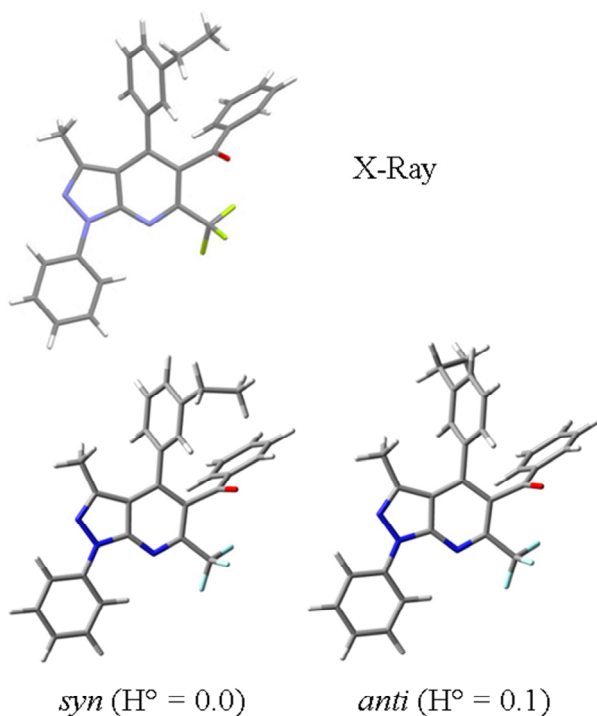


Figure 27. X-ray structure and DFT calculated structures for the two diastereoisomers of compound 3. The reported energy values are thermal-corrected enthalpies, in kcal/mol.

DFT calculations were performed to evaluate the energies of the two diastereoisomers of **3**, which have been found to be very similar. The *syn* conformer was the more stable by only 0.16 kcal/mol when the internal energy was considered, and by even less (0.10 kcal/mol) when the thermal-corrected enthalpy was taken into account (Figure 27). The four possible transition states connecting the four conformations were calculated at the same level of theory. There are two possible transition states for each moiety: for the benzoyl group, in which the CO is coplanar with the heterocyclic scaffold, it can be close either to the aryl ring in position 4 or to the CF₃ group in position 6 (TS1 and TS2 in Figure 28),

and for the *m*-ethylphenyl ring where the ethyl group points to either the methyl in position 3 of the pyrazolo[3,4-*b*]pyridine or to the benzoyl group in position 5 (TS3 and TS4 in Figure 28). For each rotational pathway, the lowest calculated energy barrier is the one to be considered for the comparison with experimental data. Calculated energies suggested that the rotation of the *m*-ethylphenyl group was higher than that of the benzoyl group (18.1 and 14.9 kcal/mol, respectively).

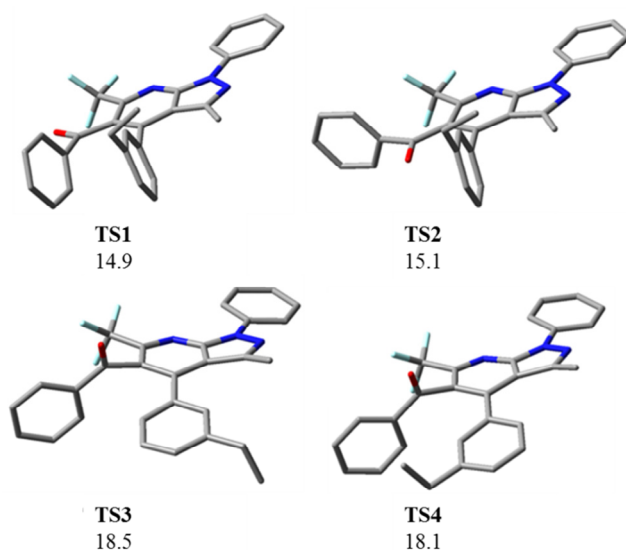


Figure 28. Calculated transition states for compound **3** at the B3LYP/6-31G(d) level. The reported energy values (relative to the ground state) are thermal-corrected enthalpies, in kcal/mol.

The NMR spectrum of compound **3** recorded at room temperature showed broad peaks for both the CH₂ and CH₃ signals of the ethyl group. On lowering the temperature of a C₂D₂Cl₄ solution of **3**, the signals of the CH₂ decoalesced and eventually split into two quartets with 55:45 relative ratio at -22 °C. The unbalanced ratio confirmed that the two conformational diastereoisomers were present, thus both rotational

barriers must be frozen in the NMR time scale. The lack of diastereotopicity on the CH₂ signals is due to a negligible chemical shift difference between the diastereotopic protons. On switching the solvent to acetonitrile-*d*₃, the same signals did show diastereotopicity at -22 °C, but the low boiling point of this solvent did not allow the measurement of the higher of the two barriers. The diastereomerization barrier, assigned to the benzoyl rotation was conveniently measured by line-shape simulation of the methyl signal in C₂D₂Cl₄ (Figure 29), yielding a barrier of 13.9 ± 0.15 kcal/mol, in agreement with the one found for **1** and **2**.

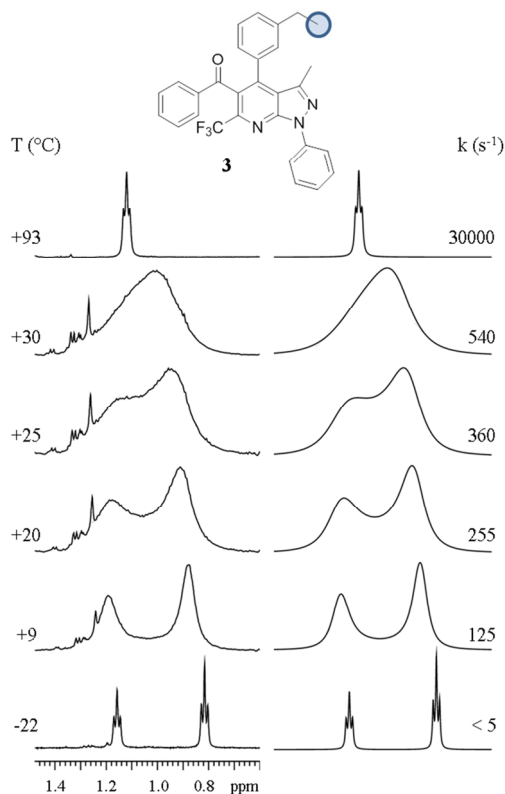


Figure 29. (Left) temperature dependence of the ¹H methyl signals of **3** (600 MHz in C₂D₂Cl₄). (Right) Lineshape simulation obtained with the rate constants reported.

The measurement of the rotational barrier of the second stereogenic axis was accomplished with compound **4** ($C_2D_2Cl_4$ sample), bearing a *m*-isopropylphenyl group. At room temperature the methyl groups show a broad signal, then on lowering the temperature, the methyl signal split at $-20\text{ }^\circ\text{C}$ into three signals with 36:32:32 ratio (bottom trace of Figure 30) where the low field triplet is ascribable to the partial overlap of two doublets with the same intensity. Integration of the isopropyl CH signal confirmed the 64:36 ratio of the two conformational diastereoisomers. On raising the temperature, the broad signal observed at room temperature sharpened and two separated signals ($\Delta\nu = 21\text{ Hz}$) were observed at $+81\text{ }^\circ\text{C}$ (top left trace of Figure 30). The two observed spectral lines correspond to the diastereotopic signals of the isopropyl group when the dynamic process with the lower barrier is fast in the NMR time scale, and the higher barrier process is still frozen (the coupling constant with the CH is hidden within the line width). On further raising the temperature, the two signals reached coalescence at $+102\text{ }^\circ\text{C}$ and a doublet due to the coupling with CH was eventually visible at $+133\text{ }^\circ\text{C}$ (right section of Figure 30). Two different sets of rate constants must be considered in the simulations. The first set accounts for the exchange between the pair of methyl signals of one diastereomeric conformation with the pair of methyl signals of the other one (diastereomerization barrier). The second set of rate constants must exchange the two diastereotopic methyl signals within the same diastereoisomer. The energy barrier derived from the simulation of the first set of rate constants was $14.3 \pm 0.15\text{ kcal/mol}$, in good agreement with the values obtained for compounds **1** – **3**. The energy barrier derived for the higher energy process was $19.2 \pm 0.2\text{ kcal/mol}$. The experimental

values have to be compared with the values of 15.6 and 18.4 kcal/mol provided by the calculations for the benzoyl and *m*-isopropylphenyl rotation, respectively.

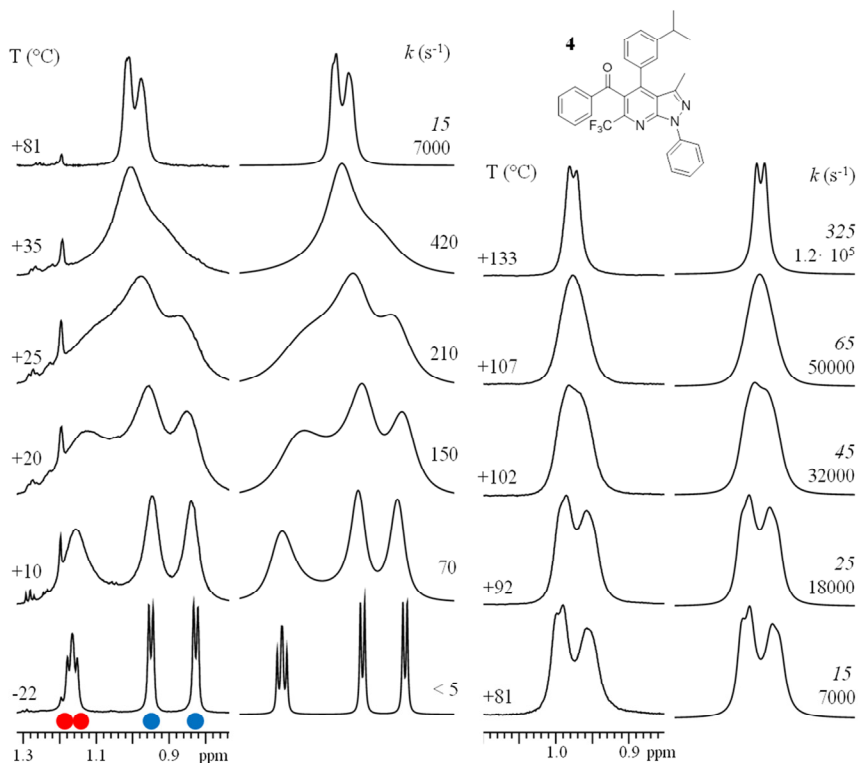


Figure 30. Temperature dependence of the ^1H NMR isopropyl methyl signal of **4** (600 MHz in $\text{C}_2\text{D}_2\text{Cl}_4$). (*Left*) low-temperature part and corresponding line-shape simulations obtained with the rate constants reported. (*Right*) high temperature spectra and line-shape simulations. Italicized rate constants are relative to the higher energy barrier, whereas the other rate constants are those for the lower barrier. The spectrum at +81 °C of the left side is the same at the bottom of the right side, where the chemical shift scale was expanded by a factor of 3.

Table 3. Experimental ^1H NMR (600 MHz, CD_2Cl_2 -67°C) and calculated chemical shifts of the two diastereoisomeric conformers of compound 3.

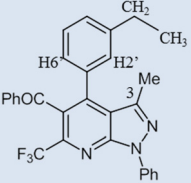
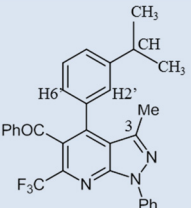
	Experimental chemical shifts (ppm)		Calculated chemical shifts (ppm)	
	Major	Minor	<i>Anti</i>	<i>Syn</i>
3-Me	2.07	2.10	2.20	2.23
Ethyl CH_2	2.36	2.57	2.65	2.67
Ethyl CH_3	0.82	1.16	0.87	1.25
$\text{H}2'$	6.75	7.08	7.34	7.69
$\text{H}6'$	7.05	6.80	7.55	7.35

Table 4. Experimental ^1H NMR (600 MHz, CD_2Cl_2 -67°C) and calculated chemical shifts of the two diastereoisomeric conformers of compound 4.

	Experimental chemical shifts (ppm)		Calculated chemical shifts (ppm)	
	Major	Minor	<i>Anti</i>	<i>Syn</i>
3-Me	2.05	2.09	2.20	2.26
CH_3	0.82	1.12	1.01	1.20
CH_3	0.95	1.14	1.32	1.24
i-PrCH	2.65	2.81	2.78	2.96
$\text{H}2'$	6.86	7.09	7.28	7.43
$\text{H}6'$	7.01	6.90	7.62	7.33

To determine the structure of the more populated conformer of compounds **3** and **4**, NOE spectra were acquired. The spectra had to be recorded at a temperature ($-67\text{ }^{\circ}\text{C}$) in which the rotation of the benzoyl was calculated to have negligible rate, to avoid saturation transfer effects arising from the irradiated peak. Unfortunately, at this temperature the signals of the benzoyl moiety were heavily broadened by a third dynamic process, thus the NOE analysis was inapplicable. In order to perform this determination we calculated NMR chemical shifts of the two diastereomeric conformations for both compound **3** and **4**. The GIAO method was used at the B3LYP/6-311++G(2d,p)//B3LYP/631G(d) level and calculations for both products **3** and **4** are reported in Table 3 and Table 4, respectively.

For both compounds calculations suggested that the major isomer has the *anti* conformation. The experimental diastereomeric ratio of **3** is 55:45 *anti/syn* ($-22\text{ }^{\circ}\text{C}$ in $\text{C}_2\text{D}_2\text{Cl}_4$), whereas for **4** is more unbalanced, being 64:36 *anti/syn* ($-22\text{ }^{\circ}\text{C}$ in $\text{C}_2\text{D}_2\text{Cl}_4$). From DFT ground state optimization, in compound **3** the *syn* conformer was calculated to be slightly more stable than the *anti* conformer, in the case of **4** the *anti* conformational isomer was calculated as more stable than the *syn* conformational isomer, probably because of the larger steric hindrance of the isopropyl with respect to the ethyl group. This is therefore in agreement with the experimental trend.

As previously mentioned, in compound **4** below $-60\text{ }^{\circ}\text{C}$ the aromatic signals of the benzoyl moiety were heavily broadened by a third dynamic process. On lowering the temperature below $-80\text{ }^{\circ}\text{C}$, the signal of the *ortho* hydrogens of the phenyl-CO ring reached coalescence and eventually split at $-118\text{ }^{\circ}\text{C}$ into two separated sets of signals in a 50:50

ratio (sample in CDFCl₂). This third dynamic process has to be assigned to the restricted rotation of the phenyl ring around the C_{ipso}-CO bond. Due to the crowding of the aromatic region and to the large chemical shift spread, a complete line-shape simulation was not workable. For this reason compound **5** has been prepared, where the phenyl moiety was substituted with a 3,5-dimethylphenyl group. For this compound the barriers for the rotation of the *m*-isopropylphenyl ring and the benzoyl were found to be identical to those of compound **4** (19.2 kcal/mol and 14.3 kcal/mol respectively). On lowering the temperature below -80°C the two unbalance signals (63:37 at -22°C) of the two CH₃ of the 3,5-dimethylphenyl group, split in four separated peaks at -118°C. Line shape simulations yielded two different rotational barriers (9.6 ± 0.2 and 9.4 ± 0.2 kcal/mol)¹³, with the major distereoisomer (*anti*) having the higher rotational barrier. Experimental values of the energy barriers measured for all the studied compounds are reported in the following table.

Table 5. Summary of the *syn:anti* ratio and of the experimental energy barriers for 4-aryl rotation and 5-benzoyl rotation ^a

Compound	Experimental <i>syn:anti</i> ratio	4-aryl rotation	5-benzoyl rotation
1	-	-(17.1)	14.3 (15.1) ^b
2	-	-(17.5)	14.1 (14.8) ^b
3	44:56 (-22°C)	-(18.1) ^b	13.9 (14.9) ^b
4	36:64 (-22°C)	19.2 (18.0) ^b	14.3 (14.7) ^b
5	37:63 (-22°C)	19.2 (18.1) ^b	14.3 (14.9) ^b
6	38:62 (-35°C)	>35 (36.4) ^b	13.0 (14.2) ^b

^a in parentheses are reported the DFT calculated values at the B3LYP/6-31G(d) level, as thermal-corrected enthalpies. All values are in kcal/mol. ^b the reported energy value is that of the lower energy transition state.

Atropisomers separation and absolute configuration

The torsional barrier found for the *meta*-aryl substituted compounds **3** and **4** were very high, due to steric constraints. For this reason we prepared compound **6**, in which the aryl ring is substituted in *ortho* position, in order to provide a torsional barrier sufficiently high to allow a physical resolution of the atropisomeric pair. In particular compound **6** is substituted with a 1-naphthyl ring, because DFT calculation suggested a rotational barrier higher than 36 kcal/mol (see Table 5).

We achieved the separation of the atropisomers by means of enantioselective HPLC, with a amylose-based stationary phase (Chiralpack AD-H). Then by means of ECD the spectra of the separated compounds were recorded, showing opposite trace (Figure 31).

We determined the experimental racemization barrier by keeping an enantiopure sample of **6** at +120 °C for 24 hours in 1,1,2,2-tetrachloroethane. Subsequent HPLC analysis did not show the presence of the second atropisomer. Assuming the second atropisomer being present less than 1 %, the lower limit to racemization barrier is about 35 kcal/mol, in good agreement with the DFT calculated value. This value corresponds to a “class 3” atropisomer in LaPlante’s scheme^{8b,c}, with half life of more than 2×10^5 years at ambient temperature.

By means of dynamic NMR, the barrier for the benzoyl rotation has been determined, being 13.0 ± 0.2 kcal/mol, a value close to that determined for all other compounds **1 – 5**.

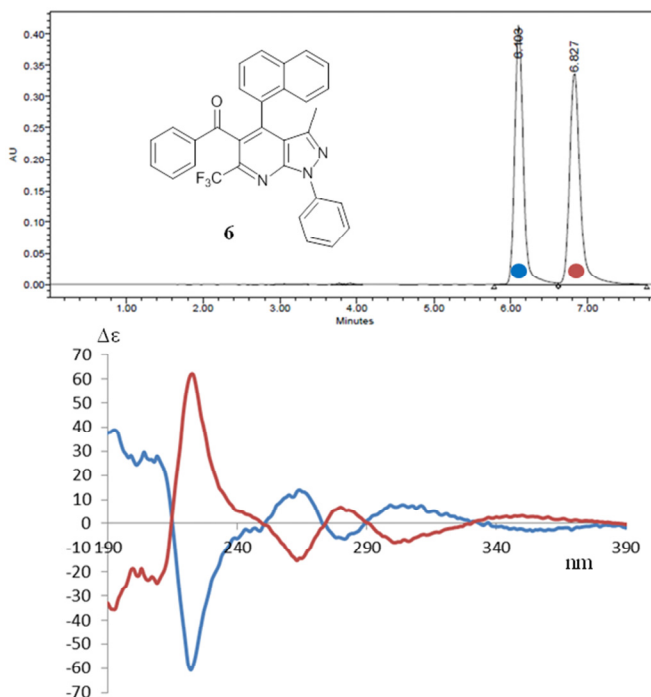


Figure 31. (Top) HPLC chromatogram of **6** on chiral stationary phase (Chiralpak AD-H). (Bottom) ECD spectra of the two atropisomers taken in acetonitrile solution.

Having in hand the two separated atropisomers of compound **6**, we pursued the determination of their absolute configuration. The reference method to assign the absolute configuration (AC) relies on the X-ray anomalous scattering¹⁴ that in the present case would require high-quality single crystals and the use of a Cu – K α X-ray source.^{15,16} Nevertheless, the determination of the AC of chiral molecules by chiro-optical techniques such as optical rotation (OR), vibrational circular dichroism (VCD), and electronic circular dichroism (ECD) has recently gained feasibility and reliability thanks to the development of the time-dependent density functional theory approach (TD-DFT).¹⁷

The experimental ECD spectrum of compound **6** shows a rather complex pattern. The typical features of the 1-naphthyl chromophore are found in the weak band at 285 nm and in the strong band at 225 nm.¹⁸ The ECD spectrum also shows two Cotton effects at 266 and 308 nm and a weak band at 355 nm. The two bands related to the two transitions of acetophenone are found at 266 and 195 nm.¹⁹

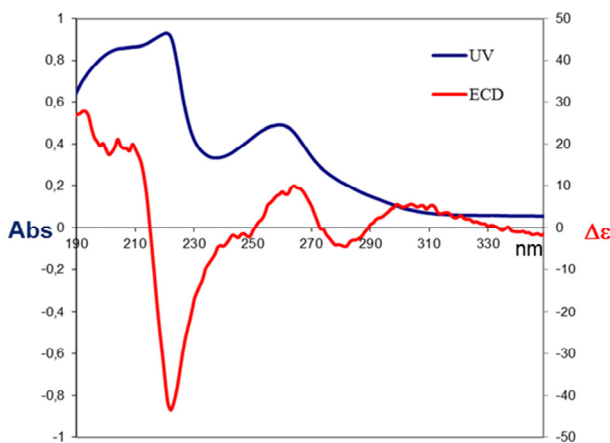


Figure 32. UV and ECD spectrum of the first eluted atropisomer of **6**.

For the simulation of the ECD spectrum the electronic excitation energies and rotational strengths were calculated for the two conformational diastereoisomers in the gas phase using the geometries optimized at the B3LYP/6-31G(d) level and using TD-DFT with four different functionals to explore whether different theoretical models provide different shapes of the simulated spectra. Simulations were performed by means of the functional: BH&HLYP,²⁰ M06-2X,²¹ ω B97XD,²² and CAM-B3LYP.²³ The simulated ECD spectra for the *anti* and *syn* conformers of the *M* atropisomer are very similar within the same conformation, but shown

early opposite trend for the two conformations. The averaged ECD spectrum will be therefore extremely sensitive to the population ratio.²⁴ Being the experimental ECD spectrum the weighted sum of the spectra of the diastereoisomers, the correct population ratio must be used to average the simulations. The ¹H NMR spectra taken at -30 °C in C₂D₂Cl₄ showed a ratio of 59:41 for the two conformational diastereoisomers.²⁵ Unfortunately the *syn:anti* attribution can't be gained by NOE spectra, being again thwarted by the slow rotation of the benzoyl moiety at the low temperatures. However, the X-ray structure of racemic **6** showed that the conformation present in the solid state was *anti*. In Figure 33 are reported the weighted ECD spectra and the resulting spectrum is in very good agreement with the experimental one of the second eluted atropisomer of compound **6**, to which *M* absolute configuration can be assigned.

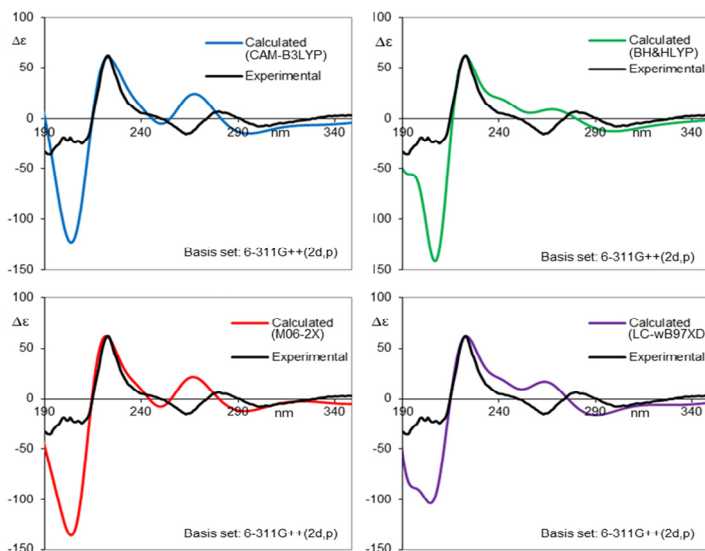


Figure 33. Colored lines: computed ECD spectra of the *M* atropisomer of **6** using different functionals and considering a 58:42

ratio of the two conformations (*anti/syn*). All the calculations employed the 6-311++G(2d,p) basis set. Black line: experimental ECD spectrum of the second eluted atropisomer of 6.

Conclusions

In this section we have analyzed the stereodynamic behavior of a series of 4-aryl-5-benzoyl-6-(trifluoromethyl)pyrazolo[3,4-*b*]pyridines. The restricted rotations of the aryl substituent in position 4 of the heteroaromatic ring and of the benzoyl group in position 5 generate conformational enantiomers or conformational diastereoisomers depending on the local symmetry of the aryl ring in position 4. The energy barriers for the rotation of the benzoyl group and for the aromatic ring were measured by dynamic NMR and rationalized by DFT calculations. In all the analyzed compounds the 4-aryl rotation was found to have a larger barrier than the benzoyl rotation, and its value was found to be quite large, despite the absence of any *ortho* substituent on the aromatic ring. At very low temperatures (i.e., < -80 °C), a third dynamic process due to rotation around the phenyl – CO bond was observed. When the 4-aryl ring was the 1-naphthyl (compound **6**), the arene – heterocyclic ring rotational barrier was larger than 35 kcal/mol, and the atropisomeric pair was resolved by means of enantioselective HPLC. Also in this case the restricted rotation of the benzoyl group yielded two conformational diastereoisomers detectable with dynamic NMR. Using the experimentally determined ratio of the two conformational diastereoisomers, the absolute configuration of the atropisomers was determined by simulating the electronic circular dichroism spectra using TD-DFT calculations. The synthesis and the chemistry of the pyrazolopyridine derivatives has attracted much attention in view of their importance as the core structure of numerous biologically active

84

compounds. However, they are not intrinsically chiral, and classical sp^3 stereocenters can be added only far away from the heterocycle. The availability and synthetic feasibility of thermally stable heteroaryl – aryl atropisomers could spread and enhance the biological activity of these compounds thanks to the newly added stereogenic moiety, directly connected to the pyrazolopyridine core.

References

¹ Gunasekaran, P.; Perumal, S.; Menéndez, J. C.; Mancinelli, M.; Ranieri, S.; Mazzanti, A. *J. Org. Chem.* **2014**, *79*, 11039 – 11050.

² a) Yu, G.; Mason, H. J.; Wu, X.; Wang, J.; Chong, S.; Dorough, G.; Henwood, A.; Pongrac, R.; Selinger, L.; He, B.; Normandin, D.; Adam, L.; Krupinski, J.; Macor, J. *J. Med. Chem.* **2001**, *44*, 1025 – 1027. b) Gunasekaran, P.; Prasanna, P.; Perumal, S. *Tetrahedron Lett.* **2014**, *55*, 329 – 332 and references cited therein.

³ a) As vasodilators: Straub, A.; Benet-Buckholtz, J.; Frode, R.; Kern, A.; Kohlsdorfer, C.; Schmitt, P.; Schwarz, T.; Siefert, H. M.; Stasch, J. P. *Bioorg. Med. Chem.* **2002**, *10*, 1711 – 1717. b) as cyclin kinase inhibitors: Huang, S.; Lin, R.; Yu, Y.; Lu, Y.; Connolly, P. J.; Chiu, G.; Li, S.; Emanuel, S. L.; Middleton, S. A. *Bioorg. Med. Chem. Lett.* **2007**, *17*, 1243 – 1245. c) as protein kinase inhibitors: Chiu, G.; Li, S.; Connolly, P. J.; Middleton, S. A.; Emanuel, S. L.; Huang, S.; Lin, R.; Lu, Y. (Janssen Pharmaceutica N.V., Belgium) *PCT Int. Appl.* WO 2006130673, **2006**.

⁴ Sagar, S. A.; Sisko, J. T.; Tucker, T. J.; Tynebor, R. M.; Su, D. S.; Anthony, N. J. (Merck & Co.) *U.S. Patent Appl.* US 2007021442, **2007**.

⁵ Boerrigter, G.; Burnett, J. C., Jr. *Cardiovasc. Drug Rev.* **2007**, *25*, 30 – 45.

⁶ Patel, J. B.; Malick, J. B.; Salama, A. I.; Goldberg, M. E. *Pharmacol, Biochem. Behav.* **1985**, *23*, 675 – 680.

⁷ a) Sanghvi, Y. S.; Larson, S. B.; Willis, R. C.; Robins, R. K.; Revankar, G. R. *J. Med. Chem.* **1989**, 32, 945 – 951. b) Schmidt, P.; Eichenberger, K.; Wilhelm, M. *Angew. Chem.* **1961**, 73, 15 – 22.

⁸ a) Clayden, J.; LaPlante, S. *Angew. Chem. Int. Ed.* **2009**, 48, 6398 – 6401. b) LaPlante, S. *ChemMedChem* **2011**, 6, 505 – 513. c) LaPlante, S. *J. Med. Chem.* **2011**, 54, 7005 – 7022. d) Zask, A.; Murphy, J.; Ellestad, G. A. *Chirality* **2013**, 25, 265 – 274.

⁹ For reviews, see: a) Hagmann, W. K. *J. Med. Chem.* **2008**, 51, 4359 – 4369. b) Purser, S.; Moore, P. R.; Swallow, S.; Gouverneur, V. *Chem. Soc. Rev.* **2008**, 37, 320 – 330. See also: c) Hiyama, T. *Organofluorine Compounds*; Springer: Berlin, 2000. d) *Fluorine in Bioorganic Chemistry*; Welch, J. T.; Eswarakrishnan, S., Eds.; Wiley: New York, **1991**.

¹⁰ Gunasekaran, P.; Indumathi, S.; Perumal, S. *RSC Adv.* **2013**, 3, 8318 – 8325.

¹¹ a) Testa, B. *Principles of organic stereochemistry*; M. Dekker: New York, **1979**, p 87. b) *IUPAC Compendium of Chemical Terminology*, 2nd ed. (the “Gold Book”); compiled by McNaught, A. D.; Wilkinson, A.; Blackwell Scientific Publications: Oxford, **1997**.

¹² a) Jennings, W. B. *Chem. Rev.* **1975**, 75, 307 – 322. b) Mislow, K.; Raban, M. *Top. Stereochem.* **1967**, 1, 1 – 38.

¹³ The indicated errors refer to the absolute errors due to the uncertainty in the temperature determination. However, the difference between the two barriers (0.2 kcal/mol) is realistic because the line-shape simulations are taken on the same spectrum, and the error due to the rate constant determination is below 0.05 kcal/mol.

¹⁴ Peerdeman, A. F.; Van Bommel, A. J.; Bijvoet, J. M. *Nature* **1951**, 168, 271 – 272.

¹⁵ The Cu-K α source is not available at the University of Bologna and enantiopure crystals couldn't be obtained.

-
- ¹⁶ Hoof, R. W. W.; Stravera, L. H.; Spek, A. L. *J. Appl. Crystallogr.* **2008**, 41, 96 – 103
- ¹⁷ For reviews, see a) Bringmann, G.; Bruhn, T.; Maksimenka, K.; Hemberger, Y. *Eur. J. Org. Chem.* **2009**, 2717 – 2727. b) Pescitelli, G.; Di Bari, L.; Berova, N. *Chem. Soc. Rev.* **2011**, 40, 4603 – 4625. c) Mazzanti, A.; Casarini, D. *WIREs Comput. Mol. Sci.* **2012**, 2, 613 – 641.
- ¹⁸ UV absorption and CD data for this chromophore can be found in: Rosini, C.; Spada, G. P.; Proni, G.; Masiero, S.; Scamuzzi, S. *J. Am. Chem. Soc.* **1997**, 109, 506 – 512.
- ¹⁹ Kimura, K.; Nagakura, S. *Theor. Chim. Acta* **1965**, 3, 164 – 173.
- ²⁰ In Gaussian 09 the BH&HLYP functional has the form: $0.5 * E_X^{HF} + 0.5 * E_X^{LSDA} + 0.5 * \Delta E_X^{Becke88} + E_C^{LYP}$.
- ²¹ Zhao, Y.; Truhlar, D. G. *Theor. Chem. Acc.* **2008**, 120, 215 – 241.
- ²² Chai, J.-D.; Head-Gordon, M. *Phys. Chem. Chem. Phys.* **2008**, 10, 6615 – 6620.
- ²³ Iikura, H.; Tsuneda, T.; Yanai, T.; Hirao, K. *J. Chem. Phys.* **2001**, 115, 3540 – 3544.
- ²⁴ Yanai, T.; Tew, D.; Handy, N. *Chem. Phys. Lett.* **2004**, 393, 51 – 54.
- ²⁵ The ratio was almost invariant when different solvents were used (61:39 in CD₃OD and 58:42 in CD₃CN).

Study of the intramolecular NO₂/CO interaction in solution¹

Weak chemical interactions play a key role in chemistry. They are effective in many biological systems and they can be employed to design supramolecular assemblies and scaffolds.² Recently, it was shown that noncovalent interactions can modulate the conformational preferences and stereoselectivity of some organocatalysts.³ A weak bond due to the electrostatic interaction between nitrogen and oxygen has been shown to be responsible for the stabilization of the crystal structure of *N,N*-dipicrylamine⁴. The intermolecular N–O interaction was one of the driving interactions for the self-assembly of *N*-oxalyl-2,4-dinitroanilide in the solid state.⁵ Through-space interactions were also observed in the solid state for a series of bipyridine *N*-oxides.⁶ Ab initio calculations had suggested that the energy involved in the N–O interaction was about 13 kJ/mol.⁷

The weak interaction between a nitro and a carbonyl group could compete with other weak interactions in the solid state, as well as in solution, in the stabilization of preferred molecular conformations, provided the correct geometries of the two acting partners are met.

In this section we studied chemical systems in which the following features are present:

- carbonyl and nitro group are linked to scaffolds that can move at a great amplitude without significant variation of the overall conformational energy
- biaryl systems in which the energy minima are quite flat
- they generate two different conformations that can be observed by dynamic-NMR spectroscopy

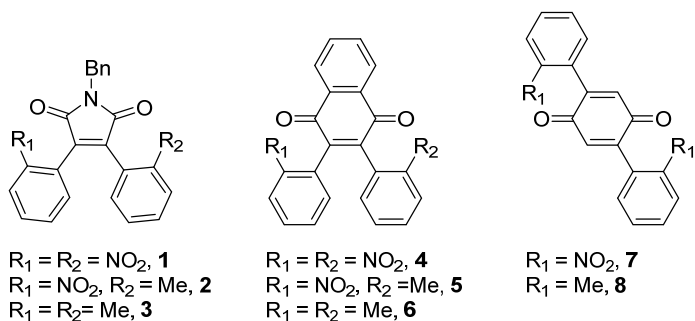


Figure 34. Structure of the compounds used in this study. (Bn = benzyl)

In order to perform these studies we synthesized compounds reported in Figure 34, in which the *ortho*-substituted aryl rings, carrying the nitro group, generate a rotational barrier that can be detected by dynamic-NMR, fulfilling the required features for us to study the intramolecular NO_2/CO interaction.

Bisarylmaleimides

In the previous work⁸ a series of 3,4 substituted benzyl maleimides have been prepared, bearing *ortho*-substituted aromatic groups which adopt tilted conformations relative to the planar scaffold. DFT computational studies and dynamic NMR spectroscopic data showed that the energies of the *syn* and *anti* conformers were very similar when aliphatic *ortho*-aryl substituents were employed. On the other hand, in the case of compound **1**, the *anti* conformer was more stable than the *syn* conformer by more than 4 kcal/mol, at the B3LYP/6-31G(d) level. This implies that in compound **1** only the *anti* conformer should be populated. From a steric point of view, the nitro group is very similar to methyl group⁹, thus steric considerations can't explain the large stabilization of the *anti* conformation.

Optimized structures showed that on each side of the maleimide ring an electrostatic interaction can take place between the electron-rich oxygen atom of the carbonyl group and the nitrogen atom of the nitro group. A second electrostatic interaction was present, with reverse polarity, between one of the oxygen atoms of the nitro group and the electron-poor carbon atom of the carbonyl group (Figure 35). Calculated distance between the oxygen atom of the carbonyl group and the nitrogen atom was very similar to that observed for *N*-oxalyldinitroanilide (2.85 Å)⁵. This interaction can take place in the *syn* conformer as well, but in this case only one can be effective: the second interaction would drive the opposite sides of the phenyl rings close to each other, generating a destabilizing steric clash. As a further investigation, compound **1** was crystallized from a solution of acetonitrile and the presence of only the *anti* conformer has been confirmed. Both nitro groups interact with the two carbonyl groups, in particular we see an electrostatic interaction of the electron-rich oxygen atom with the electron-poor nitrogen, as well as the interaction of one oxygen of the nitro group with the carbon atom of the carbonyl group. The N–O and O–C distances were very similar to those reported.⁴ The calculated skew angles of the two *o*-nitrophenyl rings were -57 °C, whereas the experimentally found angles were -49 °C and -55 °C.

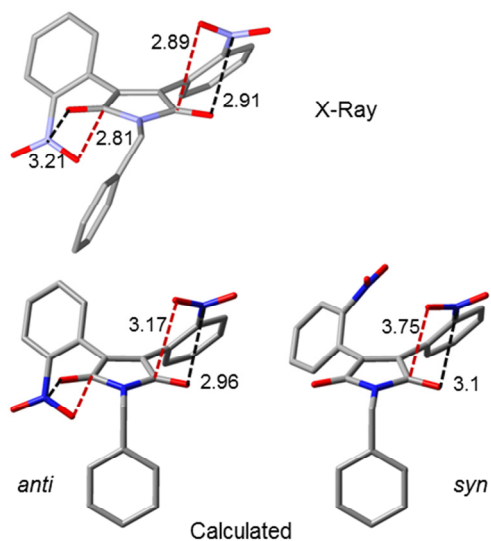


Figure 35. (Top) X-ray crystal structure of compound 1. (Bottom) calculated structures of *anti* and *syn* conformers at ω B97XD/6-311++G(2d,p) level. Distances in Å.

To experimentally observe this interaction in solution we acquired variable-temperature NMR spectra. As shown in Figure 36, a sample of compound **1** in CDCl_3 was cooled to $-24\text{ }^\circ\text{C}$, the signal of the benzylic CH_2 group split in an AB system, corresponding to the *anti* conformer (C_2 symmetry). As previously predicted by the ground state energy calculated by DFT, no signal of the *syn* conformer was present. So the rotational energy barrier corresponds to the racemization and its experimental value was derived by line shape simulation, as 14.2 ± 0.2 kcal/mol, matching very well the one found by DFT calculation (14.3 kcal/mol). In order to check whether there was a solvent effect, experiments with CD_2Cl_2 and CD_3OD as solvents have been done and the same result has been achieved.

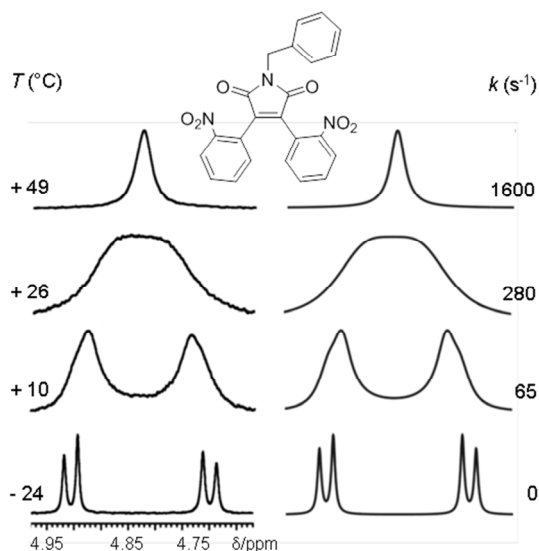


Figure 36. Variable-temperature ^1H NMR spectra of 1 (600 MHz in CDCl_3). (Left) Experimental spectra. (Right) Simulated spectra with the relative rate constants.

Because of the absence of the *syn* conformer we obtained suitable information about the stabilization energy involved in the electrostatic interactions. If a 99.5:0.5 ratio at $-24\text{ }^\circ\text{C}$ is taken into account,¹⁰ the corresponding energy difference (ΔG°) is 2.6 kcal/mol. This value is the lower limit for the stabilization of the *anti* conformation because the *syn* conformer was not detectable at all. As one NO_2/CO interaction is available in both conformations, the value should be considered a direct measurement of the strength of the electrostatic interaction. The value matches the DFT-predicted value (2.6 ± 4.1 kcal/mol).

From a geometric point of view in the ground state the electrostatic NO_2/CO interaction shrinks the angle between the maleimide plane and the *o*-nitrophenyl nearer the transition state geometry. In the transition state the motion of one *o*-nitrophenyl forces the second ring to become

perpendicular with the maleimide plane, to minimize the steric interaction between the two rings. For this reason the observed energy barrier is the result of two contributions:

- the steric clash between the rotating ring and the maleimide plane
- partial loss of the NO₂/CO stabilization for the second ring.

Naphthoquinones and benzoquinones.

We prepared more compounds in which we can perform a quantitative evaluation of the energetic contribution of the NO₂/CO interaction. For example we studied compound **2**, that bears one *o*-nitrophenyl and one *o*-tolyl ring. Whereas the nitro group can be involved in the NO₂/CO interaction, the disposition of the *o*-tolyl ring is due only to steric factors. Low temperature ¹H-NMR spectrum showed that both conformations were populated, with *syn/anti* 71:29 and NOE spectra showed that *syn* conformer was the most populated. ¹H methyl signal is split only when the two conformers are generated, thus it indicates the smaller of the two rotational barriers. On the other hand, the CH₂ group is a chirality probe that indicates the formation of the enantiomeric pair generated by the frozen rotation of the ring with the higher rotational barrier. The simulation of the methyl signal provided a value of 12.6 ± 0.2 kcal/mol for the *syn/anti* interconversion and the energy barrier derived from the simulation of the benzylic CH₂ group was 12.9 ± 0.2 kcal/mol. This values are very similar, confirming that methyl and nitro group are isosteric and a reliable assignment of the two measured barriers is impossible.^{9,11}

Both barriers are significantly lower than that of compound **1**, thus confirming a substantial stabilization of the ground-state in the case of **1**. Similarly, we found for compound **3** a *syn/anti* ratio of 55:45, equivalent

94

to $\Delta G^\circ = 0.09$ kcal/mol. All results of the calculations for compounds **1** – **3** are reported in Table 6.

Table 6. Summary of calculations.

Compd.	Level of calculation	ΔH° ^a	<i>anti/syn</i>
1	B3LYP/6-31G(d)	4.1	>99.5:0.5
1	B3LYP/def2-TZVP	4.0	
1	B97D/def2-TZVP	2.6	
1	ω B97XD/6-311++G(2d,p)	3.0	
1	ω B97XD/def2-TZVP	3.3	
2	ω B97XD/6-311++G(2d,p)	-0.6 ^b	21:79 ^c
3	ω B97XD/6-311++G(2d,p)	-0.2 ^b	45:55 ^d

^a All calculated energies are ZPE-corrected enthalpies, reported in kcal/mol.

^b A negative value means that the *syn* conformation is calculated to be more stable than the *anti* conformation. ^c The ratio was determined from NOE NMR spectrum. ^d Ref. [8].

Having in hands the experimental energy barriers for **1** - **3**, the evaluation of the electrostatic interaction can be done considering these compounds as components of a double-mutant-cycle (DMC).¹² As reported in Scheme 10, compounds **2** and **3** are respectively the single and double mutant, with respect to compound **1**. By using this approach we calculated that the stabilization due to the electrostatic interaction corresponds to 3.35 kcal/mol.

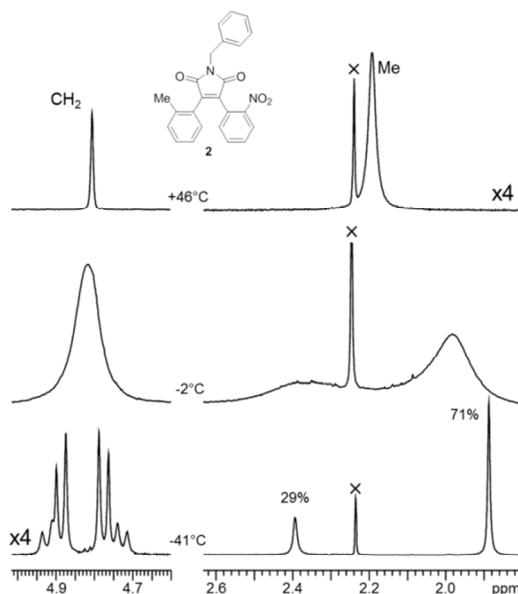
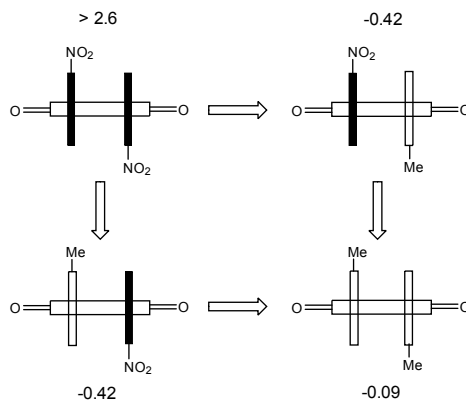


Figure 37. Variable temperature ^1H spectra of compound 2 (600 MHz in $\text{C}_2\text{D}_2\text{Cl}_4$). (Left) Signal of the benzylic CH_2 . (Right) Signal of the methyl group. The signal marked with \times is an impurity of the solvent.



Scheme 10. DMC cycle for compounds 1 – 3. Indicated values (in kcal/mol) are the energy differences (ΔG°) between *anti* and *syn* conformers as measured by NMR spectroscopy at -40°C . Negative values indicate that the *syn* conformation is more stable than the *anti*.

To check whether the NO₂/CO interaction was restricted to the geometric constraints of the pentatomic scaffold of maleimide, we prepared compounds **4** – **6** (Figure 34) containing the 1,4-naphthoquinone scaffold. Within this series, the *anti* conformer of compound **4** should gain stabilization from two NO₂/CO interactions, whereas in compounds **5** and **6** both conformers should be populated. DFT calculations at the B3LYP/def2-TZVP, ω B97XD/def2-TZVP, and ω B97XD/6-311++G(2d,p) levels, reported in Table 7 suggested that in the case of compound **4**, the *anti* conformer was more stable than the *syn* conformer by at least 4.0 kcal/mol, in fact the ¹H NMR spectrum of **4** at +25 °C showed a single set of signals. The calculated *o*-nitrophenyl rotational energy barrier was determined to be 22.7 kcal/mol.

Table 7. Summary of calculations.

Comp.	Level of calculation	ΔH^{oa}	<i>anti/syn</i>
4	B3LYP/def2-TZVP	4.6	>99.5:0.5
4	ω B97XD/6-311++G(2d,p)	4.0	
4	ω B97D/def2-TZVP	4.0	
5	ω B97XD/6-311++G(2d,p)	1.1	68:32 ^b
6	ω B97XD/6-311++G(2d,p)	0.4	59:41 ^b

^a All calculated energies are ZPE-corrected enthalpies, reported in kcal/mol.

^b The ratio was determined from NOE NMR spectrum.

For compounds **5** and **6**, the two conformers were calculated to be very close in energy and their ¹H NMR spectra revealed the presence of both the conformers in a 68:32 and 59:41 ratio, respectively. The *anti* conformation was confirmed to be the more abundant on the basis of NOE spectra. The energy barrier for the *o*-nitrophenyl rotation were calculated in compound **5** to be 22.3 kcal/mol and for the *o*-tolyl rotation

in **6** resulted 21.0 kcal/mol. As they are inaccessible for the dynamic NMR spectroscopic technique, the energy barriers for compounds **5** and **6** were determined by ^1D EXSY, which yielded barriers of 21.0 ± 0.2 and 20.7 ± 0.2 kcal/mol, respectively.

In the case of **4**, the ambient-temperature NMR spectrum should display the presence of a second conformation, if it were populated. The absence of a suitable chirality probe did not allow the determination of whether the single conformer observed corresponded to the *anti* or to the *syn* conformer. X-ray diffraction showed that only the *anti* conformer was present in the solid state, with NO_2/CO distances and geometries very similar to those in compound **1** (see Figure 38).

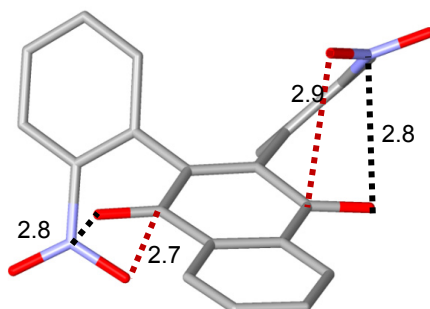


Figure 38. X-ray crystal structure of compound 4. Distances in Å.

Compound **4** was analyzed by enantioselective HPLC, which showed two peaks undergoing dynamic exchange at $+25$ °C. At 0 °C, the two chromatographic peaks were well-resolved and electronic circular dichroism (ECD) at 280 nm showed that they had opposite sign (Figure 39), confirming the presence of only the enantiomeric pair of the *anti* conformer.

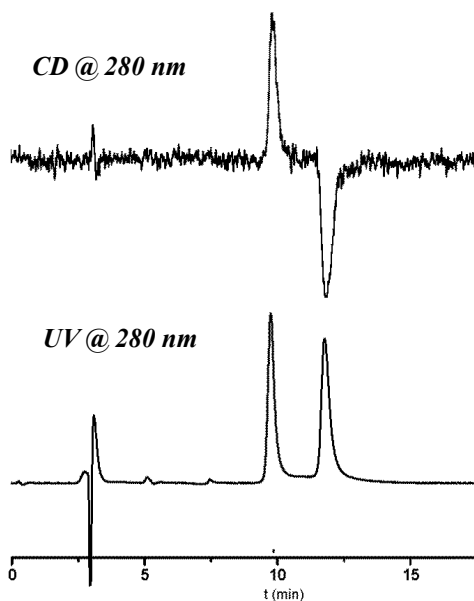


Figure 39. Chromatograms of compound 4 on an enantioselective (*R,R*)-Whelk-O1 HPLC column, recorded at 0 °C. (Bottom) UV detector. (Top) ECD detector at 280 nm.

By means of dynamic HPLC we evaluated the racemization barrier as 20.5 ± 0.3 kcal/mol.¹³ Applying the same approach used for **1** to the case of compound **4**, we determined that the stabilization energy of the *anti* conformation has to be larger than 2.6 kcal/mol. The application of the DMC approach (compounds **4** – **6**) then yielded a lower limit of 1.9 kcal/mol for the stabilization energy.

As a final attempt to experimentally measure the electrostatic interaction without any interference caused by the proximity of the aryl rings, we prepared compounds **7** and **8**. The 1,4-benzoquinone scaffold of compound **7** bears two *o*-nitrophenyl rings in the 2,5-positions and their rotations are completely independent, but two NO₂/CO interactions can be effective and the ground state of both the *syn* and *anti* conformers can be stabilized in the same way by the electrostatic interaction. Compound

8 shares the same situation, but the rotational barrier is now driven only by steric effects. As the nitro and methyl moieties are isosteric, the barrier for rotation is mainly due to the stabilization of the ground state. The calculated values are reported in Table 8.

Table 8. Summary of calculations.

Compd.	Level of calculation	ΔH° ^a	<i>anti/syn</i>
7	ω B97XD/6-311++G(2d,p)	0.9	67:33 ^b
8	ω B97XD/6-311++G(2d,p)	0.7	58:42 ^b

^a All calculated energies are ZPE-corrected enthalpies, reported in kcal/mol.

^b The ratio was assigned on the basis of calculations.

The rotational energy difference for the *syn/anti* interconversion between **7** and **8** has to be assigned to the stabilization due to a single NO₂/CO interaction. At -65 °C, the ¹H NMR spectrum of **7** showed that both conformations were populated in a 67:33 ratio, whereas the spectrum of **8** at -118 °C showed a 58:42 ratio. The energy barrier for the *syn/anti* interconversion of **7** was found to be 12.0 ± 0.2 kcal/mol and the barrier for **8** was found to be 9.1 ± 0.2 kcal/mol. Thus, the stabilization due to a single NO₂/CO interaction was evaluated to be 2.9 kcal/mol, in agreement with the previous considerations.

Conclusions

We have documented the observation of the weak NO₂/CO electrostatic interaction in solution. In order to evaluate the entity of the interaction we prepared suitable compounds, with maleimide, naphotquinone and benzoquinone scaffolds. The energetic contributions were studied by means of DFT calculations, dynamic NMR spectroscopy and by the use of the DMC approach. The stabilization due to a single NO₂/CO interaction was evaluated to be from 2.6 to 3.35 kcal/mol.

References

- ¹ Chiarucci, M.; Ciogli, A.; Mancinelli, M.; Ranieri, S.; Mazzanti, A. *Angew. Chem. Int. Ed.* **2014**, 53, 5405 – 5409.
- ² Ward, M. D.; Raithby, P. R. *Chem. Soc. Rev.* **2013**, 42, 1619 – 1636, and references therein.
- ³ Holland, M. C.; Paul, S.; Schweizer, W. B.; Bergander, K.; Mück - Lichtenfeld, C.; Lakhdar, S.; Mayr, H.; Gilmour, R. *Angew. Chem. Int. Ed.* **2013**, 52, 7967 – 7971.
- ⁴ Yin, Z.; Jiang, L.; Hea, J.; Cheng, J. - P. *Chem. Commun.* **2003**, 2326 – 2327.
- ⁵ a) Steiner, T. *Chem. Commun.* **1997**, 727 – 734. b) Desiraju, G. R.; Steiner, T.; *The Hydrogen Bond in Structural Chemistry and Biology*, Oxford University Press, Oxford, **1999**.
- ⁶ O' Learly, J.; Wallis, J. D. *CrystEngComm* **2007**, 9, 941 – 950.
- ⁷ Platts, J. A.; Howard, S. T.; Wozniak, K.; *Chem. Phys. Lett.* **1995**, 232, 479 – 485.
- ⁸ Ambrogi, M.; Ciogli, A.; Mancinelli, M.; Ranieri, S.; Mazzanti, A. *J. Org. Chem.*, **2013**, 78, 3709 – 3719.
- ⁹ Lunazzi, L.; Mancinelli, M.; Mazzanti, A.; Lepri, S.; Ruzziconi, R.; Schlosser, M. *Org. Biomol. Chem.* **2012**, 10, 1847 – 1855.
- ¹⁰ Lunazzi, L.; Mazzanti, A.; Casarini, D.; De Lucchi, O.; Fabris, F. *J. Org. Chem.* **2000**, 65, 883 – 888.
- ¹¹ Ruzziconi, R.; Spizzichino, S.; Lunazzi, L.; Mazzanti, A.; Schlosser, M. *Chem. Eur. J.* **2009**, 15, 2645 – 2652.
- ¹² a) Yang, L.; Adam, C.; Nichol, G. S.; Cockroft, S. L. *Nat. Chem.* **2013**, 5, 1006 – 1010. b) Cockroft, S. L.; Hunter, C. A. *Chem. Soc. Rev.* **2007**, 36, 172 – 188.
- ¹³ a) Wolf, C. *Chem. Soc. Rev.* **2005**, 34, 595 – 608. b) D'Acquarica, I.; Gasparrini, F.; Pierini, M.; Villani, C.; Zappia, G. *J. Sep. Sci.* **2006**, 29, 1508 – 1516. c) Piron, F.; Vanthuynne, N.; Joulin, B.; Naubron, J. -V.; Cismaş, C.; Terec, A.; Varga, R. A.; Roussel, C.; Roncali, J.; Grosu, I. *J. Org. Chem.* **2009**, 74, 9062 – 9070.

Long range bonding/non-bonding interactions: study on 2-arylpyridines

All standard criteria based on the steric effects suggest that a methoxymethyl group should be bigger than a methyl group. The Charton's "effective" epsilon parameter,¹ derived from the Van der Waals radii, puts the following scale: methyl ($v = 0.52$), ethyl ($v = 0.56$), methoxymethyl ($v = 0.63$), propyl ($v = 0.68$). Wintestein's A values² ranks methoxymethyl ($A = 1.72$) at the same level of methyl ($A = 1.74$). The B scale³, based on the torsional angle of biphenyls with one *ortho* substituent R , puts methoxymethyl ($B = 8.6$) *ex aequo* with ethyl ($B = 8.7$), on top of methyl ($B = 7.4$).

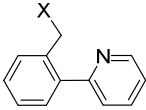
On the other hand this order of bulkiness has been found reversed, switching from 2-alkylbiphenyls to the 2-aza-analogous. A library of 2-(2'-alkylphenyl)pyridines⁴ has been prepared, reported in Table 9, finding the torsional barriers smaller up to 4 kcal/mol difference, because of the compressibility of the nitrogen lone pair.

The CH₂ signal of 2-(2-ethylphenyl)pyridine **1** did show decoalescence below -160°C ($\Delta G^\ddagger = 5.9$ kcal/mol), but in the case of 2-(*o*-tolyl)pyridine⁵ **2** and 2-(2-(methoxymethyl)phenyl)pyridine **3** neither decoalescence, nor line-broadening of the diastereotopic signals was observed at temperatures as low as -173 °C (100 K). This means the barriers were too small to allow an experimental determination by dynamic NMR measurements.⁶ These barriers were then evaluated by quantum chemical calculation. The geometries of the stationary points on the aryl-aryl rotation pathway of **1** - **3** were optimized at the B3LYP/6-31+G(d) and ω B97XD/6-31+G(d) levels of theory.

In the Ground State the pyridine ring and the 2-substituted aryl adopt a skewed disposition in order to minimize the steric hindrance. In the Transition State the rings adopt a coplanar disposition and all optimized TS showed that the lower energy transition state corresponds to the crossing of the CH₂-X group on the pyridine nitrogen (the alternative TS is higher in energy because of the steric hindrance due to the hydrogen in position 3 of pyridine).⁷

Both theoretical models suggested the energy barrier for **3** (X = OMe) was smaller than that of **1** and **2**. The calculated barrier for compound **4**, bearing the NMe₂ moiety, was found to be in the middle. The trend of calculations was then confirmed by the experimental barrier found, being 4.8 kcal/mol (coalescence found at -140 °C). This outcome could be due to a wrong estimation of the contribution due to the pyridine lone pair in the transition state.⁸ For this reason we calculated the single-point energies at the CCSD(T)/6-31+G(d)//ωB97XD/6-31+G(d) level.

Table 9. Experimental and calculated torsional barriers for arylpyridines. Calculations at the CCSD(T)/6-31+G(d)//ωB97XD/6-31+G(d) level.^a

		PlanarTS	Skewed TS	Exp. value
1	X = Me	8.4	6.2	5.9 ^b
2	X = H	5.9 ^c	5.9 ^c	-
3	X = OMe	4.9	6.7	-
4	X = NMe ₂	8.5	8.3	4.8
5^d	X = F	2.2	5.1	-

^aAll values are in kcal/mol. ^b Ref. [4]. ^c For this compound there is only one TS. ^d This compound has not been prepared, but a theoretical evaluation of the barrier has been performed.

The value suggested for the rotational barrier of 2-(2-ethylphenyl)pyridine **1** (6.2 kcal/mol) confirmed the reliability of these calculations. Nevertheless, at the CCSD(T) level of theory the activation energy for aryl-aryl rotation of **3** was again found to be smaller than that of **1** and **2**.

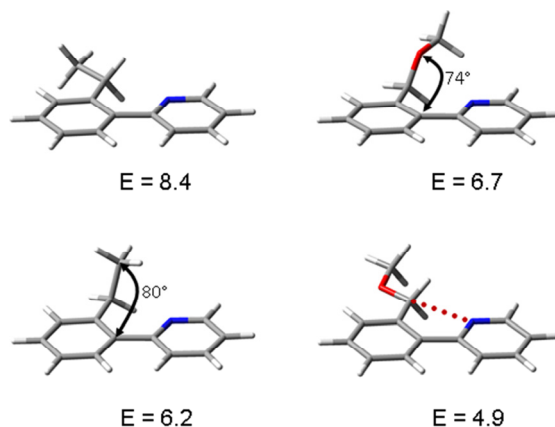
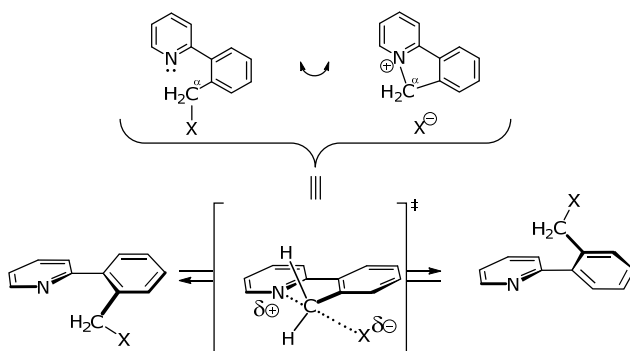


Figure 40. The two available transition states for aryl-aryl rotation of compounds **1** and **3**. Energies (in kcal/mol) were calculated at the CCSD(T)/6-31+G(d)// ω B97XD/6-31+G(d) level and they are relative to the ground states.

A close examination of the transition state geometries, as reported in Figure 40, showed that the conformation assumed by the ethyl group in the TS is substantially different from that of methoxymethyl. In the first the methyl group has a dihedral angle of 80° (Me-CH₂-C₂-C₁) with the phenyl plane, whereas the same angle is exactly 180° for the CH₂OMe group (O-CH₂-C₂-C₁ angle). When the alternative TS (i.e. Me at 180° and OMe at \approx 74°) were calculated, their energy were higher than the previous ones by 2.2 and 1.8 kcal/mol.

The energy mismatch between the planar and the skewed transition states in compounds **1** and **3** can be explained considering the stabilizing interaction due to the lone pair of the pyridine nitrogen. In fact, provided

the correct geometry, the nitrogen may share its lone pair with an electron deficient center in its closeness. In analogy with the anomeric effect⁹ and neighboring group participations¹⁰ this assistance becomes effective if the nitrogen donor and the acceptor site are part of germinal or vicinal bonding patterns. What makes unique the situation met with α -heterosubstituted 2-arylpiperidines is the distance between the nitrogen atom and the heterosubstituted α -carbon: the two centers are separated by four interposed bonds and no conjugative electron transmission chain is available. Moreover, the amplitude of the barrier-lowering donor-acceptor interaction is modulated by the nature of the heteroelement. In this way the long-range resonance interaction manifests itself as an adjustable blend of bonding (**A**) and nonbonding (**B**) limiting structures. For reasons of proximity, only the coplanar transition state of the torsional motion can benefit from this electron-density leveling interaction.



Scheme 11. Donor-acceptor interaction between pyridine nitrogen and the sp^3 carbon. In the transition state the coplanar disposition of the $C\alpha$ resembles a S_N2 type reaction.

The resonance extending from the pyridine nitrogen through the benzylic α -carbon to the heterosubstituent X is accompanied by a respectable gain

of energy. If we consider that all 2'-CH₂X substituents exert the same steric hindrance, the non-classical long-range interaction lowers the torsional barriers at an extent corresponding to the stabilization of the transition state, where this interaction can be effective. This trend was confirmed with the calculation of the energy barrier to rotation of 2-(*o*-fluoromethylphenyl)-pyridine **5**, where the calculated barrier was well lower than that of **3** and **4** (Table 9).

Within this framework it can be discussed also the behavior of the compound bearing a 2'-CH₂Br group. The reaction of 2-bromobenzylbromide with 2-pyridineboronic acid led to the prompt cyclization to 6*H*-pyrido[2,1-*a*]isoindol-5-ium bromide. The same result was found also when (2-(bromomethyl)phenyl)boronic acid was reacted with 2-bromopyridine, or when 2-(2-(hydroxymethyl)phenyl)-pyridine was treated in the Appel conditions¹¹ with CBr₄. The same results were obtained when using the 2' CH₂Cl group. These outcomes are in agreement with a strong interaction of the pyridine lone pair with the 2' carbon, leading to prompt cyclization when a good leaving group such as chloride or bromine is present.

From an alternative point of view, this interaction could also be rationalized as a pre-transition state complex for the S_N2 reaction, where the correct approach of the nucleophilic lone pair of the nitrogen can be achieved only in the TS planar geometry and the X substituent acts as a "leaving group" (see Scheme 11).

To further proof the validity of the CCSD(T) computational results, we prepared a series of compounds manageable to the dynamic NMR technique, reported in Figure 41. Compounds **6** – **8** bear two methyl groups in 3 and 5 position of the pyridine ring, compounds **9** and **10**, one

methyl in position 3 and compounds **11** - **14** bear two ethyl groups in position 3 and 5, to make the torsional barrier more hindered, without interfering with the electronic interaction of our interest.

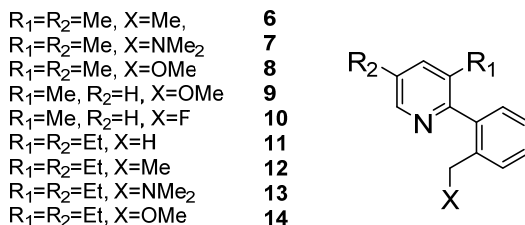


Figure 41. List of prepared pyridine type compounds.

For convenience of synthesis, the model compounds **6** – **8** were prepared by a Ziegler-type addition¹² of 2-ethylphenyllithium, [2-(dimethylamino)methyl]-phenyllithium and 2-(methoxymethyl) phenyllithium¹³ onto 3,5-dimethylpyridine followed by spontaneous lithium hydride elimination at ambient temperature. Compounds **9** - **10** were obtained by Suzuki-Miyaura cross coupling between 2-bromo-3-methylpyridine and suitable 2'-substituted phenylboronic acids. 2',3,5-Trimethyl-2-phenylpyridine lacks diastereotopic nuclei and is hence unsuitable for dynamic NMR spectroscopy. To remedy this shortcoming another set of model compounds (**11** – **14**) was designed and prepared by adding the suitable aryllithium onto the 2-position of 3,5-diethylpyridine and to rely again on thermal rearomatization.

As proven by the identity, within the experimental error, of the rotational barriers of compounds **8** and **9**, the methyl in the 5 position of pyridine does not influence the torsional barrier by inductive contribution in the TS geometry. The torsional barriers of the model compounds, as determined by line shape analysis of NMR spectra recorded at variable temperature (example in Figure 42), convey an unequivocal message:

electronegative substituents (N, O, F) lower the activation energy for the rotation about the 2-pyridyl–aryl axis substantially (Table 10).

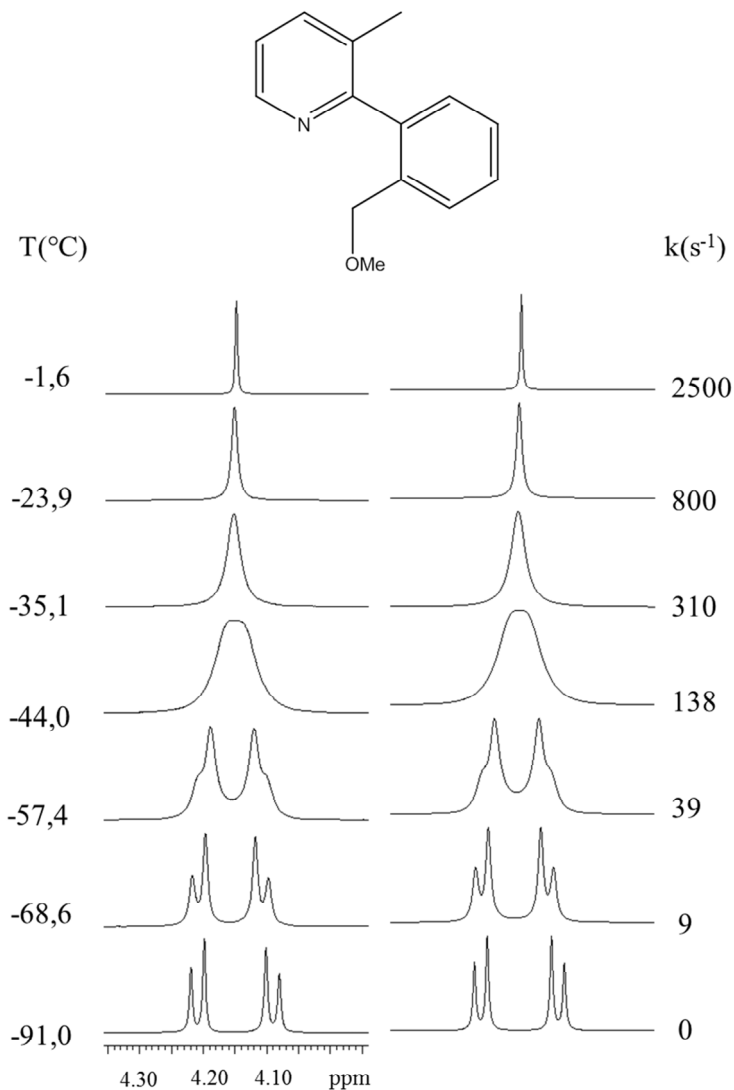


Figure 42. (Left) Temperature dependence of the ¹H benzylic CH₂ signal of compound 9 (600 MHz in CD₃CN). (Right) Line shape simulation obtained with the rate constants reported.

Table 10. Experimental and calculated torsional barriers.
Calculations at the CCSD(T)/6-31+G(d)// ω B97XD/6-31G(d) level.

Compound	X	Exp. Barrier	Calcd.
6	Me	13.1	13.1
7	NMe ₂	12.8	15.0
8	OMe	11.1	-
9	OMe	10.9	14.2
10	F	8.8	10.5
11	H	13.7	-
12	Me	14.4	-
13	NMe ₂	14.7	-
14	OMe	12.6	-

The key role played by the pyridine lone pair in the stabilization of the coplanar transition state can be confirmed by preparing the analogous biphenyls **15** – **18** (Figure 43) where the methoxy group was installed in the 2' position of phenyl to tune the rotational barriers to values similar to that of compounds **6** – **14**. In this series of compound the oxygen lone pairs does not influence the rotational barrier because the preferred transition state is that with the CH₂X group *anti* to the OMe group.

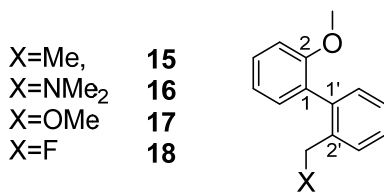


Figure 43. List of prepared biphenyl compounds.

DFT calculations suggested that in this series of compounds the rotational barrier were very similar on varying the X substituent. Between the two feasible TS, the preferred one corresponds to a C2-C1-C1'-C2' dihedral angle close to 180° to reduce the steric clash between the methoxy and

CH₂X. Within this series of compounds, the preferred conformation of the CH₂X group in the best transition state was always the skewed one. The experimental rotational barriers of these biphenyls were indeed found to be clustered in a very small range (less than 1 kcal/mol, see Table 11), thus confirming that all the CH₂-X groups have almost identical steric barriers.

Table 11. Experimental and Calculated Torsional Barriers. Calculations at the CCSD(T)/6-31+G(d)// ω B97XD/6-31G(d) level.

Compound	X	Exp. Barrier	Calcd.
14	Me	15.9	-
15	NMe ₂	15.5	-
16	OMe	15.1	-
17	F	15.1	-

The concept of long-range resonance interactions opens new perspectives. For example, it will be intriguing to compare the loosening of carbon–heteroatom bonds as experienced in the model compounds with Mayr's nucleofugality parameters.¹⁴

References

- ¹ Charton, M. *Topics Curr. Chem.* **1983**, 114, 57 – 91.
- ² a) Winstein, S.; Holness, N. J. *J. Am. Chem. Soc.* **1955**, 77, 5562 – 5578. b) Hirsch, J. A. *Top. Stereochem.* **1967**, 1, 199 – 222. c) Eliel, E. L.; Wilen, S. H. *Stereochemistry of Organic Compounds*, Wiley: New York, **1994**, pp 690 – 700. d) Kleinpeter, E.; Taddei, F. *Chem. Eur. J.* **2003**, 9, 1360 – 1368.
- ³ a) Ruzziconi, R.; Spizzichino, S.; Lunazzi, L.; Mazzanti, A.; Schlosser, M. *Chem. Eur. J.* **2009**, 15, 2645 – 2652. b) Lunazzi, L.; Mancinelli, M.; Mazzanti, A.; Lepri, S.; Ruzziconi, R.; Schlosser, M. *Org. Biomol. Chem.* **2012**, 10, 1847 – 1855.

⁴ Mazzanti, A.; Lunazzi, L.; Lepri, S.; Ruzziconi, R.; Schlosser, M. *Eur. J. Org. Chem.* **2011**, 33, 6725 – 6731.

⁵ A diastereotopic probe had been installed on the 4-position of pyridine.

⁶ In principle also a small chemical shift difference between the diastereotopic signals could prevent the detection of this energy barrier, although a large difference in chemical shift spread happens between the ethyl and methyl groups.

⁷ For a discussion about the geometries of the available ground and transition states in biaryl compounds see: Lunazzi, L.; Mazzanti, A.; Minzoni, M.; Anderson, J. E. *J. Org. Chem.* **2006**, 71, 5474 – 5481.

⁸ Dahlgren, M.K.; Schyman, P.; Tirado-Rives, J.; Jorgensen, W. L. *J. Chem. Inf. Model.*, **2013**, 53, 1191 – 1199, and references cited therein.

⁹ a) Eliel, E. L. *Angew. Chem. Int. Ed.* **1972**, 11, 739 – 750. b) Mo, Y. *Nature Chem.* **2010**, 2, 666 – 671. c) Bauerfeldt, G. F.; Cardozo, M.; Pereira, M.S.; da Silva, C.O. *Org. Biomol. Chem.* **2013**, 11, 299 – 308.

¹⁰ a) Yamada, K.; Sakata, S.; Yoshimura, Y. *J. Org. Chem.* **1998**, 63, 6891 – 6899. b) Cram, D. J. *J. Am. Chem. Soc.* **1952**, 74, 2129 – 2137. c) Winstein, S.; Lucas, H. J. *J. Am. Chem. Soc.* **1939**, 61, 1576 – 1581.

¹¹ a) Appel, R. *Angew. Chem. Int. Ed.* **1975**, 14, 801 – 811. b) Denton, R. M.; Ana, J.; Adenirana, B. *Chem. Commun.* **2010**, 46, 3025 – 3027.

¹² a) Ziegler, K.; Zeiser, K. *Ber. Dtsch. Chem. Ges.* **1930**, 63, 1847 – 1851. b) Ziegler, K.; Zeiser, K. *Justus Liebigs Ann. Chem.* **1931**, 485, 174 – 192.

¹³ Reich, H. J.; Goldenberg, W. S.; Sanders, A. W.; Jantzi, K. L.; Tzschucke, C. C. *J. Am. Chem. Soc.* **2003**, 125, 3509 – 3521.

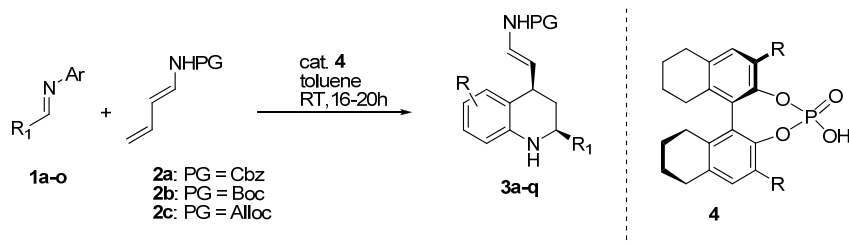
¹⁴ a) Denegri, B.; Minegishi, S.; Kronja, O.; Mayr, H. *Angew. Chem. Int. Ed.* **2004**, 43, 2302 – 2305. b) Schaller, H. F.; Tishkov, A. A.; Feng, X.; Mayr, H. *J. Am. Chem. Soc.* **2008**, 130, 3012 – 3022.

Application of conformational analysis to the absolute configuration determination

Absolute configuration of substituted 1,2,3,4-tetrahydroquinolines¹

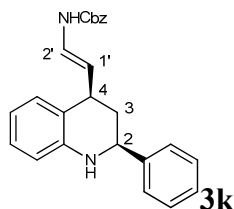
The 1,2,3,4-tetrahydroquinoline skeleton is the core of a variety of biologically active compounds (natural and synthetic), making it a key structural element in medicinal chemistry.² Among the different methods for the preparation of these compounds, the inverse electron demand aza Diels–Alder reaction between olefins and *N*-aryl imines (Povarov reaction)³ is one of the most efficient, versatile and atom-economical. Recently, the catalytic asymmetric version of this reaction has gained great progress.⁴ Bernardi and co-workers, taking advantage of their experience in chiral phosphoric acid catalyzed cycloaddition reactions,^{4d,5} focused their work in developing the enantioselective vinylogous Povarov reaction, known that the non-enantioselective counterpart has been reported.⁶

The reaction has been developed from enecarbamantes **2**, and first screening of reaction conditions lead to the choice of **4** as catalyst, operating at room temperature with toluene as solvent. (See Scheme 12) Then a broad scope for the reaction has been developed, with great yields and enantioselectivities.



Scheme 12. Vinylogous Povarov reaction.

Compound **3k** was selected as representative compound for the determination of the relative and absolute configuration by a combination of conformational analysis and theoretical simulations of chiro-optical spectra.



The relative stereochemistry was determined by means of NMR spectroscopy. Full assignment of the ^1H and ^{13}C spectra was preliminarily achieved by bi-dimensional experiments (COSY, gHSQC and gHMBC, taken in CDCl_3 solutions). The two diastereotopic hydrogens belonging to C-3 were found at 1.89 and 2.11 ppm. The COSY spectrum showed they are coupled with the hydrogens at 3.66 and 4.49 ppm. The hydrogen at 3.66 ppm showed additional coupling with the signal at 4.93 ppm (H-1). This allowed us to assign the signal at 3.66 ppm to H-4 and the signal at 4.49 ppm to H-2. The proton at 4.93 ppm, that is coupled with the signal at 6.64 ppm with a coupling constant of 14.1 Hz provided evidence of the *E*-geometry of the exocyclic double bond. The signals of the tetrahydroquinoline NH at 3.42 ppm and of the carbamate NH (6.45 ppm,

doublet, $J = 10.8$ Hz) were assigned by the lack of correlation in the ^{13}C - ^1H HSQC spectrum. One of the signals of the two diastereotopic protons at C-3 appears as a pseudo-quartet, with a large coupling constant ($J = 12.4$ Hz, H-3b in Figure 44). This implies that this proton is coupled with three hydrogens with similar and large coupling constants, which are consistent with the geminal coupling with H-3a and trans-diaxial couplings with H-2 and H-4, due to a dihedral angle close to 180° .⁷ This clearly indicates that both H-2 and H-4 are in pseudo-axial position on the tetrahydroquinoline ring, whereas the phenyl and the ene-carbamate moiety occupy the pseudo-equatorial positions. As a confirm, the signal of H-3a (the second diastereotopic hydrogen of C-3) exhibits the same large geminal constant (12.4 Hz) and two small coupling constants due to the equatorial-axial coupling, where the dihedral angle is close to 90° .

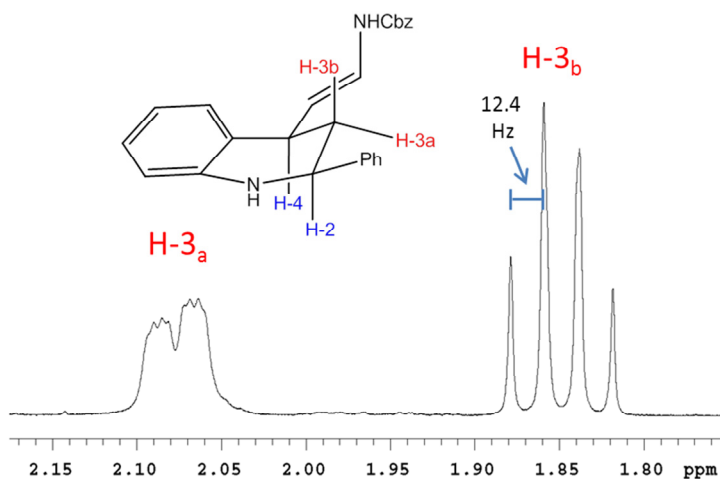


Figure 44. Expansion of the ^1H spectrum (600 MHz in CDCl_3) of **3k** showing the signals of the two diastereotopic hydrogens of C-3.

Mono-dimensional DPGSE-NOE experiments⁸ were acquired in order to confirm the relative stereochemistry at C-2 and C-4. On saturation of the vinylic hydrogen H-1' (trace a in Figure 45), NOE enhancement was

observed for one proton at C-3 (H-3b, in pseudo-axial position) and no enhancement was observed for the other ene-carbamate proton H-2'. This confirms the *E* geometry of the double bond. The large NOE on H-3b suggests that H-1' is anti to H-4. On saturation of H-4, NOE are observed on H-2 (trace c in Figure 45) and on the signal of H-3a (in pseudo-equatorial position). On saturation of H-2 (trace b in Figure 45), NOE are observed for H-4 and for H-3a, thus confirming the 1-3 diaxial relationship of H-2 and H-4, already deduced from the analysis of the *J*-couplings of the ¹H NMR spectrum. NMR analysis thus confirms the *cis* relative configuration of the two asymmetric centres of the 1,2,3,4-tetrahydroquinoline skeleton (thus 2*R**,4*S**), and the *E*-geometry of the exocyclic double bond. Having in hand the relative configuration and suitable information about the preferred conformation, the assignment of the absolute configuration was tackled by chiro-optical methods.

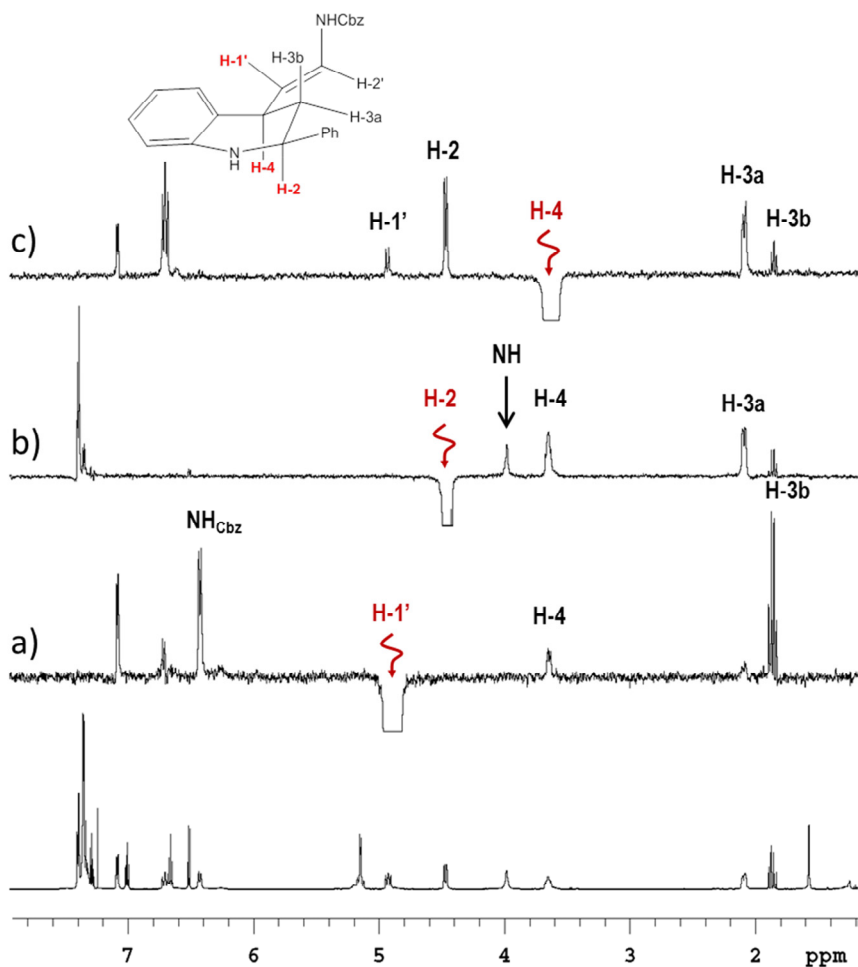
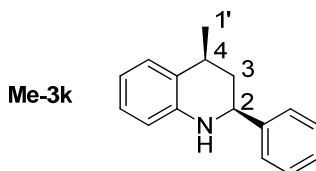


Figure 45. DPGSE-NOE spectra of **3k** (600 MHz in CDCl₃). (*Bottom*) ¹H-NMR control spectrum; *trace a*) saturation of H-1'; *trace b*) saturation of H-2; *trace c*) saturation of H-4.

The theoretical calculation of the electronic circular dichroism spectra (ECD) was selected for the absolute configuration assignment. Although the rigidity of the 1,2,3,4-tetrahydroquinoline core of compound **3k** helps in the reduction of the number of conformations to be considered,⁹ the conformational freedom of the exocyclic ene-carbamate moiety represent

a challenging issue for the conformational analysis step. As the first stage, we performed a conformational search on a model compound where all the ene-carbamate moiety (CH=CH-NH-Cbz) was reduced to a methyl group (model compound **Me-3k**).



All the conformations found by MM search within a 10 kcal/mol window (Monte Carlo searching together with the MMFF94 molecular mechanics force field as implemented in Titan 1.0.5, Wavefunction inc.) were then optimized using DFT at the B3LYP/6-31G(d) level. The harmonic vibrational frequencies of each conformation were calculated at the same level to confirm their stability (no imaginary frequencies were observed) and to evaluate the free energy of each conformation. After DFT minimization, only two conformations were found to be enclosed in the 10 kcal/mol window, and one of them (conformation **a** in Figure 46) was much more stable than the other (conformation **b**). Conformation **b** differs from **a** because of the different shape of the six-membered ring, that corresponds to a pseudo-boat conformation where the phenyl ring and the methyl occupy a pseudo-axial position. The energy gain (3.25 kcal/mol as internal energy difference, 3.71 kcal/mol as ZPE-corrected free energy) suggest that **a** should be the only populated conformer in solution. (Figure 46).

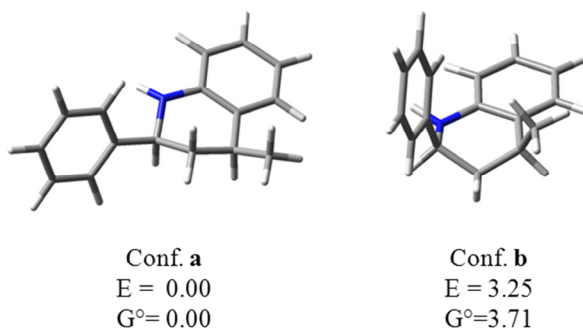


Figure 46. 3D view of the two conformations of the model compound Me-3k with a methyl group in position 4. Reported energies are in kcal/mol.

The electronic excitation energies and rotational strengths have been calculated for the isolated molecule in the gas phase for the best conformation of **Me-3k** using TD-DFT with four different methods (functionals), to ascertain if different computational approaches provide different shapes of the simulated spectra. Simulations were performed with the hybrid functionals BH&HLYP and M06-2X, the Long-range Correlated LC- ω B97XD that includes empirical dispersion, and CAM-B3LYP that includes long range correction using the Coulomb Attenuating Method. The calculations employed the 6-311++G(2d,p) basis set that proved to be sufficiently accurate at a reasonable computational cost. Rotational strengths were calculated in both length and velocity representation, the resulting values being very similar (RMS differences < 5%). For this reason the errors due to basis set incompleteness should be very small, or negligible.

As shown in Figure 47, the simulated spectra match the Cotton effects at 190 nm and 203 nm when the $2S$, $4S$ absolute configuration is assumed in the calculations. However, the lower energy Cotton effect at 229 nm is not

reproduced by the calculations. This means that the contribution of the ene-carbamate moiety on the ECD spectrum cannot be ruled out. Thus the simulation of the ECD spectra must be performed on the whole structure of **3k**.

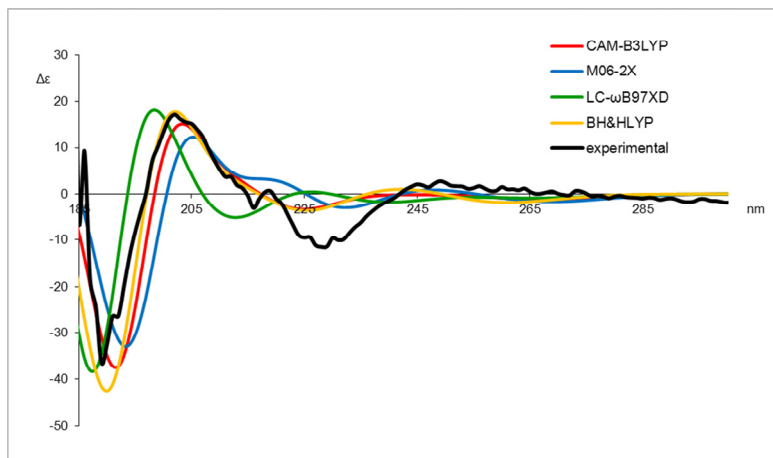


Figure 47. Black line: experimental ECD spectrum of **3k. Colored lines: TD-DFT simulated spectra calculated for Me-**3k**. All the simulated spectra were red-shifted by 15 nm to match the experimental maximum at 203 nm.**

Starting from the best conformation of **Me-3k**, a new conformational search was performed on **3k**. After DFT optimization, two conformations were found to be very close in energy. Both exhibit the pseudo-chair conformation of the tetrahydroquinoline ring and they are different because of the *E/Z* rotational isomerism of the amidic part of the carbamate. If the internal energy is considered, the *Z* conformation is favoured by 1.18 kcal/mol. On the contrary, the *E* conformation is more stable by 0.38 kcal/mol when the free energies obtained by thermochemistry corrections are applied.

Apart from the *E/Z* rotational isomerism, the calculated geometry of conformations **3k-a** and **3k-b** are in good agreement with the

experimental NOE data, whereas one of the two hydrogens belonging to C-3 (H-3b) has dihedral angles close to 180° with H-2 and H-4 (179° and 168° , respectively). Also the position of H-1' corresponds to the distance constraints extracted by NOE data, with an *anti*-relationship with H-4.

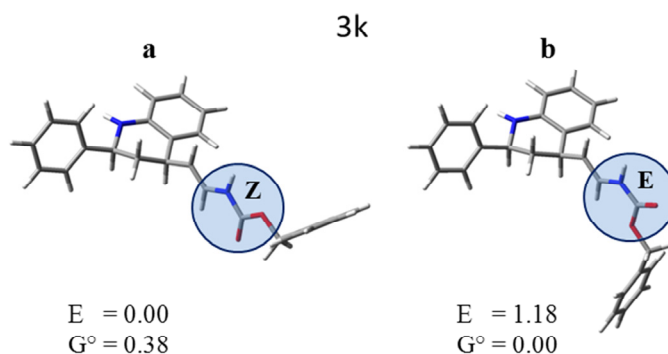


Figure 48. 3D view of the two most stable conformation of **3k**, calculated at the B3LYP/6-31G(d) level. Energy differences are in kcal/mol and represent ZPE-corrected free energy in standard conditions (G°) or uncorrected internal energies (E).

Variable temperature NMR spectra, taken down to -15°C in CD_3CN , showed that the *E/Z* interconversion due to rotation of the carbamate could be frozen in the NMR timescale. The ratio of the two conformations due to *E/Z* isomerism was 90:10, corresponding to a $\Delta G^\circ = 1.1$ kcal/mol. at $+25^\circ\text{C}$. Unfortunately, NOE spectra can't ascertain whether the *Z* or the *E* rotamer was the more populated conformation. DFT calculations of the chemical shifts at the B3LYP/6-311++G(2d,p) level (GIAO approach) suggested that the chemical shift of the NH-Cbz hydrogen in the *E*-conformer is shielded by 0.35 ppm in the *E*-rotamer with respect to the NH of the *Z*-conformer. Since the upfield signal experimentally corresponds to the most populated conformer, this theoretical result agrees well with the calculations based on the free

energies and it assigns the *E*-conformation (**b** in Figure 48) as the more stable rotamer in solution.

The electronic excitation energies and rotational strengths were calculated in the gas phase for the two conformation of **3k** using TD-DFT with the same four different methods (functionals) and basis sets used for **Me-3k** (BH&HLYP, M06-2X, LC- ω B97XD, and CAM-B3LYP with 6-311++G(2d,p) basis set). All the calculations were performed supposing *2S*, *4R* Absolute Configuration, with the results shown in Figure 49.

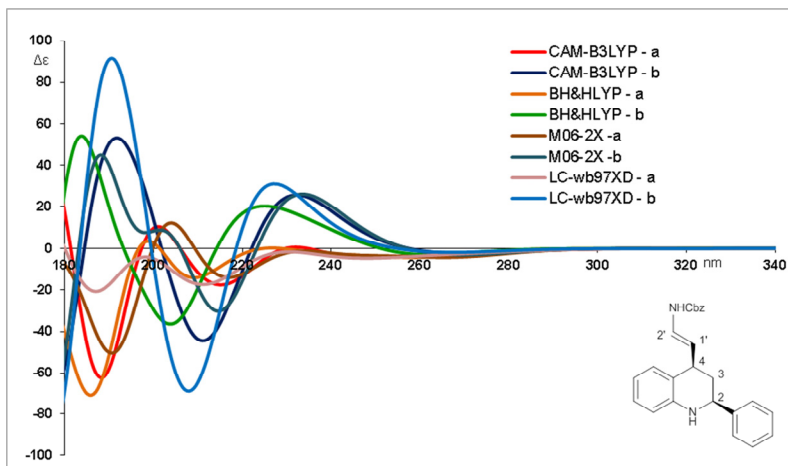


Figure 49. TD-DFT simulated spectra calculated for **3k**. The reddish set of lines correspond to conformation a (*Z*-rotamer). The bluish set correspond to conformation b (*E*-rotamer).

As shown in Figure 49, the simulated spectra are similar within the same conformation, but the two conformations show quite different spectra. In particular, they show opposite phase in the high energy region between 200 and 180 nm. However, the experimental ratio to be used to get the averaged spectrum was provided by low-temperature NMR. The simulated spectra were then obtained by using a 86:14 ratio, corresponding to a $\Delta G^\circ = 1.1$ kcal/mol at +25°C. (Figure 50). It should be

stressed that if the opposite ratio of the rotamers is used the agreement is still acceptable, but the wavelength of the highest energy Cotton does not match to the experimental value. From an alternative point of view, the ECD spectrum confirms the conformational preference toward the Z-rotamer of the ene-carbamate.

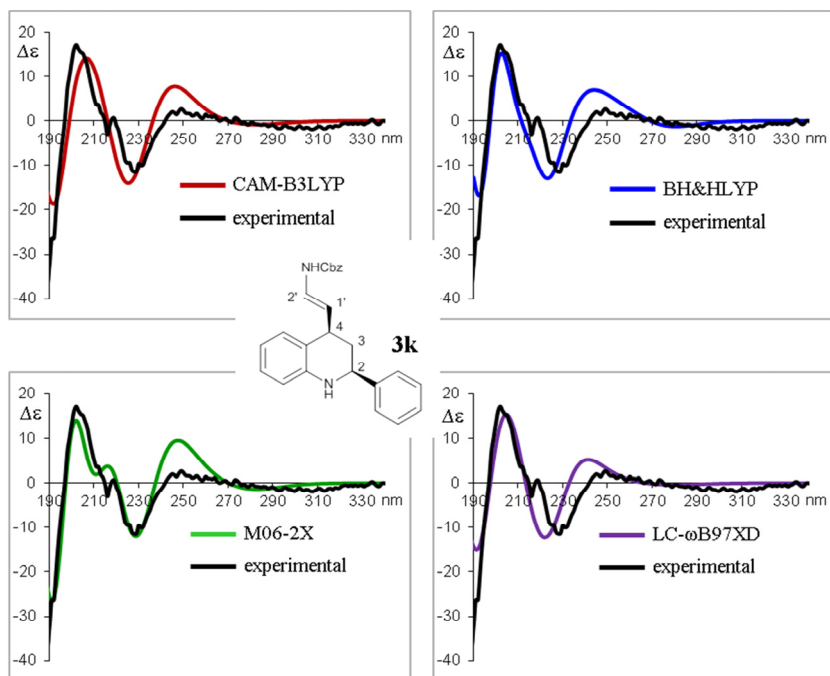


Figure 50. Simulations of the experimental ECD spectrum of **3k** (black traces). obtained with different methods of calculation. Each simulated spectrum (red, blue, green and purple lines) was obtained starting from the spectra obtained for the two conformations weighted using the experimental NMR data (86:14). The experimental spectrum of **3k** was obtained in acetonitrile solution ($5.5 \cdot 10^{-5}$ M, 0.2 cm path length). $\Delta\epsilon$ are expressed in $\text{Mol L}^{-1} \text{cm}^{-1}$. The simulated spectra were vertically scaled to match the experimental maximum at 203 nm (0.35, 0.40, 0.43 and 0.20 for CAM-B3LYP, BH&HLYP, M06-2X and LC- ω B97XD, respectively) and red shifted (by 15, 20, 15 and 15 nm, respectively).

The best simulation was obtained by the M06-2X functional, but all the simulated spectra now show a good agreement with the experimental one, also in the 230 nm region. Thus the absolute configuration could be reliably assigned as 2*S*,4*R*, which is in agreement with the proposed reaction mechanism.

References

- ¹ Caruana, L.; Fochi, M. F.; Ranieri, S.; Mazzanti, A.; Bernardi, L. *Chem. Commun.* **2013**, 49, 880 – 882.
- ² For a recent review describing both biological significance and preparation of 1,2,3,4-tetrahydroquinolines: Sridharan, V.; Suryavanshi, P. A.; Menéndez, C. *Chem. Rev.*, **2011**, 111, 7157 – 7259.
- ³ a) Povarov, V.; Mikhailov, B. M. *Izv. Akad. Nauk. SSSR, Ser. Khim.* **1963**, 955. For reviews, see: b) Kouznetsov, V. V. *Tetrahedron*, **2009**, 65, 2721 – 2750. c) Bello, D.; Ramon R.; Lavilla, R. *Curr. Org. Chem.*, **2010**, 14, 332 – 356.
- ⁴ a) Xie, M.; Chen, X.; Zhu, Y.; Gao, B.; Lin, L.; Liu, X.; Feng, X. *Angew. Chem. Int. Ed.*, **2010**, 49, 3799 – 3802. b) Dagousset, G.; Zhu, J.; Masson, G. *J. Am. Chem. Soc.*, **2011**, 133, 14804 – 14813. c) Lin, J.-H.; Zong, G.; Du, R.-B.; Xiao, J.-C.; Liu, S. *Chem. Commun.*, **2012**, 48, 7738 – 7741. d) Bergonzini, G.; Gramigna, L.; Mazzanti, A.; Fochi, M.; Bernardi, L.; Ricci, A. *Chem. Commun.* **2010**, 46, 327 – 329. e) Xu, H.; Zuend, S. J.; Woll, M. G.; Tao, Y.; Jacobsen, E. N. *Science*, **2010**, 327, 986 – 992.
- ⁵ a) Bernardi, L.; Comes-Franchini, M.; Fochi, M.; Leo, V.; Mazzanti, A.; Ricci, A. *Adv. Synth. Catal.*, **2010**, 352, 3399 – 3406. b) Duce, S.; Pesciaoli, F.; Gramigna, L.; Bernardi, L.; Mazzanti, A.; Ricci, A.; Bartoli, G.; Bencivenni, G.; *Adv. Synth. Catal.*, **2011**, 353, 860 – 864.
- ⁶ a) Sridharan, V.; Ribelles, P.; Estévez, V.; Villacampa, M.; Ramos, M. T.; Perumal, P. T.; Menéndez, J. C. *Chem. Eur. J.*, **2012**, 18, 5056 – 5063. b) Sridharan, V.; Avendaño, C.; Menéndez, J. C. *Synlett*, **2007**, 1079 – 1099.

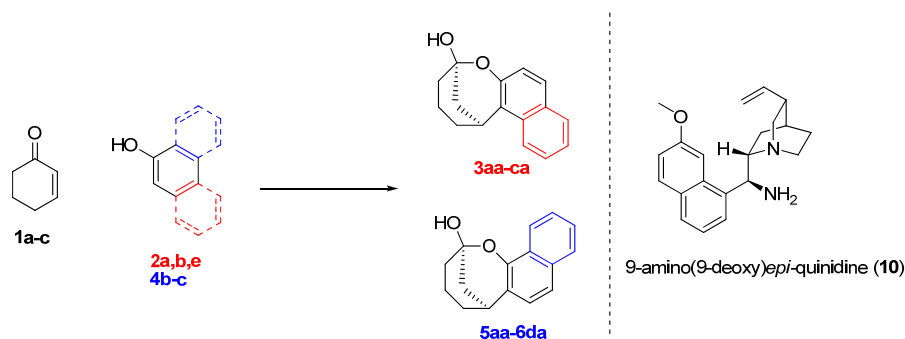
⁷ Karplus, M. *J. Am. Chem. Soc.* **1963**, 85, 2870 – 2871.

⁸ Stott, K.; Stonehouse, J.; Keeler, J.; Hwang T-L.; Shaka, A. J. *J. Am. Chem. Soc.* **1995**, 117, 4199 – 4200.

⁹ Polavarapu, P. L.; Donahue, E. A.; Shanmugam, G.; Scalmani, G.; Hawkins, E. K.; Rizzo, C.; Ibnusaud, I.; Thomas, G.; Habel, D.; Sebastian, D. *J. Phys. Chem. A* **2011**, 115, 5665 – 5673.

Absolute configuration of compounds from enantioselective Friedel-Crafts alkylation-acetalization cascade of naphthols with α,β -unsaturated cyclic ketones¹

The Friedel-Crafts (F-C) reaction represents one of the most well known ways for the generation of a new C-C bond between an electron-rich aromatic system and a suitable electrophile.² During the last few years this reaction has been performed in enantioselective fashion, via organocatalysis.³ Organocatalytic F-C alkylation has been intensively explored under different activation modes and using a large number of chiral catalysts: Brønsted acid,⁴ thiourea,⁵ base catalyzed reactions⁶ and aminocatalytic strategy mainly based on chiral secondary amines.⁷ Exploiting the capability of primary amine catalysts, in particular based on the *Cinchona* alkaloid structure,⁸ Bencivenni and co-workers developed a new asymmetric organocascade⁹ reaction of F-C alkylation, followed by acetalization, between naphthols and α,β -unsaturated ketones. (Scheme 13)

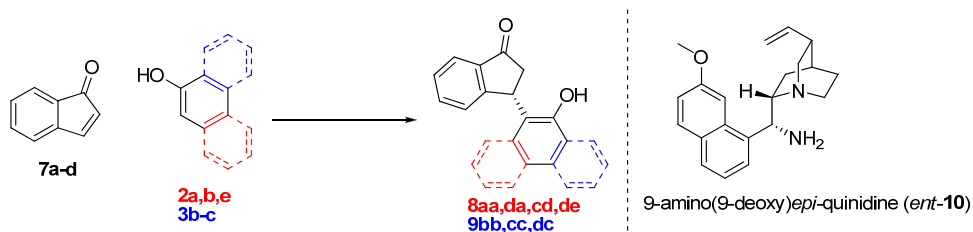


Scheme 13. F-C alkylation acetalization cascade.

The reaction between cyclohexenone **1a** and β -naphthol **2a** was chosen as model and after the screening of different primary amines, they found

that amino(9-deoxy)*epi*-quinine (**10**) in combination with 5-nitrosalicylic acid (5-NO₂-SA) was able to catalyze the reaction in toluene at 40 °C giving **3aa** as a single diastereoisomer in 88% yield and 81% *ee* after 72 hours. Then a broad scope for this reaction has been prepared, with different enones and a series of variously decorated α and β -naphthols, with good yields and enantioselectivities. (For all reaction details and substituents on the reagents, see reported paper in Ref[1]).

Finally the reactivity of 1*H*-inden-1-ones (**7a-d**) have been explored, using *ent*-**10** as catalyst (see Scheme 14). Given the severe steric hindrance¹⁰ of these substrates, the desired compounds **8aa** – **9dc** were isolated in high yields and enantioselectivities.



Scheme 14. F–C alkylation of 1*H*-inden-1-ones with α - and β -naphthols.

The absolute configuration was found for compound **8de** by means of X-ray analysis and for compounds **8aa** and **9bb**, as well as for compounds **5da** – **3ab**, by means of TD-DFT ECD simulation.

Compounds **8**

Good crystals suitable for X-ray diffraction were obtained for compound **8de** by slow evaporation of a methanol solution. The anomalous scattering determination of the absolute configuration was possible thanks to the presence of the chlorine atom. The *S* configuration was

determined for the selected crystal and its relationship to the major enantiomer obtained with ent-**10** catalyst was confirmed by means of enantioselective HPLC analysis of the very same crystal used for X-ray analysis (this was not straightforward, since the crystals were obtained from a 81% *ee* mixture of enantiomers). The crystal cell contained two conformations of the *S* enantiomers, that were different in the orientation of the OMe group on the naphthalene ring.

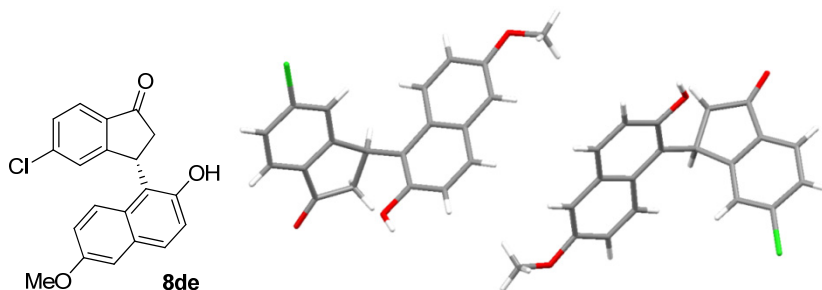


Figure 51. X-Ray structure of 8de. Two different conformations with the same *S* absolute configuration represent the asymmetric unity.

Since the prepared compounds belong to four different classes, a straight relationship of the stereochemical course of the reaction is likely, but in principle it cannot be safely assumed. However, despite many attempts, enantiopure crystals of other compounds containing a suitable heavy atom cannot be obtained. In the remaining cases, the X-ray analysis cannot determine the absolute configuration. For these reason we switched to a different approach based on conformational analysis and chiroptical methods (ECD).

From a conformational point of view, the rigidity of the scaffold of compounds **3**, **5**, **8** and **9** reduces the number of conformations to be considered and simplify the conformational analysis. In addition to this, the configuration assignment by chiroptical methods of a sample

compound of the **8** series can provide information on the reliability of this method applied to the present compounds.

A preliminary conformational search on **8aa** was carried out using Monte Carlo method together with the MMFF94 molecular mechanics force field (as implemented in Titan 1.0.5, Wavefunctioninc.). All the conformations within a 10 kcal/mol window were then optimized using DFT at the B3LYP/6-31G(d) level, the harmonic vibrational frequencies of each conformation were calculated at the same level to confirm their stability (no imaginary frequencies were observed) and to evaluate the free energy of each conformation.

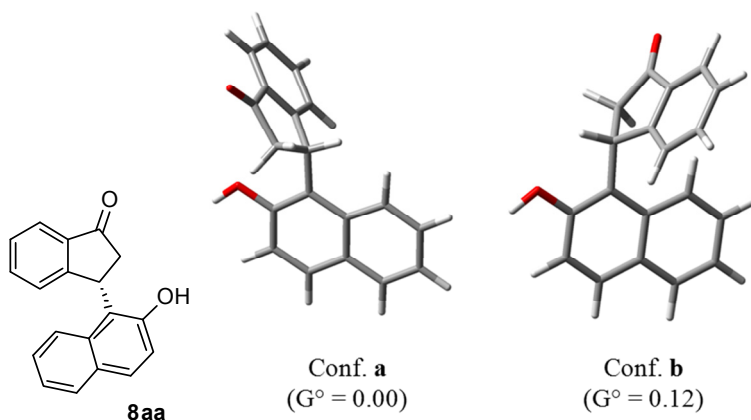


Figure 52. 3D view of the two most stable conformations of **8aa**, calculated at the B3LYP/6-31G(d) level. Energy differences are in kcal/mol and represent ZPE-corrected free energies in standard conditions.

After DFT minimization only two conformations were found to be enclosed in the 10 kcal/mol window (Figure 52). These correspond to two conformational diastereoisomers due to the rotation on the indane ring that is almost perpendicular to the naphthol ring in the ground states. The electronic excitation energies and rotational strengths have been

calculated in the gas phase for the two conformations of **8aa** using TD-DFT with four different methods (functionals) to ascertain if different calculations provide different shapes of the simulated spectra. The simulation were performed with the functionals BH&HLYP, M06-2X, LC- ω B97XD and CAM-B3LYP. All the calculations employed the 6-311++G(2d,p) basis set, that proved to be sufficiently accurate at a reasonable computational cost.

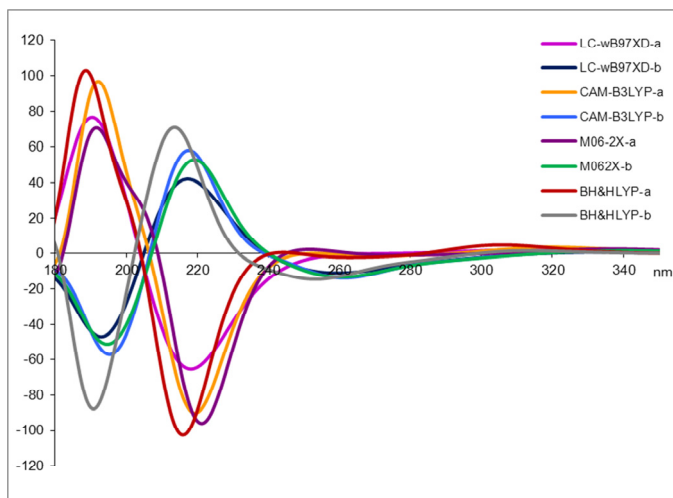


Figure 53. ECD simulations for the two conformations of **8aa, obtained with the four different functionals and the same 6-311++G(2d,p) basis set.**

The rotational strengths were calculated in both length and velocity representation with the resulting values being very similar. For this reason the errors due to basis set incompleteness should be considered very small, or negligible.¹¹ All the calculations were performed supposing *S* Absolute Configuration, with the results shown in Figure 53. The eight simulated spectra are divided into two set of opposite shaped spectra (reddish lines and bluish/greenish lines), each one corresponding to one of the two conformations of **8aa**. The opposite pattern can be attributed to

the excitonic coupling¹² to the two chromophores, i.e. the naphthyl and the indane ring, that have opposite helicity in the two conformations (R^*M^* in conformation **a** and R^*P^* in conformation **b**). Therefore the shape of the simulated spectrum that should be compared with the experimental one strongly depends on the population ratio employed. Unfortunately, the calculated energies of the two conformations are very similar ($\Delta G^\circ = 0.12$ kcal/mol), thus a correct evaluation of the populations¹³ is completely unreliable. This implies that the AC assignment is unfeasible without further experimental data.

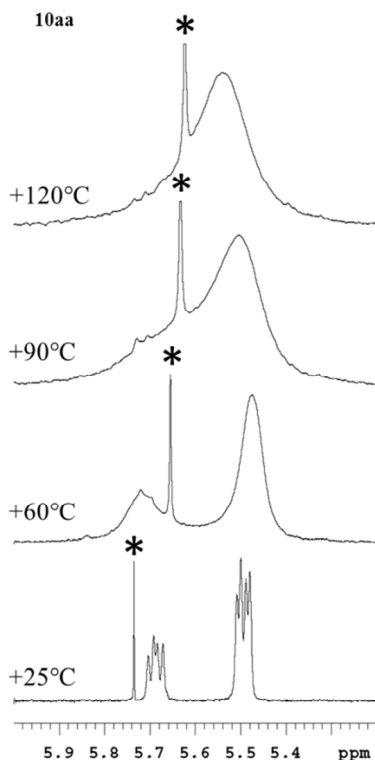


Figure 54. Variable temperature spectra ($^1\text{H-NMR}$ at 400 MHz in DMSO-d_6) of compound **8aa**. The signal of the CH of the indanone ring is showed. The asterisk marks a solvent impurity.

However, the conformational analysis of **8aa** showed that the indane ring is forced to be perpendicular to the naphthol ring by the steric hindrance exerted by the OH and the *peri* hydrogen (H-8). If the interconversion barrier is sufficiently high, two observable conformational diastereoisomers could be generated. This is what actually happened. ¹H NMR showed two sets of signals in a 69:31 ratio due to the frozen rotation around the C α - CH bond. When the temperature is raised the two multiplets broaden and show a single peak at +120°C, when the rotation is fast in the NMR time scale, (Figure 54). An energy barrier of 17.8 kcal/mol was derived at the coalescence temperature (+90°C).

NOE spectra were then acquired to determine which conformational diastereoisomer is the more populated. In the **a** diastereoisomer the CH hydrogen of indane is close to the *peri* H-8 hydrogen of the naphthol ring (1.87 Å), whereas in the **b** conformation the CH points towards the OH and it is far from H-8. DPGSE-NOE¹⁴ spectra obtained on saturation of the two CH signals showed that the major conformation has the CH close to H-8 and the minor has the CH close to OH (Figure 55).

In the present case the integration of the NMR spectra and the NOE spectra provide the exact ratio of the two conformational diastereoisomers to be used in the simulation of the experimental ECD spectrum.

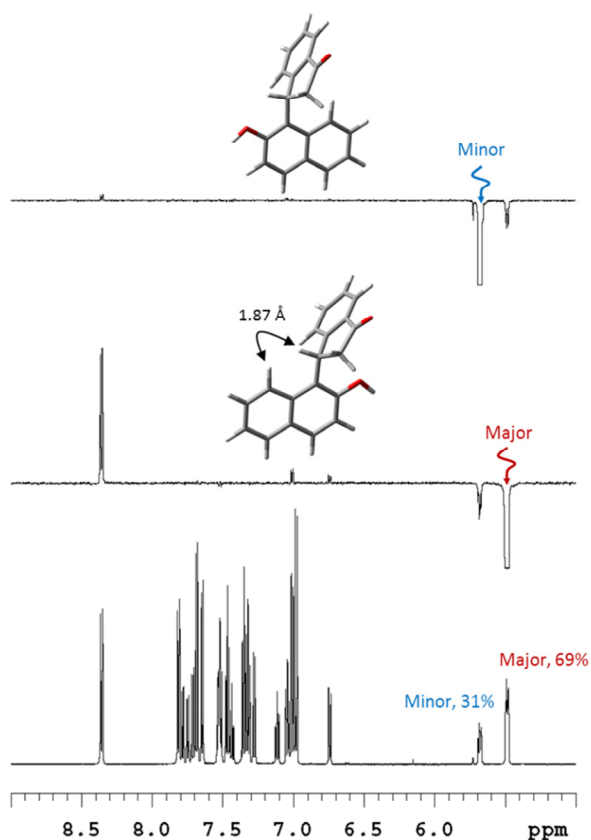


Figure 55. DPGSE-NOE spectra of 8aa (600 MHz in DMSO-d₆). (*Bottom*) control spectrum. (*Middle trace*) NOE obtained on saturation of the major CH. (*Top*) NOE spectrum obtained on saturation of the minor CH. (in both NOEs the small inverted peak of the second diastereoisomer was due to saturation transfer effects).

The simulated ECD spectrum was thus obtained for each model of calculation by taking into account the 69:31 populations ratio experimentally determined by NMR. All the four simulations obtained (Figure 56) display now a good agreement with the experimental spectrum and the best simulation was obtained with the BH&HLYP functional. Provided the experimental ratio of the two conformations,¹⁵ the ECD simulations showed to be able to tackle the absolute

configuration of **8aa**.

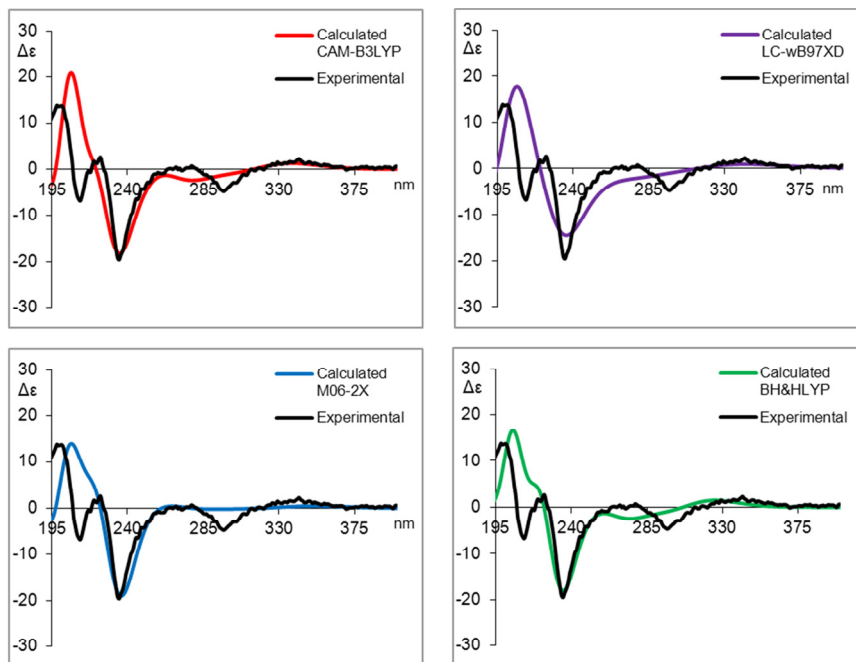


Figure 56. Simulations of the experimental ECD spectrum of **8aa** (black traces) obtained with different methods of calculation (functionals). Each simulated spectrum (red, blue, green and purple lines) was obtained starting from the spectra obtained for the two conformations weighted using the experimental NMR data. The experimental spectrum of **8aa** was obtained in acetonitrile solution ($1 \cdot 10^{-4}$ M, 0.2 cm path length). $\Delta\epsilon$ are expressed in $\text{Mol L}^{-1} \text{cm}^{-1}$. The simulated spectra were vertically scaled to match the experimental intensity and red shifted to match the experimental peak at 238 nm.

Compounds **9**

No compound of the **9** series could be crystallized as single crystals and the assignment of **9bb** was performed by means of same chiroptical methods used for **8aa**. As in the previous case, **9bb** has two conformations found by conformational analysis and subsequent DFT optimizations have the CH pointing towards the OH (**a** conformation) and

the CH in position 3 (**b** conformation), respectively. In this case, however, the steric hindrance to the rotation of the indane ring is smaller and the ^1H NMR spectrum recorded at room temperature does not show the signals corresponding to the two conformational diastereoisomers. However, since calculations estimated a very similar energy they should be both populated. For this reason, variable temperature NMR spectra were recorded down to -100°C . Below -60°C the signal of the CH broadened and split at -100°C into two signals with a 90:10 ratio. Following the trend observed for **8aa**, the lower field signal (90%) can be attributed to the conformation in which the CH hydrogen is close to OH. Comfortably, this is also the lowest energy conformation and also the evaluation of the energy difference matched well the experimental ratio (calculated ΔG^\ddagger : 0.56 kcal/mol; experimental: 0.75 kcal/mol at -100°C). By applying Boltzmann statistics, the ratio at room temperature is 78:22.

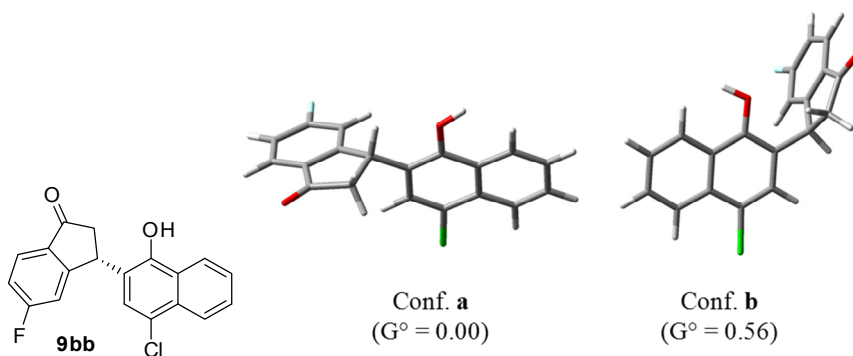


Figure 57. 3D view of the two stable conformations of **9bb**, calculated at the B3LYP/6-31G(d) level. Energy differences are in kcal/mol and represent ZPE-corrected free energies in standard conditions.

The rotational strengths and electronic excitation energies were calculated in the gas phase for the two conformations of **9bb** using TD-DFT and the same four different methods used for **8aa**. All the

calculations employed the 6-311++G(2d,p) basis set and supposing *S* Absolute Configuration (Figure 58).

As for **8aa**, the opposite helicity generated by the out-of-plane disposition of the indane ring yields two set of calculated ECD spectra with opposite pattern. However, when the final simulated spectra are obtained using the population ratio determined by low-temperature NMR, the agreement with the experimental trace is very good (Figure 59), and the *S* absolute configuration can be assigned to compound **9bb**. In addition to this, the agreement of the four methods and the similarity of the spectra enhances the reliability of the assignment.

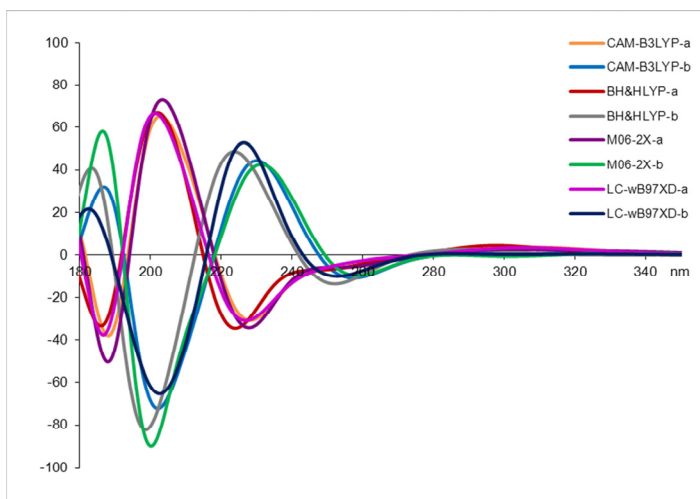


Figure 58. TD-DFT simulations for the two conformations of **9bb**, obtained with the four functionals and the 6-311++G(2d,p) basis set.

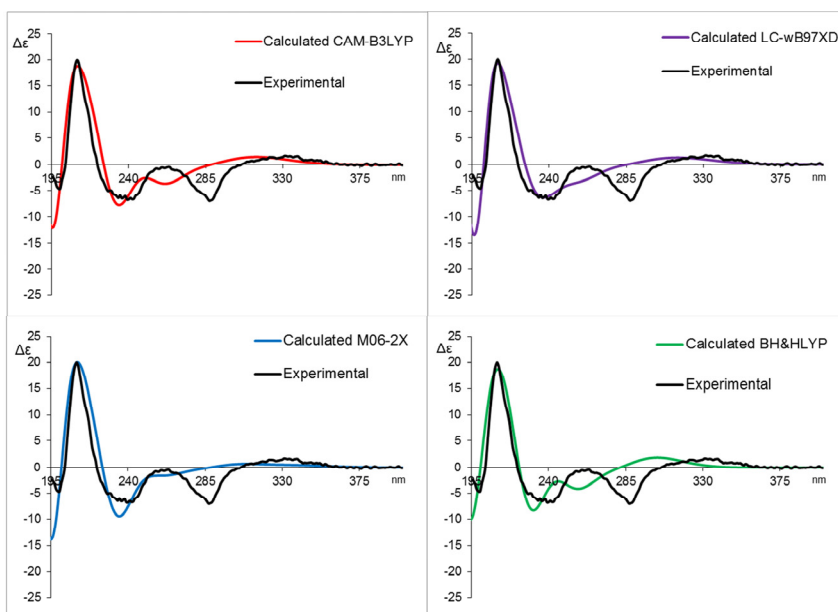


Figure 59. Simulations of the experimental ECD spectrum of **9bb** (black traces) obtained with different methods of calculation. Each simulated spectrum (red, blue, green and purple lines) was obtained starting from the spectra obtained for the four conformations weighted using Boltzmann statistics at +25°C. The experimental spectrum was obtained in acetonitrile solution ($1 \cdot 10^{-4}$ M, 0.2 cm path length). $\Delta\epsilon$ are expressed in $\text{Mol L}^{-1} \text{cm}^{-1}$. The simulated spectra were vertically scaled to match the experimental intensity, and red shifted to match the experimental maxima.

Compounds 5

As reported in the text, compounds **5** correspond to the hemiacetalic form. From a conformational point of view, these structures are completely blocked, and only one conformation is supposed to be populated. This correspond to the chair conformation of the cyclohexane part of the bicyclic system. Compound **5da**, containing a phenyl group in position 4 was selected for the spectroscopic analysis because the

presence of a second chromophore that could couple with the naphthalene ring to cause a stronger ECD spectrum.

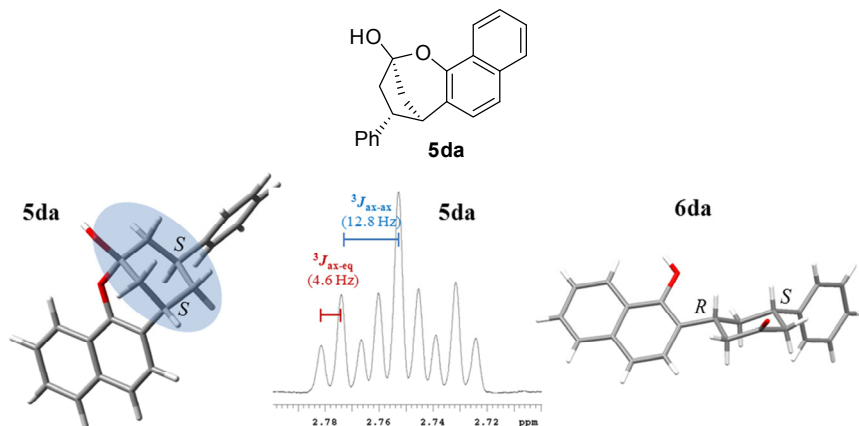


Figure 60. (Left) 3D view of the optimized conformation of **5da**, calculated at the B3LYP/6-31G(d) level. The chair-shaped cyclohexane ring is shaped. (Center) ^1H multiplet of the CH in position 4 showing the trans-diaxial and axial-equatorial coupling constants. (Right) X-ray structure of **6da**.

The analysis of the ^1H spectrum of compound **5da** showed that the phenyl ring in position 4 occupies the equatorial position. The signal of benzylic CH shows a trans-diaxial coupling constant of 12.8 Hz and an axial-equatorial constant of 4.6 Hz. The $2R^*,4S^*,6S^*$ relative configuration can be therefore assumed in the following discussions (Figure 60). It is worth to note that the second diastereoisomer produced by the reaction (**6da**) does not evolve to the hemiacetalic form because in this compound the phenyl ring should occupy the axial position. Although the absolute configuration of **6da** could not be established by anomalous scattering, the X-ray structure confirmed that the two chiral carbons have opposite chirality (thus $3R^*,5S^*$).

To exclude the presence of other low-energy conformations, the conformational search by MM methods was performed as above, but no

other conformations were found. As in the previous cases, DFT optimization at the B3LYP/6-31G(d) level provided the final geometry to be used in the TD-DFT simulations. The rotational strengths and electronic excitation energies were calculated in the gas phase by TD-DFT and the same four different methods used for **8aa** and **9bb**. All the calculations employed the 6-311++G(2d,p) basis set and supposed *S* Absolute Configuration at the reaction center. (thus *2R,4S,6S*) (Figure 61). In this case the simulation of the experimental spectrum is straightforward, since no conformational averaging is needed and the four calculated spectra are very similar. As shown in Figure 61, the experimental trace is well matched by all the simulation obtained for the *2R,4S,6S* absolute configuration.

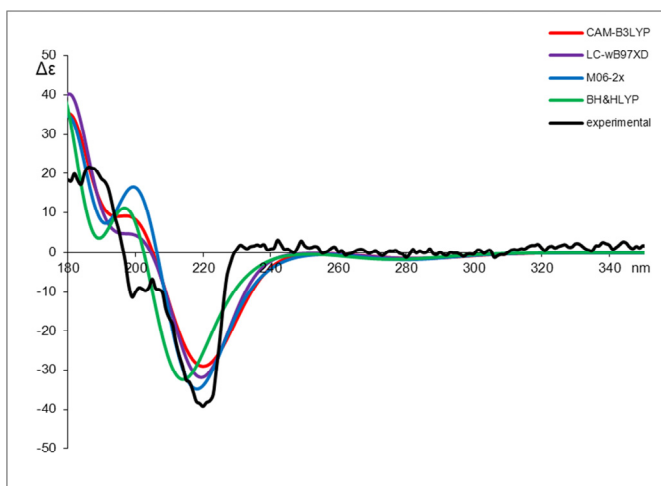


Figure 61. TD-DFT simulations for **5da**, obtained with the four different functionals and the 6-311++G(2d,p) basis set. The black line corresponds to the experimental spectrum obtained in acetonitrile solution ($1 \cdot 10^{-4}$ M, 0.05 cm path length). $\Delta\epsilon$ are expressed in $\text{Mol L}^{-1} \text{cm}^{-1}$. The simulated spectra were vertically scaled to match the experimental intensity, and red shifted to match the experimental maxima.

Compounds 3

Compounds **3** has the same hemiacetalic scaffold of compounds **5**, thus a second chiral carbon is generated with complete stereocontrol during the cyclization. With respect to the cyclohexane scaffold the two substituents must occupy the 1-3 diaxial positions (Figure 62). Compound **3ab** was selected for the stereochemical assignment.

As in the case of **5**, the bicyclic structure is very rigid, and only a single conformation was found by MM search. In this case, however, a second conformation with a boat-shaped cyclohexane cannot be excluded in principle. When optimized by DFT, this conformation showed to be about 5 kcal/mol higher in energy with respect to the conformation found by conformational search, and it can be neglected in the ECD simulations. Compound **3ab** lacks a second chromophore on the cyclohexane ring and the experimental ECD is rather weak. However, the TD-DFT simulations performed assuming the *1S,5R* absolute configuration satisfactorily followed the experimental trend (Figure 63). It should be pointed out that the same *S* configuration at the reaction center was assigned as in the three previous cases.

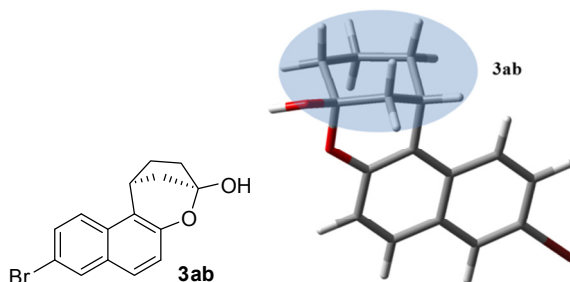


Figure 62. 3D view of the optimized conformation of **3ab**, calculated at the B3LYP/6-31G(d) level.

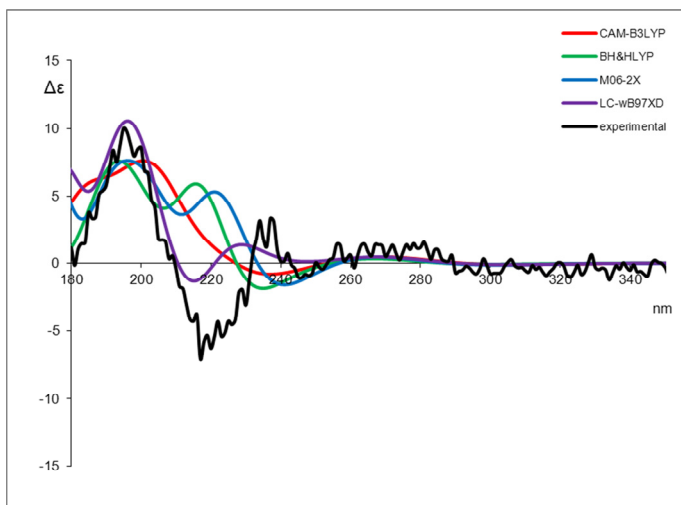


Figure 63. TD-DFT simulations for **3ab**, obtained with the four different functionals and the same 6-311++G(2d,p) basis set. The black line corresponds to the experimental spectrum obtained in acetonitrile solution ($5 \cdot 10^{-5}$ M, 0.2 cm path length). $\Delta\epsilon$ are expressed in $\text{Mol L}^{-1} \text{cm}^{-1}$. The simulated spectra were vertically scaled to match the experimental intensity, and red shifted to match the experimental maxima.

References

- ¹ Paradisi, E.; Righi, P.; Mazzanti, A.; Ranieri, S.; Bencivenni, G. *Chem. Commun.* **2012**, 48, 11178 – 11180.
- ² a) *Friedel–Crafts Chemistry*, ed. G. A. Olah, Wiley, New York, **1973**. b) Bandini, M.; Melloni, A.; Umani-Ronchi, A. *Angew. Chem., Int. Ed.* **2004**, 43, 550 – 556. c) *Catalytic Asymmetric Friedel–Crafts Alkylations*, ed. M. Bandini and A. Umani-Ronchi, Wiley-VCH, Weinheim, **2009**. d) Bolm, C.; Hildebrand, J. P.; Muiñz, K.; Hermanns, N. *Angew. Chem., Int. Ed.* **2001**, 40, 3284 – 3308. e) Poulsen, T. B.; Jørgensen, K. A. *Chem. Rev.* **2008**, 108, 2903 – 2915. f) Dalpozzo, R.; Bartoli, G.; Bencivenni, G. *Symmetry* **2011**, 3, 84 – 125. g) Chauhan, P.; Chimni, S. S. *RSC Adv.* **2012**, 2, 6117 – 6134.

-
- ³ a) Terrasson, V.; de Figueiredo, R. M.; Campagne, J. M. *Eur. J. Org. Chem.* **2010**, 14, 2635 – 2655. b) You, S.-L.; Cai, Q.; Zeng, M. *Chem. Soc. Rev.* **2009**, 38, 2190 – 2201.
- ⁴ a) Uraguchi, D.; Sorimachi, K.; Terada, M. *J. Am. Chem. Soc.* **2004**, 126, 11804 – 11805. b) Seayad, J.; Seayad, A. M.; List, B. *J. Am. Chem. Soc.* **2006**, 128, 1086 – 1087. c) Rueping, M.; Nachtsheim, B. J.; Moreth, S. A.; Bolte, M. *Angew. Chem., Int. Ed.* **2008**, 47, 593 – 596. d) Duce, S.; Pesciaioli, F.; Gramigna, L.; Bernardi, L.; Mazzanti, A.; Ricci, A.; Bartoli, G.; Bencivenni, G.; *Adv. Synth. Catal.* **2011**, 353, 860 – 864.
- ⁵ a) Herrera, R. P.; Sgarzani, V.; Bernardi, L.; Ricci, A. *Angew. Chem., Int. Ed.* **2005**, 44, 6576 – 6579. b) Taylor, M. S.; Jacobsen, E. N. *J. Am. Chem. Soc.* **2004**, 126, 10558 – 10559. c) Ganesh, M.; Seidel, D. *J. Am. Chem. Soc.* **2008**, 130, 16464 – 16465.
- ⁶ a) Marcelli, T.; Hiemstra, H. *Synthesis* **2010**, 8, 1229 – 1279. b) Chauhan, P.; Chimni, S. S. *Eur. J. Org. Chem.* **2011**, 9, 1636 – 1640.
- ⁷ a) Paras, N. A.; MacMillan, D. W. C. *J. Am. Chem. Soc.* **2001**, 123, 4370 – 4371. b) Paras, N. A.; MacMillan, D. W. C.; *J. Am. Chem. Soc.* **2002**, 124, 7894 – 7895. c) Chi, Y.; Scroggins, S. T.; Fréchet, J. M. J. *J. Am. Chem. Soc.* **2008**, 130, 6322 – 6323. d) Nicolaou, K. C.; Reingruber, R.; Sarlah, D.; Bräse, S. *J. Am. Chem. Soc.* **2009**, 131, 2086 – 2087.
- ⁸ a) Bartoli, G.; Melchiorre, P. *Synlett*, **2008**, 12, 1759 – 1772. b) Chen, Y.-C. *Synlett*, **2008**, 13, 1919 – 1930. c) Melchiorre, P. *Angew. Chem., Int. Ed.*, **2012**, 39, 9748 – 9770.
- ⁹ a) Grondal, C.; Jeanty, M.; Enders, D. *Nat. Chem.* **2010**, 2, 167 – 178. c) Nicolaou, K. C.; Edmonds, D. J.; Bulger, P. G. *Angew. Chem., Int. Ed.* **2006**, 45, 7134 – 7186.
- ¹⁰ De Vincentiis, F.; Bencivenni, G.; Pesciaioli, F.; Mazzanti, A.; Bartoli, G.; Galzerano P.; Melchiorre, P. *Chem. Asian J.* **2010**, 5, 1652 – 1656.

¹¹ Stephens, P. J.; McCann, D. M.; Devlin, F. J.; Cheeseman, J. R.; Frisch, M. J. *J. Am. Chem. Soc.* **2004**, 126, 7514 – 7521.

¹² a) Harada, N.; Nakanishi, K. *Acc. Chem. Res.* **1972**, 5, 257 – 263. b) Harada, N.; Nakanishi, K. *Circular Dichroic Spectroscopy: Exciton Coupling in Organic Stereochemistry*; University Science Books: Mill Valley, CA, **1983**. c) *Circular Dichroism: Principle and Applications*; Berova, N.; Nakanishi, K.; Woody, R.W. Eds; VCH: New York, **2000**; Chapter 12, p 337.

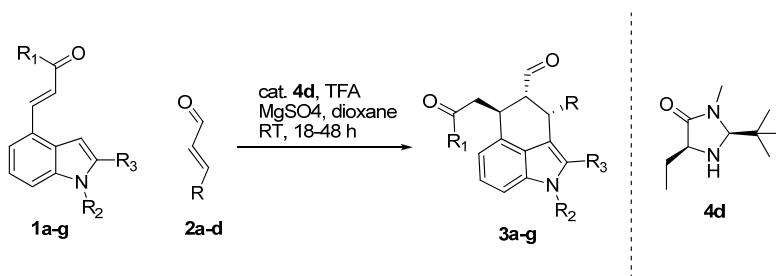
¹³ Mazzeo, G.; Giorgio, E.; Zanasi, R.; Berova, N.; Rosini, C. *J. Org. Chem.* **2010**, 75, 4600 – 4603.

¹⁴ a) Stott, K.; Stonehouse, J.; Keeler, J.; Hwand, T. L.; Shaka, A. J. *J. Am. Chem. Soc.* **1995**, 117, 4199 – 4200. b) Stott, K.; Keeler, J.; Van, Q. N.; Shaka, A. J. *J. Magn. Resonance* **1997**, 125, 302 – 324. c) See also: *High Resolution NMR Techniques in Organic Chemistry*. Claridge, T. D. W. Pergamon: Amsterdam, **1999**.

¹⁵ Casarini, D.; Lunazzi, L.; Mancinelli, M.; Mazzanti, A.; Scafato, P. *Chirality* **2009**, 21, 16 – 23.

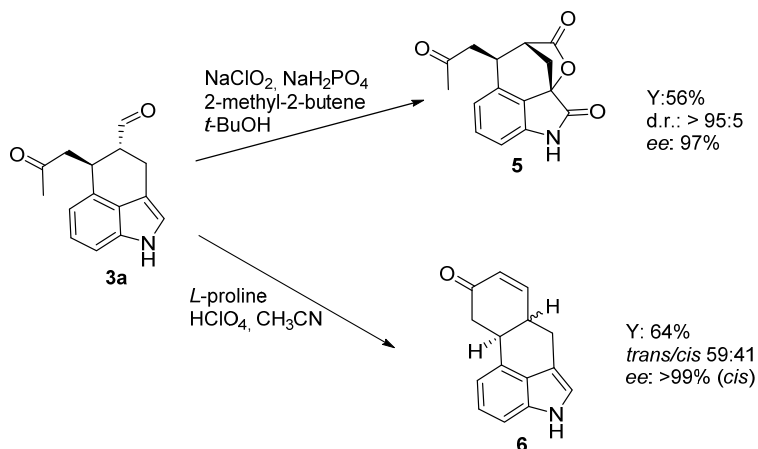
Absolute configuration of substituted 3,4-annulated indoles¹

The construction of enantioenriched carbo- and hetero-cycles by domino organocatalytic processes has been intensively studied in the last few years.² In this context, great focus has been set on the preparation of various benzo-fused heterocycles, by using aromatic rings bearing nucleophilic and electrophilic moieties in *ortho* positions in combination with activated olefins.³ These organocatalytic sequences are generally initiated by a hetero-Michael⁴ addition of a sulphur, oxygen or nitrogen nucleophile, which promotes the formation of an enolate/enamine that adds to the *ortho* electrophile terminating the cascade reaction. An elimination step, or an additional cyclization event, eventually follows. In particular, the cascade of iminium ion and enamine catalyses,⁵ in which a nucleophilic enamine is formed upon the conjugated addition to an enal or an enone activated by an amine catalyst, has been particularly effective in these cascade processes.² On these grounds, we hypothesized that 4-substituted indoles **1** could be productively engaged in organocatalytic iminium ion–enamine cascade reactions, giving a new synthetic route to 3,4-annulated indoles (Scheme 15).



Scheme 15. Reaction between **1** and acrolein **2** with the selected catalyst **4d**.

We envisaged that the indole C-3 of polyfunctional compounds **1** could act as a nucleophile in an iminium ion promoted Friedel–Crafts (F–C)⁶ process, triggering an intramolecular Michael addition⁷ of the enamine to the activated double bond placed at its ortho position. The resulting all-carbon 3,4-ring fused indole core (1,3,4,5-tetrahydrobenzo[*cd*]indole) of products **3** is widespread in natural products and biologically relevant compounds, as exemplified by the ergot alkaloid family⁸ and by steroidal indoles.⁹ Bernardi and co-workers selected the indole **1a** as first substrate and acrolein **2a** as the enal partner. After the screenings, the optimal catalyst and all other conditions have been found and a library of 3,4-annulated indoles **3** have been prepared.



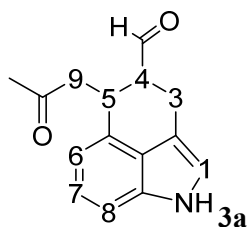
Scheme 16. Synthetic manipulations in the products **3. (Top) Pinnick conditions. (Bottom) Robinson annulation.**

The possibility of performing synthetic manipulations in the products **3** was briefly explored (Scheme 16). Treatment of **3a** under Pinnick conditions^{6a} oxidized both the aldehyde and the indole, furnishing the intriguing spirocyclic lactone **5**, whereas a Robinson annulation reaction¹⁰ rendered the tetracyclic derivative **6** as a mixture of diastereoisomers, due

to a partial epimerisation of the chiral centre a to the aldehyde during the reaction.

The absolute configuration was found for compound **3a** and **3h**, as well as for compounds **6**, by means of TD-DFT ECD simulation.

All the attempts to obtain good crystals of the prepared compounds were not successful. Moreover, with the exception of **3c**, a suitable heavy atom ($Z > \text{Si}$ using standard Mo-K α radiation¹¹) was not available for the assignment of the absolute configuration by the anomalous dispersion X-ray method.¹² For this reason the relative and absolute configuration was determined by a combination of conformational analysis and theoretical simulations of ECD spectra. Compound **3a** was selected as representative compound.



The relative stereochemistry of the two stereogenic centres at C-4 and C-5 was determined by means of NMR spectroscopy. Full assignment of the ¹H and ¹³C spectra was preliminarily achieved by bi-dimensional experiments (gHSQC and gHMBC, taken in CDCl₃ solutions). The two diastereotopic hydrogens belonging to C-3 were found at 3.00 and 3.38 ppm whereas the two diastereotopic hydrogens belonging to C-9 were found at 2.77 and 2.85 ppm (by long-range correlation with the C=O). The latter showed an additional coupling with the signal at 4.14 ppm (H-5). The signal of the NH (7.98 ppm) was assigned by the lack of correlation in the ¹³C-¹H HSQC spectrum. DPGSE-NOE experiments¹³

were acquired in order to assign the relative stereochemistry at C-4 and C-5. These carbons bear respectively the CHO and the CH₂COCH₃ moieties, that can assume a *cis* or *trans* relative disposition. On saturation of the aldehyde hydrogen (9.54ppm , trace *b*) in Figure 64), NOE enhancement was observed for H-5 and for one of the diastereotopic hydrogens at C-3 (3.38 ppm, H-3_a). No enhancement was observed for the other hydrogen H-3_b, and on the two hydrogens belonging to C-9. The observed NOEs suggested that the aldehyde and the CH₂COCH₃ substituents lie on opposite sides of the exa-atomic cycle. On saturation of both the diastereotopic C-9 hydrogens (trace *a*) in Figure 64), large NOEs were observed at 4.14 ppm (H-5), 2.92ppm (H-4) and 3.0 ppm (H-3_b). While the first two NOEs have to be visible independently from the relative configuration of the two stereogenic centres, the latter confirmed that the CH₂COCH₃ group is on the opposite side of the cycle with respect to the CHO. On saturation of H-5 (trace *c*) of Figure 64), NOEs were observed on the aldehyde hydrogen, on the two hydrogens at C-9, but no enhancement was observed on the two hydrogens at C-3. This confirms that H-5 occupies a pseudo-equatorial position. Finally, on saturation of the COMe signal (not shown in figure), NOE were observed only on H-9_a and H-9_b, suggesting that the COMe moiety adopts a conformation that places the methyl far from the cycle. NMR analysis thus suggests the *trans* relationship of the two stereogenic centres (thus 4*R**,5*S** relative configuration).

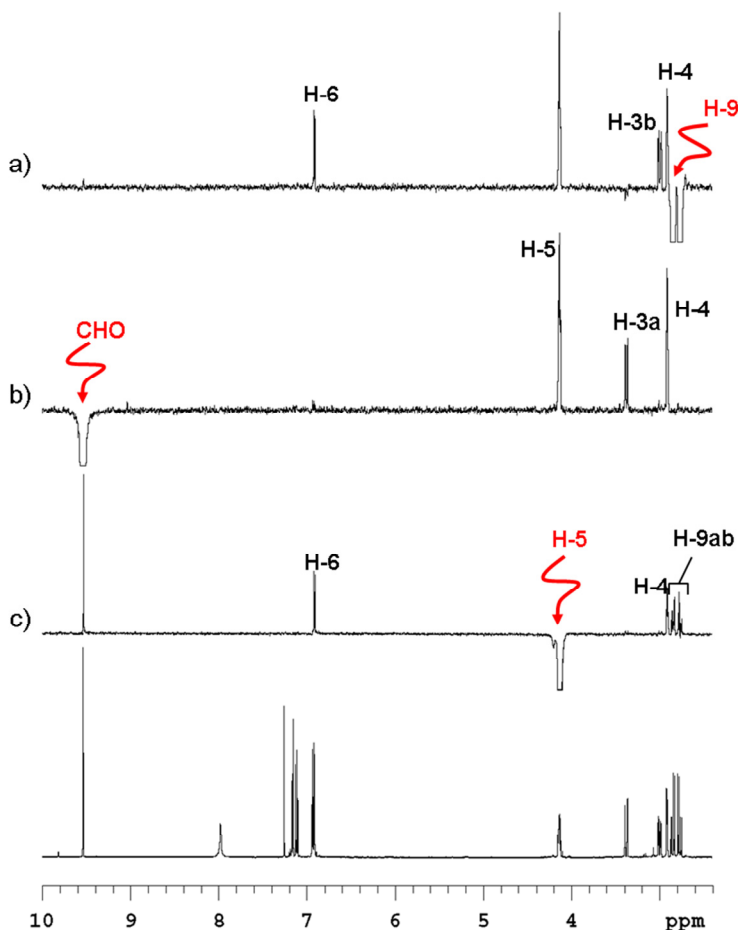
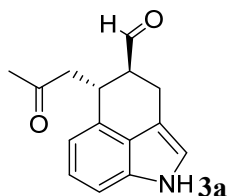


Figure 64. DPGSE-NOE spectra of **3a** (600 MHz in CDCl_3). (*Bottom*) ^1H -NMR control spectrum; trace *a*) saturation of H-9; trace *b*) saturation of CHO; trace *c*) saturation of H-5.

Although the rigidity of the heterocyclic core of compound **3a** helps in the reduction of the number of conformations to be considered,¹⁴ the conformational degrees of freedom due to the rotation of the aldehyde and CH_2COCH_3 moieties represent a challenging issue for the conformational analysis step. As the first stage, we performed a

conformational search on compound **3a**, with the 4*R**,5*S**relative configuration. The whole conformational space was explored by means of Monte Carlo searching together with the MMFF94 molecular mechanics force field as implemented in Titan 1.0.5 (Wavefunctioninc.)



All the conformations found by MM search within a 10 kcal/mol window were then optimized using DFT at the B3LYP/6-31G(d) level using the Gaussian 09 suite of programs. The harmonic vibrational frequencies of each optimized conformation were calculated at the same level to confirm their stability (no imaginary frequencies were observed) and to evaluate the free energy of each conformation. After DFT minimization, five conformations were found to be enclosed in a 2 kcal/mol window, as reported in Figure 65 and Table 12. All of them exhibit the same shape of the six-membered ring, that corresponds to a pseudo boat conformation where both the aldehyde and the CH_2COCH_3 moiety occupies a pseudo-axial position. Conformation **b** differs from **a** because of the different disposition of the ketone chain, and they both have the CH of the aldehyde pointing towards the H-5. Conformations **c** and **d** have a different orientation of the aldehyde moiety, so the CH of the aldehyde is pointing toward H-3_a. The relative internal and free energies suggested that all these conformations should be populated (Figure 65).

To check whether a different theoretical level provide different results, the four ground states were optimized again at the M06-2X/6-31+G(d,p) level obtaining similar results. Conformation **a** is always the most stable,

150

and **d** the less stable, whereas the energies of **b** and **c** are reversed on varying the theoretical level of calculation.

Table 12. Relative energies of the four conformations of 3a evaluated using ZPE-corrected free energies and different optimization levels: B3LYP/6-31G(d) and M06-2X/6-31+G(d,p). Populations are calculated using Boltzmann distribution at 298 K.

Conform.	G°	G°	Pop.	Pop.
	(B3LYP)	(M06-2X)	(B3LYP)	(M06-2X)
a	0.0	0.0	48	53
b	0.80	0.46	12	25
c	0.20	0.79	34	14
d	1.29	1.10	6	8

Albeit with different intensity, NMR spectra showed large NOE effects on H-5 and H-3_a when the CHO signal was saturated, thus confirming that both conformations of the CHO are populated in solution. The stronger NOE enhancement observed for H-5 confirms the conformational preference suggested by DFT calculations for the **a**-type conformation. The CHO-H₅ and CHO-H_{3a} calculated distances in conformations **a** and **c** are 2.30 and 2.33 Å respectively. Being the expected NOE almost equivalent, the observed difference can provide a good estimate of the experimental ratio of the conformations. The experimental NOE ratio was 63:37, that is matched very well by the ratio suggested by calculations (60:40 by B3LYP and 78:22 by M06-2X).

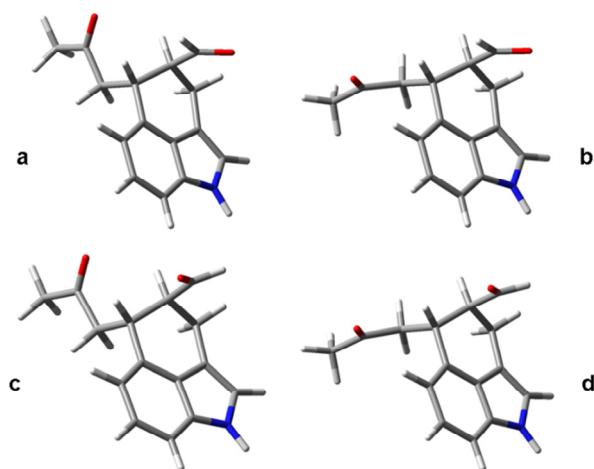


Figure 65. 3D view of the four conformations of the model compound 3a.

Having in hand the relative configuration and suitable experimental data supporting the preferred conformations, the assignment of the absolute configuration was tackled by ECD. The electronic excitation energies and rotational strengths have been calculated for the isolated molecule in the gas phase for the four conformation of **3a** using TD-DFT with four different methods (functionals), to ascertain if different computational approaches provide different shapes of the simulated spectra (see Figure 66). Simulations were performed with the four functionals: BH&HLYP,¹⁵ M06-2X,¹⁶ ω B97XD¹⁷ and CAM-B3LYP.¹⁸ The calculations employed the 6-311++G(2d,p) basis set that proved to be sufficiently accurate at a reasonable computational cost. Rotational strengths were calculated in both length and velocity representation, the resulting values being very similar (RMS differences < 5%). For this reason the errors due to basis set incompleteness should be very small, or negligible.¹⁹

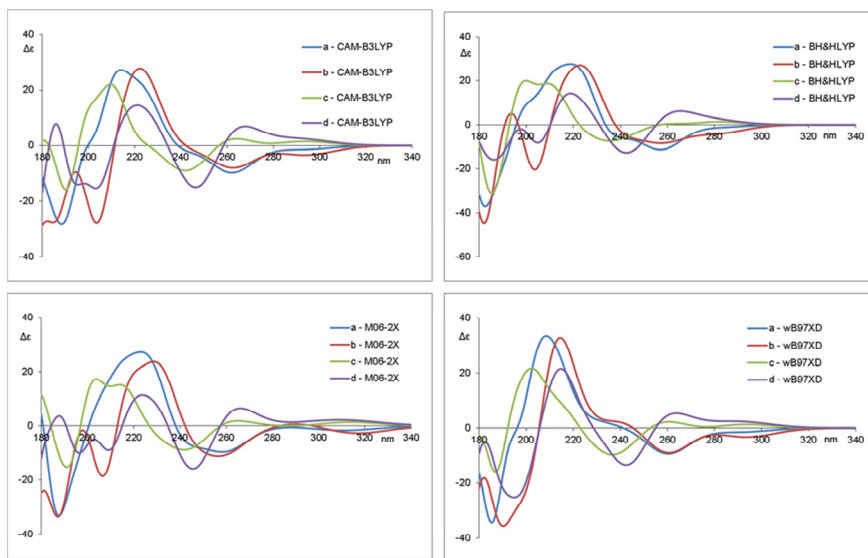


Figure 66. TD-DFT simulated spectra calculated for the four conformations of 3a using four different functionals (CAM-B3LYP, BH&HLYP, M06-2X, ω B97-XD) and the same 6-311++G(2d,p) basis set. For each conformation the first 50 excited states were calculated, and the spectrum was obtained using a 0.40 eV line width at half height.

Although the spectra simulated within the same functional for the four conformation are quite different, they are nevertheless consistent with the simulation of the positive Cotton effect at about 220 nm, and with the negative part in the 240-260 nm region. The almost coincidence of the simulated spectra for the same conformation on varying the functional represent a good proof of the simulations consistency.

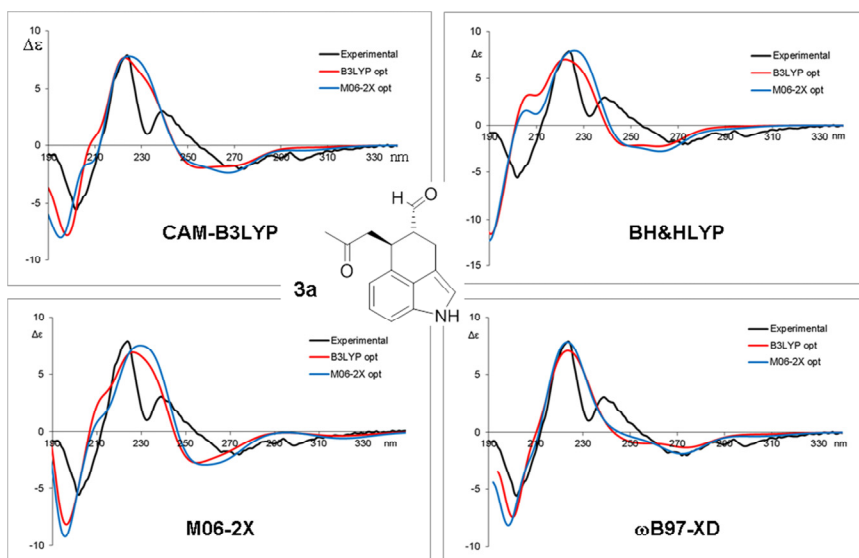


Figure 67. Simulations of the experimental ECD spectrum of **3a** (black traces). For each section, the black line corresponds to the experimental spectrum (acetonitrile solution, $1.5 \cdot 10^{-4}$ M, 0.2 cm path length $\Delta\epsilon$ in $\text{Mol L}^{-1} \text{cm}^{-1}$). The red lines correspond to the simulations obtained using the populations derived from B3LYP/6-31G(d) optimization. The blue lines correspond to the simulations obtained using the populations derived from M06-2X/6-31+G(d,p) optimization. The simulated spectra were vertically scaled and red-shifted by 7-14 nm to get the best match with the experimental spectrum. All the simulations are for the 4*R*, 5*S* absolute configuration.

The population-weighted spectra to be compared with the experimental spectrum were obtained using the percentages of Table 12. As shown in Figure 67, the simulated spectra match well the Cotton effects at 224 nm and 270 nm when the 4*R*, 5*S* absolute configuration is assumed in the calculations. The best simulation was obtained by the ω B97-XD functional, but all the simulated spectra show a good agreement with the experimental one. It has to be noted that the simulated spectra derived from the conformational geometries and energies obtained with

B3LYP/6-31G(d) optimization have the same level of accuracy with respect to those obtained with the more recent and computationally heavier M06-2X/6-31+G(d,p) optimization level. This seems to confirm the good performance of B3LYP in the conformational analysis of organic molecules.

Compounds 6

Due to the epimerization process observed in the Robinson annulation of **3a** to compounds *cis-6* and *trans-6*, the determination of their relative and absolute configuration was desirable. During the reaction, only the stereogenic centre in position 4 of **3a** could be racemized. Being more conformationally constrained by the tetracyclic scaffold, compounds *cis-6a* and *trans-6* are very rigid. This helps in the conformational analysis to reduce the populated conformations.

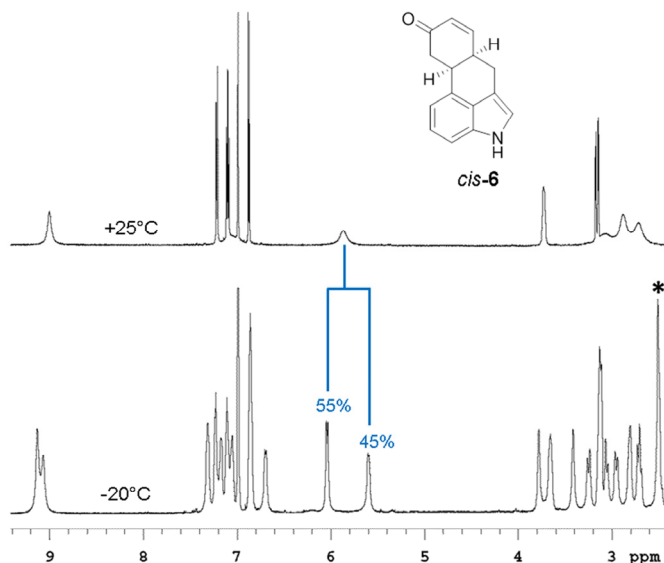


Figure 68. ^1H spectra of compound *cis-6* (600 MHz in CD_3CN). (Top) ambient temperature spectrum. (Bottom) spectrum recorded at -20°C . The asterisk indicates the water signal of the solvent.

The two diastereoisomers *cis-6a* and *trans-6* were separated by means of semi-preparative HPLC on a C18 column (Phenomenex® Synergi Hydro-RP) using Acetonitrile/H₂O 70:30. The ¹H spectra of the first eluted peak showed very broad lines in the aliphatic part and for the two vinylic hydrogens (see Figure 68, top trace). On lowering the temperature these lines broaden further and they eventually split at -20°C into two set of signals in a 55:45 ratio (Figure 68, bottom). This dynamic behaviour can be explained considering the optimized structures of the two diastereoisomers. In the case of *trans-6* isomer a single conformation should be populated. In this conformation the two bridgehead hydrogens occupy the pseudo-axial positions. In the case of the *cis-6* isomer, the same hydrogens occupy one pseudo-axial and one pseudo-equatorial position, thus two conformation obtained by exchanging the positions of these hydrogens can be envisaged (Figure 69).

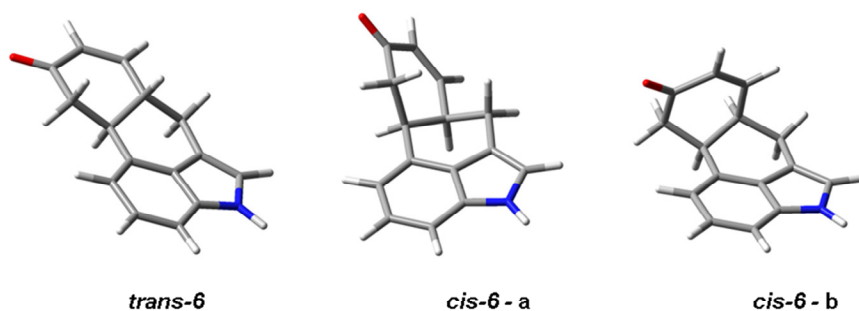


Figure 69. Optimized structures for the ground state conformations of *trans-6* and *cis-6*.

The conformational search found only one conformation for the *trans-6* isomer, and confirmed that both the proposed conformation of *cis-6* corresponded to energy minima. When optimized at the M06-2X/6-31G(d) level, the two conformations of the *cis* isomer were found to be

very close in energy (0.67 kcal/mol), and the transition state for their interconversion was found to be 14.1 kcal/mol. This explains the dynamic behaviour observed in the NMR spectra of the first eluted compound, that can be thus assigned to the *cis*-6 isomer. The *trans*-6 isomer was calculated to be slightly more stable than the *cis* (0.33 kcal/mol). When the calculation of the two ground states of *cis*-6 were repeated using a larger basis set and including the solvent (acetonitrile) in the calculations (PCM-M06-2X/6-31+G(d,p)), the energy difference between the two conformations reduced to 0.05 kcal/mol, thus reproducing well also the experimentally observed ratio.

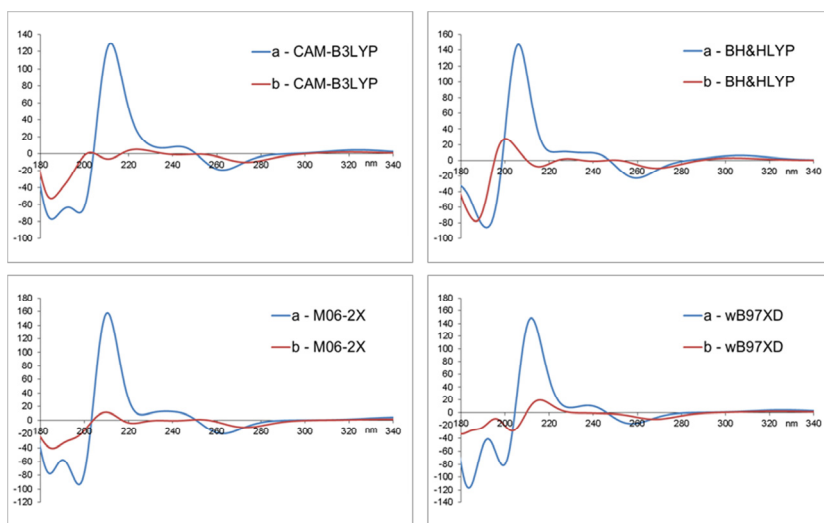


Figure 70. TD-DFT simulated spectra calculated for the two conformations of *cis*-6 using four different functionals (CAM-B3LYP, BH&HLYP, M06-2X, ω B97XD) and the same 6-311++G(2d,p) basis set. For each conformation the first 50 excited states were calculated, and the spectrum was obtained using a 0.40 eV line width at half height. All the simulations are for the 6aR,10aS absolute configuration.

As said before, compound *cis-6* is very rigid and the exact ratio of the two populated conformations can be provided by low-temperature NMR. For this reason the simulation of the ECD spectrum is straightforward. Having already established the absolute configuration of **3a**, a new assignment of the absolute configuration could appear an overkill, but it is not. Compound **3a** had a considerable conformational mobility while **6a** is rigid. The stereogenic centre at C-5 of **3a** should be left unchanged, but the reaction conditions are severe. For these reasons the independent assignment of the absolute configuration of *cis-6* provides a validation about the retention of configuration at C-5. As for **3a**, the electronic excitation energies and rotational strengths have been calculated for the isolated molecule in the gas phase for the two conformations of *cis-6* using TD-DFT with CAM-B3LYP, BH&HLYP, M06-2X, ω B97XD and the 6-311++G(2d,p) (Figure 70). Although the experimental assignment of the two conformations of *cis-6* is not available, the ratio is very close to 50:50. Moreover, the spectrum simulated for the **b** conformation is very weak. For these reason the spectrum resulting from Boltzmann distribution does not change on reversing the conformers population. All the simulated spectra agree well with the 6a*R*,10a*S* absolute configuration. Taking into account the different numbering of *cis-6*, the 10a*S* configuration matches the 5*S* configuration of the starting compound **3a**.

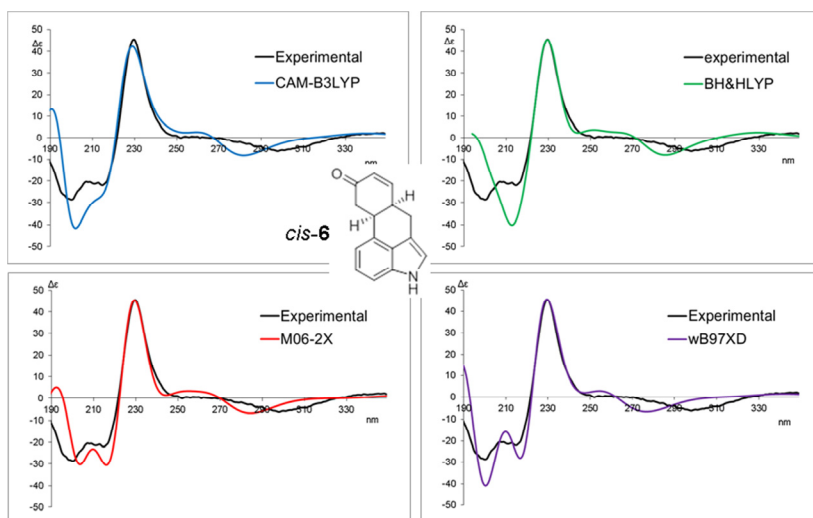


Figure 71. Simulations of the experimental ECD spectrum of *cis-6* (black traces). For each section, the black line correspond to the experimental spectrum (acetonitrile solution, $1.5 \cdot 10^{-4}$ M, 0.2 cm path length, $\Delta\epsilon$ in $\text{Mol L}^{-1} \text{cm}^{-1}$). The simulated spectra were vertically scaled and red-shifted by 7-18 nm to get the best match with the experimental spectrum. All the simulations are for the 6*aR*,10*aS* absolute configuration.

References

- ¹ Caruana, L.; Fochi, M.; Comes Franchini, M.; Ranieri, S.; Mazzanti, A.; Bernardi, L. *Chem. Commun.* **2014**, 50, 445 – 447.
- ² For reviews, see: a) Grondal, C.; Jeanty, M.; Enders, D. *Nat. Chem.* **2010**, 2, 167 – 178. b) H. Pellissier, *Adv. Synth. Catal.* **2012**, 354, 237 – 294. c) Gouedranche, S.; Raimondi, W.; Bugaut, X.; Costantieux, T.; Bonne, D.; Rodriguez, J. *Synthesis* **2013**, 45, 1909 – 1930. d) Walji, A. M.; MacMillan, D. W. C. *Synlett* **2007**, 10, 1477 – 1489.
- ³ a) Bhanja, C.; Jena, S.; Nayak, S.; Mohapatra, S. *Beilstein J. Org. Chem.* **2012**, 8, 1668 – 1694. b) Wang, W.; Li, H.; Wang, J.; Zu, L. *J. Am. Chem. Soc.* **2006**, 128, 10354 – 10355. c) Wang, J.; Xie, H.; Li, H.; Zu, L.; Wang, W. *Angew.*

Chem. Int. Ed. **2008**, 47, 4177 – 4179. *d)* Hou, W.; Zheng, B.; Chen, J.; Peng, Y. *Org. Lett.* **2012**, 14, 2378 – 2381.

⁴ *a)* Enders, D.; Wang, C.; W.; Bats, J. *Synlett* **2009**, 11, 1777 – 1780. *b)* Enders, D.; Hahn, R.; Atodiresei, I. *Adv. Synth. Catal.* **2013**, 355, 1126 – 1136.

⁵ Landmark reports: *a)* Huang, Y.; Walji, A. M.; Larsen, C. H.; MacMillan, D. W. C. *J. Am. Chem. Soc.* **2005**, 127, 15051 – 15053. *b)* Marigo, M.; Schulte, T.; Franzén, J.; Jørgensen, K. A. *J. Am. Chem. Soc.* **2005**, 127, 15710 – 15711. *c)* Yang, J. W.; Fonseca, M. T. H.; List, B. *J. Am. Chem. Soc.* **2005**, 127, 15036 – 15037. *d)* Enders, D.; Hüttl, M. R. M.; Grondal, C.; Raabe, G. *Nature* **2006**, 441, 861 – 863. *e)* Melchiorre, P.; Marigo, M.; Carlone, A.; Bartoli, G. *Angew. Chem. Int. Ed.* **2008**, 47, 6138 – 6171.

⁶ *a)* Austin, J. F.; MacMillan, D. W. C. *J. Am. Chem. Soc.* **2002**, 124, 1172 – 1173. *b)* Hong, L.; Wang, L.; Chen, C.; Zhang, B.; Wang, R. *Adv. Synth. Catal.* **2009**, 351, 772 – 778. *c)* Rueping, M.; Nachtsheim, B. J. *Beilstein J. Org. Chem.* **2010**, 6, 6.

⁷ *a)* Hechavarria Fonseca, M. T.; List, B. *Angew. Chem., Int. Ed.* **2004**, 43, 3958 – 3960. *b)* Hayashi, Y.; Gotoh, H.; Tamura, T.; Yamaguchi, H.; Masui, R.; Shoji, M. *J. Am. Chem. Soc.* **2005**, 127, 16028 – 16029.

⁸ *a)* Schardl, C. L.; Panaccione D. G.; Tudzynski, P. *The Alkaloids*, ed. G. A. Cordell, Elsevier, **2006**, vol. 63, pp. 45–86. *b)* Somei, M.; Yokoyama, Y.; Murakami, Y.; Ninomiya, I.; Kiguchi, T.; Naito, T. *The Alkaloids*, ed. G. A. Cordell, Academic Press, San Diego, **2000**, vol. 54, pp. 191–257.

⁹ Xiong, Q.; Zhu, X.; Wilson, W. K.; Ganesan, A.; Matsuda, S. P. T. *J. Am. Chem. Soc.* **2003**, 125, 9002 – 9003.

¹⁰ Eder, U.; Sauer, G.; Wiechert, R. *Angew. Chem. Int. Ed.* **1971**, 10, 496 – 497.

¹¹ Hooft, R. W. W.; Stravera, L. H.; Spek, A. L. *J. Appl. Cryst.* **2008**, 41, 96 – 103.

¹² Bijvoet, J. M.; Peerdeman, A. F.; Van Bommel, A. J. *Nature* **1951**, 168, 271 – 272.

-
- ¹³ Stott, K.; Stonehouse, J.; Keeler, J.; Hwang, T-L.; Shaka, A. J. *J. Am. Chem. Soc.* **1995**, 117, 4199 – 4200.
- ¹⁴ Polavarapu, P. L.; Donahue, E. A.; Shanmugam, G.; Scalmani, G.; Hawkins, E. K.; Rizzo, C.; Ibnusaud, I.; Thomas, G.; Habeland, D.; Sebastian, D. *J. Phys. Chem. A* **2011**, 115, 5665 – 5673.
- ¹⁵ In Gaussian 09 the BH&HLYP functional has the form: $0.5 * E_X^{HF} + 0.5 * E_X^{LSDA} + 0.5 * \Delta E_X^{Becke88} + E_C^{LYP}$
- ¹⁶ Zhao, Y.; Truhlar, D. G. *Theor. Chem. Acc.* **2008**, 120, 215 – 241.
- ¹⁷ Chai, J-D.; Head-Gordon, M. *Phys. Chem. Chem. Phys.* **2008**, 10, 6615 – 6620.
- ¹⁸ Yanai, T.; Tewand, D.; Handy, N. *Chem. Phys. Lett.* **2004**, 393, 51 – 57.
- ¹⁹ Stephens, P. J.; McCann, D. M.; Devlin, F. J.; Cheeseman, J. R.; Frisch, M. J. *J. Am. Chem. Soc.* **2004**, 126, 7514 – 7521.

Experimental section

Atropisomers of arylmaleimides

Materials

3,4-Dibromo-1*H*-pyrrole-2,5-dione, benzyl bromide, 1-bromo-2-methylnaphthalene, *n*-butyllithium, and the boronic acids **2a–e** were commercially available. 2-Methylnaphthylboronic acid¹ and 3,4-dibromo-1-benzylpyrrole-2,5-dione² were prepared according to known procedures. Diethyl ether and THF have been dried before use by distillation on Na/benzophenone. Chromatography employed the following stationary phases: silica gel 60 F254 for the TLC and silica gel 60 Å (230–400 mesh) for prepurification. All reactions were performed in dried glassware and under dry nitrogen atmosphere. Glassware was dried at 70 °C for at least 3 h before use. A Phenomenex Luna C18 (10 µm, 100 Å, 250 × 21.2 mm) semipreparative column was used to purify the compounds using mixtures of CH₃CN and H₂O as eluent. Enantioselective HPLC columns were used to separate the stable atropisomers of **4f** and **3f** (Phenomenex LUX-cellulose-2 250 × 10 mm and Daicel Chiralpak AD-H 250 × 21.2 mm, respectively). Detection wavelength was 254 nm. NMR spectra were recorded using a spectrometer operating at a field of 14.4 T (600 MHz for ¹H, 150.8 for ¹³C). Chemical shifts are given in ppm relative to the internal standards

¹ Joyce, R. P.; Gainor, J. A.; Weinreb, S. M. *J. Org. Chem.* **1987**, 52, 1177 – 1185.

² Thompson, W. J.; Gaudino, J. *J. Org. Chem.* **1984**, 49, 5237 – 5243. See also: Pathak, R.; Nhlapo, J. M.; Govender, S.; Michael, J. P.; Van Otterlo, W. A. L.; De Koning, C. B. *Tetrahedron* **2006**, 62, 2820 – 2830.

tetramethylsilane (^1H and ^{13}C) or relative to the residual peak of the solvents. The 600 MHz ^1H spectra were acquired using a 5 mm dual direct probe with a 9000 Hz spectral width, 2.0 μs (20° tip angle) pulse width, 3 s acquisition time, and 1 s delay time. A shifted sine bell weighting function equal to the acquisition time (i.e., 3 s) was applied before the Fourier transformation. The 150.8 MHz ^{13}C spectra were acquired under proton decoupling conditions with a 38000 Hz spectral width, 4.2 μs (60° tip angle) pulse width, 1 s acquisition time and 1 s delay time. A line broadening function of 1–2 Hz was applied before the Fourier transformation. Assignment of the carbons multiplicity were obtained by means of the DEPT sequences.

General Synthetic Procedure

1-Benzyl-3,4-dibromo-1*H*-pyrrole-2,5-dione (**1**) (1 mmol) was dissolved in dry THF (5 mL), and then the appropriate boronic acid (2 mmol), cesium carbonate (2.5 mmol), and the palladium catalyst $\text{Pd}(\text{PPh}_3)_4$ or $\text{Pd}(\text{OAc})_2$ were added. The stirred solution was kept at reflux for 2 h or at 40°C overnight (Table 13 summarizes the experimental conditions). Et_2O and H_2O were then added, and the extracted organic layer was dried (Na_2SO_4), filtered on silica gel, and concentrated at reduced pressure. The crude products were purified by semipreparative HPLC on C18 column to obtain analytically pure samples of **3a–f** and **4a–f**.

1-Benzyl-3-bromo-4-(*o*-tolyl)-1*H*-pyrrole-2,5-dione (**3a**).

Yield: 0.104 g (30%) as a white waxy solid.

^1H NMR (600 MHz, CD_2Cl_2 , 5.33 ppm, 25°C): δ 2.27 (s, 3 H), 4.79 (s, 2 H), 7.22 (d, $J = 7.7$ Hz, ^1H), 7.28–7.44 (m, 8H).

^{13}C NMR (150.8 MHz, CD_2Cl_2 , 54.0 ppm, 25°C): δ 20.6 (CH_3), 43.1 (CH_2), 12.3 (CH), 127.1 (Cq), 128.0 (Cq), 128.5 (CH), 128.9 (2 CH), 164

129.3 (2 CH), 129.8 (CH), 130.8 (CH), 131.3 (CH), 136.6 (Cq), 137.7 (Cq), 144.3 (Cq), 165.7 (Cq), 168.6 (Cq).

HPLC: CH₃CN/H₂O 82:18 v/v, *t_R* = 7.78 min. HRMS (EI): *m/z* calcd for C₁₈H₁₄BrNO₂ [M⁺] 355.02079, found 355.0210.

Table 13. Summary of the Synthetic Details

Entry (yield %)	Entry (yield %)	catalyst	temp (°C)	time (h)
3a (30)	4a (32)	Pd(PPh ₃) ₄	reflux	2
3b (37)	4b (18)	Pd(OAc) ₂	40	overnight
3c (35)	4c (30)	Pd(OAc) ₂	reflux	2
3d (27)	4d (10)	Pd(PPh ₃) ₄	40	overnight
3e (28)	4e (20)	Pd(OAc) ₂	reflux	2
3f (13)	4f (6)	Pd(OAc) ₂	reflux	2

1-Benzyl-3,4-di-*o*-tolyl-1*H*-pyrrole-2,5-dione (4a)

Yield: 0.118 g (32%) as a white amorphous solid.

¹H NMR (600 MHz, CD₂Cl₂, 5.33 ppm, 25 °C): δ 2.06 (s, 6 H), 4.84 (s, 2 H), 7.09 (d, *J* = 7.6 Hz, 2 H), 7.17 (t, *J* = 7.6 Hz, 2 H), 7.21 (d, *J* = 7.6 Hz, 2 H), 7.29 (td, *J* = 7.6, 1.1 Hz, 2 H), 7.31 - 7.35 (m, 1 H), 7.38 (t, *J* = 7.43 Hz, 2 H), 7.44 (d, *J* = 7.1 Hz, 2 H).

¹³C NMR (150.8 MHz, CD₂Cl₂, 54.0 ppm, 25 °C): δ 20.6 (2 CH₃), 42.6 (CH₂), 126.2 (2 CH), 128.3 (CH), 128.7 (2 CH), 129.2 (2 CH), 129.4 (2 Cq), 130.1 (2 CH), 130.6 (bs, 2 CH), 131.2 (2 CH), 137.3 (2 Cq), 137.7 (Cq), 141.1 (2 Cq), 170.8 (2 Cq).

HPLC: CH₃CN/H₂O 82:18 v/v, *t_R* = 10.58 min. HRMS (EI): *m/z* calcd for C₂₅H₂₁NO₂ [M⁺] 367.15723, found 367.1572.

1-Benzyl-3-bromo-4-(2-ethylphenyl)-1H-pyrrole-2,5-dione (3b).

Yield: 0.135 g (37%) as a white waxy solid.

^1H NMR (600 MHz, $\text{C}_2\text{D}_2\text{Cl}_4$, 6.00 ppm, 25 °C): δ 1.17 (t, $J = 7.5$ Hz, 3 H), 2.55 (q, $J = 7.5$ Hz, 2 H), 4.80 (bs, benzylic CH_2), 7.18 (d, $J = 7.6$ Hz, 1 H), 7.30-7.42 (m, 7 H), 7.48 (t, $J = 7.6$, 1 H).

^{13}C NMR (150.8 MHz, $\text{C}_2\text{D}_2\text{Cl}_2$, 74.0 ppm, 25 °C): δ 15.25 (CH_3), 26.9 (CH_2), 42.8 (CH_2), 126.1 (CH), 126.6 (Cq), 126.9 (CH), 128.3 (CH), 128.6 (CH), 129.0 (2 CH), 129.4 (CH), 130.7 (Cq), 135.8 (Cq), 143.1 (Cq), 144.2 (Cq), 165.2 (Cq), 168.4 (Cq).

HPLC: $\text{CH}_3\text{CN}/\text{H}_2\text{O}$ 82:18 v/v, $t_{\text{R}} = 9.25$ min. HRMS (EI): calcd for $\text{C}_{19}\text{H}_{16}\text{BrNO}_2$ [M^{+}] 369.03644, found 369.0360.

1-Benzyl-3,4-bis(2-ethylphenyl)-1H-pyrrole-2,5-dione (4b).

Yield: 0.070 g (18%) as a white amorphous solid.

^1H NMR (600 MHz, CD_3CN , 1.96 ppm, 60 °C): δ 1.07 (t, $J = 7.6$ Hz, 6 H), 2.49 (q, $J = 7.6$ Hz, 4 H), 4.82 (s, 2 H), 7.11 (d, $J = 7.7$ Hz, 2 H), 7.17 (t, $J = 7.6$ Hz, 2 H), 7.30 – 7.37 (m, 5 H), 7.40 (bd, 4 H).

^{13}C NMR (150.8 MHz, CD_3CN , 118.3 ppm, 60 °C): δ 15.2 (2 CH_3), 27.3 (2 CH_2), 43.1 (CH_2), 126.8 (2 CH), 128.8 (2CH), 128.9 (CH), 129.6 (2 Cq), 129.7 (2 CH), 129.9 (2 CH), 130.9 (2 CH), 131.3 (2 CH), 138.4 (Cq), 142.6 (2Cq), 144.5 (2 Cq), 171.9 (2 Cq).

HPLC: $\text{CH}_3\text{CN}/\text{H}_2\text{O}$ 82:18v/v, $t_{\text{R}} = 15.10$ min. HRMS (EI): m/z calcd for $\text{C}_{27}\text{H}_{25}\text{NO}_2$ [M^{+}] 395.18853, found 395.1881.

1-Benzyl-3-bromo-4-(2,3-dimethylphenyl)-1H-pyrrole-2,5-dione (3c).

Yield: 0.130 g (35%) as a white waxy solid.

^1H NMR (600 MHz, $\text{C}_2\text{D}_2\text{Cl}_4$, 6.00 ppm, 25 °C): δ 2.16 (s, 3 H), 2.35 (s, 3 H), 4.78 (d, $J = 14.59$ Hz, 1 H), 4.82 (d, $J = 14.59$ Hz, 1 H), 7.09 (d, $J = 7.6$ Hz, 1 H), 7.235 (t, $J = 7.6$ Hz, 1 H), 7.28 – 7.44 (m, 6 H).

^{13}C NMR (150.8 MHz, $\text{C}_2\text{D}_2\text{Cl}_4$, 74.0 ppm, 25 °C): δ 18.0 (CH_3), 20.5 (CH_3), 42.7 (CH_2), 125.8 (CH), 126.3 (Cq), 127.1 (CH), 128.3 (2 CH), 129.0 (2 CH), 132.0 (Cq), 135.6 (Cq), 135.8 (Cq), 138.2 (Cq), 144.2 (Cq), 165.3 (Cq), 168.5 (Cq).

HPLC: $\text{CH}_3\text{CN}/\text{H}_2\text{O}$ 82:18 v/v, $t_{\text{R}} = 9.20$ min. HRMS (EI): m/z calcd for $\text{C}_{19}\text{H}_{16}\text{BrNO}_2 [\text{M}^+]$ 369.03644, found 369.0358.

1-Benzyl-3,4-bis(2,3-dimethylphenyl)-1H-pyrrole-2,5-dione (4c).

Yield: 0.118 g (30%) as a white amorphous solid.

^1H NMR (600 MHz, CDCl_3 , 50 °C): δ 1.96 (s, 6 H), 2.22 (s, 6 H), 4.83 (s, 2 H), 6.88 (bd, 2 H), 7.02 (bt, 2 H), 7.12 (bd, 2 H), 7.21 – 7.40 (m, 3 H), 7.45 (bd, 2 H).

^{13}C NMR (150.8 MHz, CDCl_3 , 77.0 ppm, 50 °C): δ 17.4 (2 CH_3), 20.2 (2 CH_3), 42.2 (CH_2), 125.5 (2 CH), 127.8 (3 CH), 128.6 (2 CH), 128.7 (2 CH), 128.9 (2 Cq), 131.0 (2 CH), 135.4 (2 Cq), 136.7 (Cq), 137.4 (2 Cq), 141.2 (2 Cq), 170.4 (2 Cq).

HPLC: $\text{CH}_3\text{CN}/\text{H}_2\text{O}$ 82:18 v/v, $t_{\text{R}} = 14.51$ min. HRMS (EI): m/z calcd for $\text{C}_{27}\text{H}_{25}\text{NO}_2 [\text{M}^+]$ 395.18853, found 395.1880.

1-Benzyl-3-bromo-4-(2-isopropylphenyl)-1H-pyrrole-2,5-dione (3d).

Yield: 0.104 g (27%) as a white waxy solid.

^1H NMR (600 MHz, $\text{C}_2\text{D}_2\text{Cl}_4$, 6.00 ppm, 25 °C): δ 1.18 (d, $J = 6.7$ Hz, 3 H), 1.24 (d, $J = 6.7$ Hz, 3 H), 2.69 (sett, $J = 6.7$ Hz, 1 H), 4.77 (d, $J = 14.6$ Hz, 1 H), 4.81 (d, $J = 14.6$ Hz, 1 H), 7.13 (d, $J = 7.7$ Hz, 1 H), 7.30 (t, $J = 7.5$ Hz, 1 H), 7.32–7.42 (m, 5 H), 7.43–7.52 (m, 2 H).

^{13}C NMR (150.8 MHz, $\text{C}_2\text{D}_2\text{Cl}_4$, 74.0 ppm, 25 °C): δ 23.9 (CH_3), 24.5 (CH_3), 31.9 (CH), 42.8 (CH_2), 126.0 (Cq), 126.1 (CH), 126.2 (CH), 127.1 (Cq), 128.3 (CH), 128.6 (2 CH), 129.0 (2 CH), 129.2 (CH), 130.8 (CH), 135.8 (Cq), 144.6 (Cq), 148.0 (Cq), 165.2 (Cq), 168.5 (Cq).

HPLC:CH₃CN/H₂O 82:18 v/v, t_R = 12.15 min. HRMS (EI): m/z calcd for C₂₀H₁₈BrNO₂ [M⁺] 383.05209, found 383.0525.

1-Benzyl-3,4-bis(2-isopropylphenyl)-1H-pyrrole-2,5-dione (4d).

Yield: 0.042 g (10%) as a white amorphous solid. NMR spectra showed the presence of the two conformations *syn* (49%) and *anti* (51%).

¹H NMR (600 MHz, CDCl₃, 0 °C): δ 0.72 (d, 6 H *anti*, J = 6.4 Hz), 0.81 (d, 6 H *syn*, J = 6.4 Hz), 1.145 (d, 6 H *anti*, J = 6.4 Hz), 1.22 (d, 6 H *syn*, J = 6.4 Hz), 2.65 (quint, 2 H *anti*, J = 6.4 Hz), 2.70 (quint, 2 H *syn*, J = 6.8 Hz), 4.79 (d, 1 H *anti*, J = 14.5 Hz), 4.835 (s, 2 H *syn*), 4.88 (d, 1 H *anti*, J = 14.5 Hz), 6.99 (bt, 4 H), 7.08 – 7.16 (m, 4 H), 7.24 – 7.40 (m, 14 H), 7.49 (bt, 4 H).

¹³C NMR (150.8 MHz, CDCl₃, 77.0 ppm, 0 °C): δ 23.0 (2 CH₃), 23.2 (2 CH₃), 24.7 (2 CH₃), 25.1 (2 CH₃), 31.1 (4 CH), 42.15 (CH₂), 42.2 (CH₂), 125.6 (2 CH), 125.7 (2 CH), 126.1 (2 CH), 126.4 (2 CH), 126.6 (2 Cq), 126.7 (2 Cq), 127.8 (2 CH), 128.7 (4 CH), 128.8 (2 CH), 128.9 (2 CH), 129.8 (2 CH), 129.9 (2 CH), 129.9 (2 CH), 130.4 (2 CH), 136.4 (2 Cq), 136.5 (2 Cq), 140.3 (2 Cq), 140.6 (2 Cq), 147.7 (2 Cq), 148.0 (2 Cq), 170.6 (4 Cq).

HPLC: CH₃CN/H₂O 82:18 v/v, t_R = 21.34 min. HRMS (EI): m/z calcd for C₂₉H₂₉NO₂ [M⁺] 423.21983, found 423.2192.

1-Benzyl-3-bromo-4-(naphthalen-1-yl)-1H-pyrrole-2,5-dione (3e).

Yield: 0.110 (28%) as a white amorphous solid.

¹H NMR (600MHz, CDCl₃, 25 °C): δ 4.85 (s, 2 H), 7.29 – 7.4 (m, 3 H), 7.46 (d, J = 7.2 Hz, 2 H), 7.48 – 7.63 (m, 5 H), 7.92 (d, J = 8.3 Hz, 1 H), 7.995 (d, J = 8.3 Hz, 1 H).

¹³C NMR (150.8 MHz, CDCl₃, 77.0 ppm, 25 °C): δ 42.8 (CH₂), 124.9 (CH), 125.0 (Cq), 125.5 (CH), 126.5 (CH), 126.8 (CH), 127.1 (Cq), 128.2
168

(CH), 128.5 (CH), 128.81 (CH), 128.83 (2 CH), 128.9 (2 CH), 129.9 (Cq), 131.1 (CH), 133.6 (Cq), 135.8 (Cq), 142.4 (Cq), 165.1 (Cq), 168.4 (Cq).

HPLC: CH₃CN/H₂O 90:10 v/v, t_R = 5.94 min. HRMS (ESI-Orbitrap): m/z calcd for C₂₁H₁₅BrNO₂⁺ [M + H⁺] 392.02807, found 392.02914.

1-Benzyl-3,4-di(naphthalen-1-yl)-1H-pyrrole-2,5-dione (4e). Yield: 0.088 g (20%) as a white amorphous solid.

¹H NMR (600MHz, C₂D₂Cl₄, 6.00 ppm, 60 °C): δ 4.92 (s, 2 H), 7.24 (t, J = 7.6 Hz, 2 H), 7.32 – 7.38 (m, 7 H), 7.40 (t, J = 7.6 Hz, 2 H), 7.50 (d, J = 7.6 Hz, 2 H), 7.59 (bd, 2 H), 7.74 (d, J = 8.1 Hz, 2 H), 7.78 (d, J = 7.6 Hz, 2 H).

¹³C NMR (150.8 MHz, C₂D₂Cl₄, 74.0 ppm, 60 °C): δ 42.5 (CH₂), 125.1 (2 CH), 125.2 (2 CH), 126.1 (2 CH), 126.4 (2 CH), 126.6 (2 Cq), 127.9 (CH), 128.4 (2 CH), 128.5 (2 CH), 128.7 (2 CH), 128.8 (2 CH), 130.3 (2 CH), 130.7 (2 Cq), 133.4 (2 Cq), 136.5 (Cq), 140.4(2 Cq), 170.4 (2 Cq).

HPLC: CH₃CN/H₂O 90:10 v/v, t_R = 7.23 min. HRMS (ESI-Orbitrap): m/z calcd for C₃₁H₂₂NO₂⁺ [M + H⁺] 440.16451, found 440.16529.

1-Benzyl-3-bromo-4-(2-methylnaphthalen-1-yl)-1H-pyrrole-2,5-dione (3f).

Yield: 0.053 g (13%) as white amorphous solid.

¹H NMR (600 MHz, CDCl₃, 25 °C): δ 2.37 (s, 3 H), 4.87 (s, 2 H), 7.30 – 7.36 (m, 1 H), 7.37 – 7.40 (m, 2 H), 7.41 – 7.49 (m, 6 H), 7.86 – 7.90 (m, 2 H).

¹³C NMR (150.8 MHz, CDCl₃, 77.0 ppm, 25 °C): δ 20.6 (CH₃), 42.8 (CH₂), 123.2 (Cq), 124.3 (CH), 125.6 (CH), 127.0 (CH), 128.1 (CH), 128.4 (CH), 128.5 (3 CH), 128.8 (2 CH), 129.2 (Cq), 130.2 (CH), 130.6

(Cq), 131.8 (Cq), 135.2 (Cq), 135.8 (Cq), 143.6 (Cq), 164.9 (Cq), 168.0 (Cq).

ChiralPak AD-H (5 μm , 250 \times 20 mm, 20 mL/min, 254 nm, 25 $^{\circ}\text{C}$) semipreparative HPLC column has been used for the separation of the atropisomers and for the kinetic study; hexane/2-propanol 90:10 v/v, t_{R} = 6.89 and 9.55 min. HRMS (ESI-Orbitrap): m/z calcd for $\text{C}_{22}\text{H}_{17}\text{BrNO}_2^+$ [$\text{M} + \text{H}^+$] 406.04372, found 406.04453.

1-Benzyl-3,4-bis(2-methylnaphthalen-1-yl)-1*H*-pyrrole-2,5-dione (4f).

Total yield (as *syn anti*): 0.028 g (6%) as slightly yellow waxy solid.

Syn. ^1H NMR (600 MHz, CDCl_3 , -10 $^{\circ}\text{C}$): δ 2.24 (s, 6 H), 4.95 (s, 2 H), 7.12 (t, $J = 7.6$ Hz, 2 H), 7.20 (d, $J = 8.3$, 2 H), 7.27 – 7.29 (m, 2 H), 7.34 – 7.42 (m, 3 H), 7.51 (d, $J = 7.0$ Hz, 2 H), 7.60 (d, $J = 8.6$ Hz, 2 H), 7.64 – 7.70 (m, 4 H).

^{13}C NMR (150.8 MHz, CDCl_3 , 77.00 ppm, -10 $^{\circ}\text{C}$): δ 21.13 (CH_3), 42.29 (CH_2), 124.30 (2 Cq), 124.80 (2 CH), 125.06 (2 CH), 126.11 (2 CH), 127.86 (CH), 128.15 (2 CH), 128.45 (2 CH), 128.59 (2 CH), 128.80 (2 CH), 129.71 (2 CH), 131.00 (2 Cq), 131.58 (2 Cq), 135.41 (2 Cq), 136.44 (Cq), 141.92 (2 Cq), 170.13 (2 Cq).

Anti. ^1H NMR (600 MHz, CDCl_3 , -10 $^{\circ}\text{C}$): δ 2.03 (s, 6 H), 4.95 (AB system, $J = 14.75$ Hz, 2 H), 7.15 (d, $J = 8.44$ Hz, 2 H), 7.27 – 7.42 (m, 7 H), 7.52 (d, $J = 7.73$ Hz, 2 H), 7.56 (d, $J = 7.73$ Hz, 2 H), 7.69 (d, $J = 8.5$ Hz, 2 H), 7.72 – 7.76 (m, 2 H).

^{13}C NMR (150.8 MHz, CDCl_3 , 77.0 ppm, -10 $^{\circ}\text{C}$): δ 21.5 (CH_3), 42.3 (CH_2), 124.1 (2 Cq), 125.0 (2 CH), 125.2 (2 CH), 126.2 (2 CH), 127.9 (CH), 128.3 (2 CH), 128.5 (2 CH), 128.6 (2 CH), 128.8 (2 CH), 129.7 (2 CH), 131.0 (2 Cq), 131.7 (2 Cq), 136.0 (2 Cq), 136.4 (Cq), 142.2 (2 Cq), 170.3 (2 Cq).

Lux Cellulose-2 HPLC column was used to separate the three stereoisomers. (5 μm , 100 \AA , 250 \times 10.00 mm, hexane/2-propanol 90:10 v/v, 5 mL/min, detection at 254 nm, 25 $^{\circ}\text{C}$); $t_{R\text{syn}}$ = 15.88 min, $t_{R\text{anti}}$: 12.62 and 16.92 min. HRMS (ESI-Orbitrap): m/z calcd for $\text{C}_{33}\text{H}_{26}\text{NO}_2^+$ $[\text{M} + \text{H}^+]$ 468.19581, found 468.19726.

Atropisomers of 4-arylpyrazolo[3,4-b]pyridines

Materials

Compounds **1** and **2** were known and compounds **3** –**6** were prepared as reported in the literature.³

n-Butyllithium (1.6 M in hexane), dimethylformamide, 4,4,4-trifluoroacetoacetic acid ethylester, 3-isopropylbenzaldehyde, 3,5-dimethylacetophenone, 5-amino-3-methyl-1-phenylpyrazole, and L-proline were commercially available. 1-(3,5-Dimethylphenyl)-4,4,4-trifluoro-1,3-butanedione was prepared according to the literature.⁴ Diisopropylamine was freshly distilled from CaH_2 prior to use. Et_2O and THF were dried before use by distillation over Na/benzophenone. CDFCl_2 was prepared according to a known procedure.⁵

4,4,4-Trifluoro-1-(3,5-dimethylphenyl)butane-1,3-dione (7)

Diisopropylamine (1.14 mL, 0.82 g, 8.1 mmol) was dissolved in 40 mL of THF. The solution was cooled to $-20\text{ }^{\circ}\text{C}$, and then a solution of *n*-BuLi in hexane (1.6 M, 5 mL, 8 mmol) was added dropwise. The mixture was

³ Gunasekaran, P.; Indumathi, S.; Perumal, S. *RSC Adv.* **2013**, 3, 8318–8325.

⁴ Büttner, S.; Riahi, A.; Hussain, I.; Yawer, M. A.; Lubbe, M.; Villinger, A.; Reinke, H.; Fischer, C.; Langer, P. *Tetrahedron* **2009**, 65, 2124 – 2135.

⁵ Siegel, J. S.; Anet, F. A. L. *J. Org. Chem.* **1988**, 53, 2629 – 2630.

stirred for 30 minutes at $-20\text{ }^{\circ}\text{C}$, and then the temperature was allowed to rise to $+5\text{ }^{\circ}\text{C}$ and then cooled down to $-78\text{ }^{\circ}\text{C}$. A solution of 3,5-dimethylacetophenone (1.00 g, 6.7 mmol) was then added dropwise to the solution of LDA. The reaction mixture was stirred for 30 min at $-78\text{ }^{\circ}\text{C}$, and its color went from colorless to yellow. A solution of 4,4,4-trifluoroacetoacetic acid ethyl ester (0.97 mL, 1.15 g, 8.1 mmol in 5 mL of THF) was added dropwise to the solution of enolate. The reaction was stirred at $-78\text{ }^{\circ}\text{C}$ for 1 h and then allowed to warm to ambient temperature overnight. Saturated NH_4Cl solution was then added, and the mixture was extracted with diethyl ether ($3 \times 30\text{ mL}$). The combined organic layers were dried (Na_2SO_4), filtered, and concentrated under reduced pressure. The residue was purified by dissolving the impurities in CHCl_3 and by recrystallization from acetonitrile, yielding the title compound as a white solid (798 mg, 40%). mp $+280\text{ }^{\circ}\text{C}$ (decomp).

^1H NMR (600 MHz, CD_3CN , 1.96 ppm, $+25\text{ }^{\circ}\text{C}$): δ 2.35 (s, 6 H), 2.32 (s, OH), 6.23 (s, 1 H), 7.15 (s, 1 H), 7.51 (s, 2 H).

^{13}C NMR (150.8 MHz, CD_3CN , 1.79 ppm, $+25\text{ }^{\circ}\text{C}$): δ 21.8 (CH_3), 90.9 (CH), 121.1 (q, $J = 279\text{ Hz}$, CF_3), 126.4 (CH), 134.1 (Cq), 139.4 (CH), 172.4 (q, $J = 35\text{ Hz}$, CO- CF_3), 190.5 (CO).

^{19}F NMR (376 MHz, CD_3CN , $+25\text{ }^{\circ}\text{C}$): δ -76.3 (s). HRMS (ESI-TOF- MS^-) m/z : $[\text{M} - \text{H}]^-$ calcd for $\text{C}_{12}\text{H}_{10}\text{F}_3\text{O}_2$: 243.06329; found: 243.06369.

General Procedure for the Synthesis of 3-Methyl-1-phenyl-1H-pyrazolo[3,4-*b*]pyridines (3 – 6)

A mixture of 4,4,4-trifluoro-1-phenylbutane-1,3-dione (1 mmol), the appropriate aromatic aldehyde (1 mmol), 3-methyl-1-phenyl-1H-pyrazol-5-amine (1 mmol), and L-proline (0.20 mmol) in ethanol (15 mL) was stirred at $+60\text{ }^{\circ}\text{C}$ overnight. The reaction mixture was then extracted with

ethyl acetate (2 × 40 mL), and after removal of the solvent, the crude was chromatographed over silica gel using petroleum ether – ethyl acetate mixture (4:1 v/v), which afforded pure compounds **3**, **4**, and **6**.

4,4,4-Trifluoro-1-(3,5-dimethylphenyl)butane-1,3-dione **7** (0.2 mmol), *m*-isopropylbenzaldehyde (0.2 mmol), 3-methyl-1-phenyl-1H-pyrazol-5-amine (0.2 mmol), and L-proline (0.05 mmol) in ethanol (5 mL) were used for the preparation of compound **5**.

4-(4-Methoxyphenyl)-(3-methyl-1-phenyl-6-(trifluoromethyl)-1H-pyrazolo[3,4-*b*]pyridine-5-yl)(phenyl)methanone (1).

Yield: 400 mg (82%, relative to *p*-methoxybenzaldehyde). White solid, mp 150 – 151 °C.

¹H NMR (600 MHz, CD₃CN, +50 °C): δ 2.11(s, 3 H), 3.77 (s, 3 H), 6.85 (bs, 2 H), 7.17 (d, *J* = 8.0 Hz, 2 H), 7.37 (t, *J* = 7.9 Hz, 2 H), 7.43 (t, *J* = 7.5 Hz, 1 H), 7.55 (t, *J* = 7.5 Hz, 1 H), 7.60 – 7.65 (m, 4 H), 8.32 (d, *J* = 8.1 Hz, 2 H).

¹³C NMR (150.8 MHz, CD₃CN, +50 °C): δ 15.4 (CH₃), 56.7 (OCH₃), 115.0 (CH), 118.9(Cq), 122.6 (CH), 123.4 (q, *J* = 275.4 Hz, CF₃), 126.9 (Cq), 128.1(CH), 128.9 (Cq), 130.1 (CH), 130.9 (CH), 130.9 (CH), 132.8 (CH), 135.4 (CH), 139.2 (Cq), 140.6 (Cq), 144.2 (q, *J* = 35.1 Hz, C-CF₃), 145.7 (Cq), 147.8 (Cq), 150.7 (Cq), 162.0 (Cq), 196.0 (CO).

¹⁹F NMR (376.3 MHz, CD₃CN, +25 °C): δ –61.61 (s). HRMS(ESI-TOF-MS⁺) *m/z*: [M + H]⁺ calcd for C₂₈H₂₁F₃N₃O₂: 488.15859; found: 488.15805.

(3-Methyl-1-phenyl-4-(*p*-tolyl)-6-(trifluoromethyl)-1H-pyrazolo[3,4-*b*]pyridine-5-yl)(phenyl)methanone (2).

Yield: 372 mg (79%, relative to *p*-methylbenzaldehyde). White solid, mp 155 – 156 °C.

¹H NMR (600 MHz, CD₃CN, +50 °C): δ 2.05 (s, 3 H, CH₃), 2.32 (s, 3 H, CH₃), 7.14 (br, 4H, Ar - H), 7.38 (t, *J* = 8.3 Hz, 7.6 Hz, 2 H), 7.42 (tt, *J* = 7.5 Hz, 1.2 Hz, 1 H), 7.55 (tt, *J* = 7.4 Hz, 1.2 Hz, 1 H), 7.63 (m, 4 H), 8.31 (m, 2 H).

¹³C NMR (150.8 MHz, CD₃CN, +50 °C): δ 15.3 (CH₃), 21.8 (CH₃) 122.6 (CH), 123.5 (q, *J* = 275.1 Hz, CF₃) 128.1 (CH), 128.7 (Cq), 130.0 (CH, br), 130.1 (CH), 130.9 (CH), 131.0 (CH), 131.2 (CH, br), 131.9 (Cq), 135.4 (CH), 139.3 (Cq), 140.6 (Cq), 140.9 (Cq), 144.1 (*J* = 34.5 Hz, C-CF₃), 145.7 (Cq), 148.0 (Cq), 150.6 (Cq), 195.8 (CO).

¹⁹F NMR (376.3 MHz, CD₃CN, +25 °C): δ -61.61. HRMS (ESI-TOF-MS⁺) *m/z*: [M + H]⁺ calcd for C₂₈H₂₁F₃N₃O (M + H)⁺: 472.16367. found: 472.16116.

(4-(3-Ethylphenyl)-(3-methyl-1-phenyl-6-(trifluoromethyl)-1 *H* - pyrazolo[3,4-*b*]pyridine-5-yl)(phenyl)methanone (3)

Yield: 266 mg (55%, relative to *m*-ethylbenzaldehyde). White solid, mp 101 – 102 °C.

¹H NMR (600 MHz, CD₃CN, +50 °C): δ 1.07 (bs, 3 H), 2.07 (bs, 3 H), 2.54 (bs, 2 H), 7.03 – 7.09 (m, 2 H), 7.16 – 7.26 (m, 2 H) 7.36 (t, *J* = 7.6 Hz, 2 H), 7.43 (t, *J* = 7.6 Hz, 1 H), 7.54 (t, *J* = 7.6 Hz, 1 H), 7.60 – 7.65 (m, 4 H), 8.32 (d, *J* = 7.6 Hz, 2 H).

¹³C NMR (150.8 MHz, CD₃CN, +50 °C): δ 15.3 (CH₃), 16.4 (CH₃), 29.8 (CH₂), 122.6 (2 CH), 123.4 (q, *J* = 275.0 Hz, CF₃), 128.1 (CH), 128.5 (CH), 129.5 (CH), 130.0 (2 CH), 130.1 (CH), 130.8 (CH), 130.9 (2 CH), 131.0 (2 CH), 131.1 (Cq), 134.9 (Cq), 135.3 (CH), 139.3 (Cq), 140.6 (Cq), 144.2 (q, *J* = 34.4 Hz, C-CF₃), 145.7 (Cq), 145.8 (Cq), 148.1 (Cq), 150.6 (Cq), 195.8 (CO).

¹⁹F NMR (376.3 MHz, CD₃CN, +25 °C): δ -61.42 (s). HRMS (ESI-TOF-MS⁺): *m/z*: [M + H]⁺ calcd for C₂₉H₂₃F₃N₃O: 486.17932; found: 486.17912. Crystals suitable for X-ray analysis (colorless bricks) were obtained by slow evaporation of a hexane/ethyl acetate 4:1 v:v solution.

(4-(3-Isopropylphenyl)-3-methyl-1-phenyl-6-(trifluoromethyl)-1 H - pyrazolo[3,4- b]pyridine-5-yl)(phenyl)methanone (4)

Yield: 255 mg (51%, relative to *m*-isopropylbenzaldehyde). White solid, mp 119 – 120 ° C.

¹H NMR (600 MHz, CD₃CN, +50 °C): δ 1.07(bs, 3 H), 1.11 (bs, 3 H), 2.07 (s, 3 H), 2.80 (bs, 1 H), 7.05 (d, *J* = 7.4 Hz, 1 H), 7.09 (bs, 1 H), 7.20 (d, *J* = 7.4 Hz, 1 H), 7.32 (bs, 1 H), 7.36 (t, *J* = 7.5 Hz, 2 H), 7.42 (t, *J* = 7.5 Hz, 1 H), 7.42 (t, *J* = 7.5 Hz, 1 H), 7.61 (d, *J* = 7.5 Hz, 2 H), 7.63 (t, *J* = 7.8 Hz, 2 H), 8.32 (d, *J* = 8.2 Hz, 2 H).

¹³C NMR (150.8 MHz, CD₃CN, +50 °C): δ 15.2 (CH₃), 24.4 (CH₃), 24.7 (CH₃), 35.3(CH), 118.6 (Cq), 122.6 (CH), 123.4(q, *J* = 275.2 Hz, CF₃), 128.1 (CH), 128.7 (CH), 128.7 (Cq), 128.8(CH), 129.3 (CH), 129.5 (CH), 130.0 (CH), 130.9 (CH), 131.0 (CH), 134.8 (Cq), 135.3 (CH), 139.3 (Cq), 140.6 (Cq), 144.2 (q, *J* = 34.4 Hz, C-CF₃), 145.7 (Cq), 148.2 (Cq), 150.3 (Cq), 150.6 (Cq), 195.8 (CO).

¹⁹F NMR (376.3 MHz, CD₃CN, +25 °C): δ -61.60 (s). HRMS (ESI-TOF-MS⁺): *m/z*: [M + H]⁺ calcd for C₃₀H₂₅F₃N₃O: 500.19497; found: 500.19449.

(4-(3-Isopropylphenyl)-3-methyl-1-phenyl-6-(trifluoromethyl)-1 H - pyrazolo[3,4-*b*]pyridine-5-yl)(3,5-dimethylphenyl)-methanone (5)

Yield: 29 mg, 28%, relative to *m*-isopropylbenzaldehyde). Waxy solid.

¹H NMR (600 MHz, CD₃CN, +50 °C): δ 1.00 – 1.18 (bs, 6 H), 2.05 – 2.08 (bs, 6 H), 2.24 (s, 3 H), 2.82 (bs, 1 H), 7.06 (d, *J* = 7.6 Hz, 1 H),

7.09 (bs, 1 H), 7.18 (s, 1 H), 7.20 – 7.28 (m, 4 H), 7.43 (t, $J = 7.5$ Hz, 1 H), 7.64 (t, $J = 8.0$, 2 H), 8.33 (d, $J = 8.2$ Hz, 2 H).

^{13}C NMR (150.8 MHz, CD_3CN , +50 °C): δ 15.2 (CH_3), 21.6 (CH_3), 24.4 (CH_3), 24.6 (CH_3), 35.3 (CH), 122.6 (CH), 123.5 (q, $J = 275$ Hz, CF_3), 128.1 (CH), 128.7 (CH), 128.8 (CH), 129.1 (Cq), 129.2(CH), 129.4 (CH), 130.9 (CH), 135.0 (Cq), 136.8 (CH), 139.5 (Cq), 140.0 (Cq), 140.6 (Cq), 144.2 (q, $J = 35.1$ Hz, C- CF_3), 145.7 (Cq), 148.1 (Cq), 150.2 (Cq), 150.6 (Cq), 196.0 (CO).

^{19}F NMR (376.3 MHz, CD_3CN , +25 °C): δ -61.60 (s). HRMS (ESI-TOF-MS⁺): m/z : $[\text{M} + \text{H}]^+$ calcd for $\text{C}_{32}\text{H}_{29}\text{F}_3\text{N}_3\text{O}$: 528.22627; found: 528.22702.

(3-Methyl-4-(1-naphthyl)-1-phenyl-6-(trifluoromethyl)-1H-pyrazolo[3,4-*b*]pyridine-5-yl)(phenyl)methanone (6).

Yield: 131mg (36%, relative to 1-naphthaldehyde). White solid, mp 185 – 187 °C.

^1H NMR (600 MHz, CD_3CN , +50 °C): δ 1.60 (s, 3 H), 7.21 (bs, 2 H), 7.30 (d, $J = 6.5$ Hz, 1 H), 7.35 – 7.47 (m, 5 H), 7.50 (t, $J = 7.6$ Hz, 1 H), 7.55 (d, $J = 7.7$ Hz, 2 H), 7.65 (t, $J = 7.9$ Hz, 2 H), 7.88 (d, $J = 8.4$ Hz, 1 H), 7.90 (d, $J = 8.4$ Hz, 1 H), 8.34 (d, $J = 8.4$ Hz, 2 H).

^{13}C NMR (150.8 MHz, CD_3CN , +50 °C): δ 14.1 (CH_3), 119.7 (CH), 122.7 (CH), 123.5 (q, $J = 275.1$ Hz, CF_3), 126.2 (CH), 127.4 (CH), 128.0 (CH), 128.2 (CH), 128.4 (CH), 129.6 (CH), 129.7 (CH), 129.8 (CH), 129.9 (bs, CH), 130.7 (CH), 130.9 (CH), 131.2 (CH), 132.2, 133.2, 134.6, 135.1 (CH), 138.9, 140.6, 144.8 (q, $J = 34.4$ Hz, C- CF_3), 145.5, 146.2, 150.6, 195.6 (CO).

^{19}F NMR (376.3 MHz, CD_3CN , +25 °C): δ -61.40 (s). HRMS (ESI-TOF-MS⁺): m/z : $[\text{M} + \text{H}]^+$ calcd for $\text{C}_{31}\text{H}_{21}\text{F}_3\text{N}_3\text{O}$ 508.16367; found:

508.16539. HPLC resolution of the atropisomeric pair: Daicel ChiralPak AD-H (5 μm , 250 \times 20 mm), 18 mL/min flowrate, 254 nm detection, +25 $^{\circ}\text{C}$; eluent: hexane:2-propanol 98:2 v:v; t_R 6.10 and 6.83 min. Crystals of the racemic mixture suitable for X-ray analysis (colorless sticks) were obtained by slow evaporation of a $\text{CH}_3\text{OH}/\text{CH}_2\text{Cl}_2$ 3:1 v:v solution.

Study of the intramolecular NO₂/CO interaction in solution

Materials

Compounds **1**, **2**, **3** were prepared using a known procedure⁶. Compounds **4**, **5**, **6**, **7**, **8** were prepared starting from 2,3-dibromo-1,4-naphthoquinone and 2,5-dibromo-1,4-*p*-hydroquinone⁷ by Suzuki coupling.

1-benzyl-3,4-bis(2-nitrophenyl)-1*H*-pyrrole-2,5-dione (**1**)

In an oven dried round bottom flask under nitrogen atmosphere, 1-benzyl-3,4-dibromo-1*H*-pyrrole (1 mmol, 1 eq) and 2-nitrophenylboronic acid (3 mmol, 3 eq) were dissolved in 5 ml of dry THF. Cs_2CO_3 (2.5 eq) was added and the reaction mixture was degassed by nitrogen bubbling for 5-10 minutes. $\text{Pd}(\text{OAc})_2$ (0.05 eq) was added and the reaction was heated at 40 $^{\circ}\text{C}$ until complete consumption of the starting material (GC-MS, 6 hours). The solution was then diluted with water (10 ml) and extracted with Et_2O (3 \times 10 ml). The combined organic layers were dried over Na_2SO_4 and the solvent were evaporated under reduced pressure. The crude reaction mixture was purified with semi-preparative HPLC on

⁶ Ambroggi, M.; Ciogli, A.; Mancinelli, M.; Ranieri, S.; Mazzanti, A., *J. Org. Chem.*, **2013**, 78, 3709–3719.

⁷ Yu, D.; Mattern, D. L. *Synth. Commun.* **1999**, 29, 821 – 825.

C18 column, to obtain analytically pure samples. (10 μm , 250 x 10.0 mm, 20 mL/min, ACN/H₂O 75:25 v/v).

¹H-NMR (600 MHz, CD₃CN, 1.96 ppm, 25 °C): δ 4.79 (s, 2 H), 7.30 - 7.36 (m, 5 H), 7.35 - 7.42 (m, 2 H), 7.65 (t, $J = 7.2$ Hz, 2 H), 7.70 (td, $J = 7.9$ Hz, 1.5 Hz, 2 H), 8.26 (d, $J = 8.2$ Hz, 2 H).

¹³C-NMR (150.8 MHz, CD₃CN, 118.3 ppm, 25 °C): δ 42.7 (CH₂), 124.5 (2 Cq), 126.1 (2 CH), 128.3 (2 CH), 128.7 (CH), 129.7 (2 CH), 132.5 (2 CH), 133.0 (2 CH), 135.3 (2 CH), 137.4 (2 Cq), 138.3 (2 Cq), 149.6 (Cq), 169.5 (2Cq).

HRMS (ESI-Orbitrap) m/z calcd for C₂₃H₁₅N₃O₆Na⁺ [M+Na]⁺: 452.0585, found 452.0589.

1-benzyl-3-(2-nitrophenyl)-4-(*o*-tolyl)-1H-pyrrole-2,5-dione (2)

In an oven dried round bottom flask under nitrogen atmosphere, 1-benzyl-3-bromo-4-(*o*-tolyl)-1H-pyrrole-2,5-dione (1 eq) and *o*-nitrophenylboronic acid (2.0 eq) (1 mmol, 1 eq) were dissolved in 5 ml of dry THF. Cs₂CO₃ (2.5 eq) was added and the reaction mixture was degassed by nitrogen bubbling for 5-10 minutes. Pd(OAc)₂ (0.05 eq) was added and the reaction was heated at 40 °C until complete consumption of the starting material. (GC-MS, 6 hours). The solution was then diluted with water (10 ml) and extracted with Et₂O (3 x 10 ml). The combined organic layers were dried over Na₂SO₄ and the solvent were evaporated under reduced pressure. The crude reaction mixture was purified with semi-preparative HPLC on C18 column, to obtain analytically pure samples. (10 μm , 250 x 10.0 mm, 20 mL/min, ACN/H₂O 67:33 v/v).

¹H-NMR (600 MHz, CD₂Cl₂, 5.33 ppm, 25 °C): δ 2.11 (bs, 3 H), 4.81 (s, 2 H), 7.08 (d, $J = 7.63$ Hz, 1 H), 7.15 - 7.29 (bs, 3 H), 7.29-7.42 (m, 6 H),

7.52 (t, $J = 7.73$ Hz, 1 H), 7.58 (t, $J = 7.73$ Hz, 1 H), 8.17 (d, $J = 8.25$ Hz, 1 H).

^{13}C -NMR (150 MHz, CD_2Cl_2 , 53.4 ppm, 25 °C): δ 19.7 (b, CH_3), 42.0 (CH_2), 124.6 (Cq), 125.0 (CH), 125.7 (CH), 127.7 (CH), 128.0 (CH), 128.6 (CH), 129.8 (CH), 130.1 (CH), 130.7 (CH), 130.8 (CH), 131.5 (CH), 133.6 (CH), 136.3 (Cq), 137.4 (Cq), 148.4 (Cq), 168.5 (CO), 169.8 (CO). HRMS (ESI-Orbitrap) m/z : calcd for $\text{C}_{24}\text{H}_{19}\text{N}_2\text{O}_4^+$ $[\text{M}+\text{H}]^+$: 399.13393, found: 399.13492, $\text{C}_{24}\text{H}_{18}\text{N}_2\text{O}_4\text{Na}^+$ 421.1164; found 421.1168.

2,3-bis(2-nitrophenyl)naphthalene-1,4-dione (4)

In an oven dried round bottom flask under nitrogen atmosphere, 2,3-dibromonaphthalene-1,4-dione (0.5 mmol, 1 eq) and 2-nitrophenylboronic acid (1.1 mmol, 2.2eq) were dissolved in 5 ml of 1,4-dioxane. 2 M aqueous solution of K_2CO_3 (1 ml, 4 eq) was added and the reaction mixture was degassed by nitrogen bubbling for 5-10 minutes. $\text{Pd}(\text{PPh}_3)_4$ (0.025 mmol, 0.05 eq) was added and the reaction was heated at 90 °C until complete consumption of the starting material (GC-MS, 6 hours). The solution was then diluted with water (10 ml) and extracted with ethyl acetate (3 x 10 ml). The combined organic layers were dried over Na_2SO_4 and the solvent was evaporated under reduced pressure. The crude reaction mixture was purified with silica-gel flash chromatography eluting with petrol ether/AcOEt mixture (95:5 \rightarrow 7:3) to afford the product as a brown solid in 14 % yield. An analytic sample of the compound was obtained by semi-preparative HPLC on a Synergy Polar-RP column (4 μm , 250 x 10.0 mm, 5 mL/min, ACN/ H_2O 70:30 v/v).

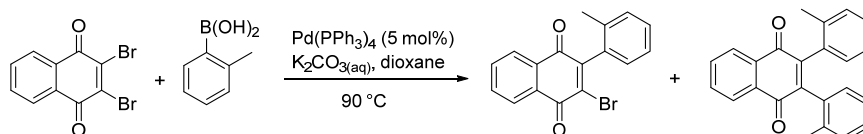
^1H NMR (600 MHz, CDCl_3): δ 7.24 (dd, $J_1 = 7.8$ Hz, $J_2 = 1.2$ Hz, 2 H), 7.44 (dt, $J_1 = 7.8$ Hz, $J_2 = 1.2$ Hz, 2 H), 7.49 (dt, $J_1 = 7.8$ Hz, $J_2 = 1.2$ Hz,

2 H), 7.82 (dd, $J_1 = 6.0$ Hz, $J_2 = 3.6$ Hz, 2 H), 8.17 (dd, $J_1 = 6.0$ Hz, $J_2 = 3.6$ Hz, 2H), 8.20 (dd, $J_1 = 7.8$ Hz, $J_1 = 1.2$ Hz, 2 H).

^{13}C -NMR (150 MHz, CDCl_3): δ 124.3 (2 CH), 127.1 (2 CH), 129.5 (2 Cq), 130.1 (2 CH), 131.1 (2 CH), 131.8 (2 Cq), 134.0 (2 CH), 134.3 (2 CH), 143.3 (2 Cq), 148.9 (2 Cq), 182.4 (2 Cq).

HRMS (ESI-Orbitrap) m/z : calcd for $\text{C}_{22}\text{H}_{12}\text{N}_2\text{O}_6 \text{Na}^+[\text{M}+\text{Na}]^+$: 423.0593; found 423.0587.

2-bromo-3-(*o*-tolyl)naphthalene-1,4-dione and 2,3-di-*o*-tolyl naphthalene-1,4-dione



In an oven dried round bottom flask under nitrogen atmosphere, 2,3-dibromonaphthalene-1,4-dione (0.22 mmol, 1.1 eq) and *o*-tolylboronic acid (0.2 mmol, 1.0 eq) were dissolved in 2 ml of 1,4-dioxane. 2 M aqueous solution of K_2CO_3 (0.4 ml, 4 eq) was added and the reaction mixture was degassed by nitrogen bubbling for 5-10 minutes. $\text{Pd}(\text{PPh}_3)_4$ (0.011 mmol, 0.05 eq) was added and the reaction was heated at 90°C until complete consumption of the starting material (GC-MS, 6 hours). The solution was then diluted with water (10 ml) and extracted with DCM (3 x 10 ml). The combined organic layers were dried over Na_2SO_4 and filtered through a short pad of silica-gel. The volatiles were removed under reduced pressure and the crude product was purified by semipreparative HPLC on a Luna C18 column (10 μm , 250 x 21.2 mm, 25 mL/min, ACN/ H_2O 80:20 v/v) to afford 22 mg of 2-bromo-3-(*o*-tolyl)naphthalene-1,4-dione and 14 mg of 2,3-di-*o*-tolyl naphthalene-1,4-dione, with 54 % overall yield.

2-bromo-3-(*o*-tolyl)naphthalene-1,4-dione

¹H-NMR (400 MHz, CDCl₃): δ 2.19 (s, 3 H), 7.10 (d, *J* = 7.2 Hz, 1 H), 7.30 - 7.34 (m, 2 H), 7.37 - 7.41 (m, 1 H), 7.79 - 7.84 (m, 2 H), 8.14 - 8.19 (m, 1 H), 8.24 - 8.29 (m, 1 H).

¹³C-NMR (100 MHz, CDCl₃): δ 19.7 (CH₃), 125.8 (CH), 127.4 (CH), 127.6 (CH), 127.9 (CH), 129.2 (CH), 130.2 (CH), 131.2 (Cq), 131.7 (Cq), 134.1 (CH), 134.4 (CH), 134.6 (Cq), 135.1 (Cq), 140.0 (Cq), 151.0 (Cq), 178.1 (Cq), 181.3 (Cq).

MS (EI) *m/z*: 247 (100) [M-Br]⁺, 219 (30), 189 (45).

2,3-di-*o*-tolyl naphthalene-1,4-dione (6)

¹H-NMR (600 MHz, C₂D₂Cl₄) δ 2.07 (s, 6H_{syn}), 2.24 (s, 6H_{anti}), 6.75 (d, *J*₁ = 7.2 Hz, 2H_{anti}), 6.99 (dt, *J*₁ = 7.2 Hz, *J*₂ = 1.8 Hz, 2H_{anti}), 7.02 (d, *J* = 7.8 Hz, 2H_{syn}), 7.10 (t, *J* = 7.8 Hz, 2H_{syn}), 7.12 (d, *J* = 7.8 Hz, 2H_{syn}), 7.16-7.21 (m, 4H_{anti} + 2H_{syn}), 7.84-7.87 (m, 2H_{anti} + 2H_{syn}), 8.19-8.21 (m, 2H_{anti} + 2H_{syn}).

¹³C-NMR (150 MHz, C₂D₂Cl₄): δ 20.5 (2CH₃), 20.8 (2CH₃), 125.2 (2CH), 125.8 (2CH), 127.0 (2CH), 127.1 (2CH), 128.0 (2CH), 128.7 (2CH), 128.8 (2CH), 130.0 (2CH), 130.2 (2CH), 130.7 (2CH), 132.2 (2Cq), 132.3 (2Cq), 132.8 (2Cq), 133.9 (2Cq), 134.4 (2CH), 134.5 (2CH), 136.1 (2Cq), 136.3 (2Cq), 147.8 (2Cq), 148.1 (2Cq), 184.6 (2Cq), 184.8 (2Cq). HRMS-(ESI-Orbitrap) *m/z*: calcd for C₂₄H₁₈O₂Na⁺[M+Na]⁺: 361.1204; found 361.1193.

2-(2-nitrophenyl)-3-(*o*-tolyl)naphthalene-1,4-dione (5)

In an oven dried round bottom flask under nitrogen atmosphere, 2-bromo-3-(*o*-tolyl)naphthalene-1,4-dione (0.2 mmol, 1 eq) and 2-nitrophenylboronic acid (0.4 mmol, 2.0 eq) were dissolved in 2 ml of 1,4-dioxane. 2 M aqueous solution of K₂CO₃ (0.2 ml, 4 eq) was added and

the reaction mixture was degassed by nitrogen bubbling for 5-10 minutes. Pd(PPh₃)₄ (0.010 mmol, 0.05 eq) was added and the reaction was heated at 90 °C until complete consumption of the starting material (GC-MS, 3 hours). The solution was then diluted with water (5 ml) and extracted with DCM (3 x 5 ml). The combined organic layers were dried over Na₂SO₄ and the solvent were evaporated under reduced pressure. The crude reaction mixture was purified with silica-gel flash chromatography eluting with petrol ether/AcOEt mixture (9:1 → 8:2) to afford the product as a brown solid in 35 % yield. An analytic sample of the compound was obtained by recrystallization from *n*-Hex:*i*-PrOH:THF 1:1:1 mixture.

¹H-NMR (600 MHz, C₂D₂Cl₄): δ 1.97 (s, 3 H_{syn}), 2.31 (s, 3 H_{anti}), 6.86 (d, *J* = 7.2 Hz, 1 H_{anti}), 6.91 - 6.94 (m, 1 H_{anti}), 6.97 (t, *J* = 7.2 Hz, 1 H_{anti}), 7.09 (d, *J* = 7.8 Hz, 2 H_{syn}), 7.16 - 7.25 (m, 3 H_{syn} + 2 H_{anti}), 7.43 - 7.47 (m, 2 H_{anti}), 7.48 (dd, *J*₁ = 7.8 Hz, *J*₂ = 1.2 Hz, 1 H_{syn}), 7.52 (dt, *J*₁ = 7.8 Hz, *J*₂ = 1.2 Hz, 1 H_{syn}), 7.83 - 7.88 (m, 2 H_{syn} + 2 H_{anti}), 8.11 (dd, *J*₁ = 8.4 Hz, *J*₂ = 1.2 Hz, 1 H_{syn}), 8.14 - 8.18 (m, 1 H_{syn} + 2 H_{anti}), 8.21 - 8.23 (m, 1 H_{syn} + 1 H_{anti}).

¹³C-NMR (150 MHz, C₂D₂Cl₄): δ 19.7 (CH₃), 20.9 (CH₃), 120.6 (Cq), 124.6 (CH), 124.9 (CH), 125.2 (CH), 126.3, (CH), 127.1 (CH), 127.20 (CH), 127.23, 127.3 (CH), 128.5 (CH), 129.0 (Cq), 129.1 (CH), 129.3 (CH), 129.4 (Cq), 130.0 (CH), 130.1 (CH), 130.2 (CH), 130.4 (CH), 130.7 (CH), 130.9 (CH), 131.9 (Cq), 132.0 (Cq), 132.1 (Cq), 132.3 (Cq), 132.4 (Cq), 132.9 (CH), 133.5 (CH), 133.6 (Cq), 134.0 (CH), 134.5 (CH), 134.6 (CH), 134.7 (CH), 134.8 (CH), 136.5 (Cq), 136.7 (Cq), 145.5 (Cq), 145.72 (Cq), 145.74 (Cq), 146.2 (Cq), 147.8 (Cq), 183.5 (Cq), 183.7 (Cq), 183.9 (Cq), 184.8 (Cq). HRMS-(ESI-Orbitrap) *m/z*: calcd for C₂₃H₁₅NO₄Na⁺[M+Na]⁺: 392.0899; found 392.0886.

2,5-bis-*o*-tolylbenzoquinone (8)

In an oven dried Schlenk tube, under nitrogen atmosphere, 2,5-dibromo-*p*-benzoquinone (100 mg, 0.379 mmol, 1 eq) and *o*-tolylboronic acid (129 mg, 0.948 mmol, 2.5 eq) were dissolved in 3 ml of dry THF. 2 M aqueous solution of K₂CO₃ (0.75 ml, 4 eq) was added and the reaction mixture was degassed by nitrogen bubbling for 5-10 minutes. Pd(PPh₃)₄ (0.038 mmol, 0.1 eq) was added and the solution was stirred 6 hours at 60 °C. The reaction mixture was then diluted with 1 M HCl (5 ml) and extracted with ethyl acetate (3 x 5 ml). The combined organic layers were dried over Na₂SO₄ and the solvent was evaporated under reduced pressure. The crude reaction mixture was dissolved in 4 ml of MeCN and a solution of CAN (1.04 g, 5 eq) in 4 ml of water was added at room temperature. The reaction mixture was stirred overnight and then the aqueous layer was extracted with DCM (3 x 10 ml), the combined organic layers were dried over Na₂SO₄ and the volatiles were removed under reduced pressure. The crude product was purified with silica-gel flash chromatography (petrol ether/ethyl acetate 95/5) affording the product in 14% yield as a sticky yellow solid. Further purification of the product with preparative HPLC (Kinetex C18 5μm, 100 Å, 250 x 21.2 mm, MeCN/H₂O 70/30, 20 ml/min and Chiralpak AD-H 2x25 cm *n*-Hex/*i*-PrOH 90/10, 20 ml/min) provide the product with 95% purity.

¹H-NMR (600 MHz, CDCl₃): δ 2.26 (s, 6 H), 6.82 (s, 2 H), 7.18 (dd, *J*₁ = 7.8 Hz, *J*₂ = 1.2 Hz, 2 H), 7.28 (d, *J* = 7.8 Hz, 2 H), 7.30 (d, *J* = 7.8 Hz, 2 H), 7.37 (dd, *J*₁ = 7.8 Hz, *J*₂ = 1.2 Hz, 2 H).

¹³C-NMR (100 MHz, CDCl₃): δ 20.5 (2 CH₃), 125.8 (2 CH), 129.4 (2 CH), 129.5 (2 CH), 130.5 (2 CH), 132.9 (2 Cq), 134.8 (2 CH), 136.2 (2 Cq), 148.2 (2 Cq), 186.6 (2 Cq).

HRMS-(ESI-Orbitrap) m/z : calcd for $C_{20}H_{16}O_2Na^+$ $[M+Na]^+$: 311.1048; found 311.1042.

2,5-dibromo-*p*-hydroquinone

According to the procedure described, *p*-benzoquinone (1 eq) was dissolved in dry Et_2O (0.2M) at 0 °C, under N_2 flow, then bromine (2 eq, 2 M solution in dry Et_2O) was added over 10 minutes. The mixture was stirred at room temperature for 15 minutes, returned to the ice bath, and treated with concentrated H_2SO_4 (2 eq). After 30 minutes the mixture was poured onto iced water and extracted 3 times with Et_2O and the extracted organic layer was dried (Na_2SO_4), filtered and concentrated at reduced pressure. The crude mixture of 2,5-dibromo-*p*-hydroquinone containing a small amount of 2,3-dibromo-*p*-hydroquinone was used without any further purification.

1H -NMR (600 MHz, CD_3CN , +25°C): δ 7.10 (s, 1 H), 6.87 (s, 1 H).

^{13}C -NMR (150.8 MHz, CD_3CN , +25°C): δ 105.95 (Cq), 109.71 (Cq), 116.50 (CH), 120.68 (CH), 148.34 (Cq), 148.98 (Cq).

2,5-bis-*o*-nitrophenylbenzoquinone (7)

The mixture of 2,5-dibromo-*p*-hydroquinone and 2,3-dibromo-*p*-hydroquinone (1 eq) were dissolved in dry THF (0.067 M), then the *o*-nitrophenylboronic acid (4 eq), potassium carbonate (5 eq, 2 M solution) and the palladium catalyst $Pd(PPh_3)_4$ were added. The stirred solution was kept at reflux for 2 hours. Et_2O and H_2O were then added and the extracted organic layer was dried (Na_2SO_4), filtered on silica gel and concentrated at reduced pressure. The crude products were purified by semi-preparative HPLC on C18 column (60:40 v/v acetonitrile/ H_2O), to obtain a mixture of 2,5-bis-*o*-nitrophenylhydroquinone and 2,3-bis-*o*-

nitrophenyl hydroquinone(about 3%). The oxidation⁸ to benzoquinone was then performed as described. The crude products were then purified and separated by semi-preparative HPLC on Synergi-hydro column (70:30 v/v acetonitrile/H₂O).

¹H-NMR (600 MHz, CD₃CN, +25°C): δ 7.03 (s, 1 H), 7.62 (dd, $J_1 = 7.69$ Hz, $J_2 = 1.20$ Hz, 1 H), 7.77 (dt, $J_1 = 8.08$ Hz, $J_2 = 1.39$ Hz, 1 H), 7.87 (dt, $J_1 = 7.67$ Hz, $J_2 = 1.30$ Hz, 1 H), 8.22 (dd, $J_1 = 8.21$, $J_2 = 0.98$ Hz, 1 H).

¹³C-NMR (150.8 MHz, CD₃CN, +25°C): δ 124.68 (CH), 128.34 (Cq), 131.34 (CH), 132.00 (CH), 132.26 (CH), 134.56 (CH), 147.20 (Cq), 148.50 (Cq), 184.98 (Cq).

HRMS-(ESI-Orbitrap) m/z : calcd for C₁₈H₁₀N₂O₆Na⁺[M+Na]⁺: 373.0431; found. 373.042.

⁸Minisci,F.; Citterio,A.; Vismara,E.; Fontana,F.; De Bernardinis, S.; Correale, M. *J. Org. Chem.* **1989**, 54, 728 – 731.

Long range bonding/non-bonding interactions: study on 2-arylpyridines

2-(2-ethylphenyl)-3,5-dimethylpyridine (6)

¹H-NMR (600 MHz, CD₂Cl₂, 5.32 ppm, +25°C): δ 1.00 (t, *J* = 7.4 Hz, 3 H), 2.04 (s, 3 H), 2.35 (s, 3 H), 2.39 (bs, 2 H), 7.09 (d, *J* = 7.7 Hz, 1 H), 7.23 (dt, *J* = 7.0, 2.2 Hz, 1 H), 7.33 (dt, *J* = 7.8, 1.5 Hz, 1 H), 7.50 (s, 1 H), 8.30 (s, 1 H).

¹³C-NMR (150.8 MHz, CD₃CN, 118.69 ppm, +25°C): δ 14.497 (CH₃), 17.086 (CH₃), 18.254 (CH₃), 25.715 (CH₂), 125.499 (CH), 127.908 (CH), 128.563 (CH), 128.878 (CH), 130.822 (Cq), 131.851 (Cq), 138.144 (CH), 140.092 (Cq), 142.025 (Cq), 146.737 (CH), 156.556 (Cq).

1-(2-(3,5-dimethylpyridin-2-yl)phenyl)-*N,N*-dimethylmethanamine (7)

¹H-NMR (600 MHz, CD₂Cl₂, 5.32 ppm, +25°C): δ 2.04 (s, 9 H), 2.35 (s, 3 H), 3.17 (s, 2 H), 7.11 (d, *J* = 7.1 Hz, 1 H), 7.29 (t, *J* = 7.1 Hz, 1 H), 7.36 (t, *J* = 7.1 Hz, 1 H), 7.39 (s, 1 H), 7.56 (d, *J* = 7.7 Hz, 1 H), 8.28 (s, 1 H).

¹³C-NMR (150.8 MHz, CD₂Cl₂, 54 ppm, +25°C): δ 18.353 (CH₃), 19.382 (CH₃), 45.757 (2 CH₃), 61.258 (CH₂), 126.957 (CH), 128.121 (CH), 129.377 (CH), 129.875 (CH), 131.585 (Cq), 132.046 (Cq), 138.131 (Cq), 138.552 (CH), 141.210 (Cq), 147.262 (CH), 156.978 (CH).

2-(2-(methoxymethyl)phenyl)-3,5-dimethylpyridine (8)

¹H-NMR (600 MHz, CD₂Cl₂, 5.32 ppm, +25°C): δ 2.05 (s, 3 H), 2.35 (s, 3 H), 3.16 (s, 3 H), 4.20 (bs, 2 H), 7.16 (d, *J* = 8.1 Hz, 1 H), 7.34 (t, *J* = 7.1 Hz, 1 H), 7.40 (t, *J* = 8.1 Hz, 1 H), 7.43 (s, 1 H), 7.53 (d, *J* = 7.6 Hz, 1 H), 8.29 (s, 1 H).

¹³C-NMR (150.8 MHz, CD₃CN, 118.69 ppm, +25°C): δ 17.097 (CH₃), 18.239 (CH₃), 57.395 (CH₃), 71.483 (CH₂), 125.517 (Cq), 127.150 (CH), 186

127.717 (CH), 128.157 (CH), 128.911 (CH), 136.643 (Cq), 138.228 (CH), 139.825 (Cq), 146.645 (CH), 147.161 (Cq), 155.626 (Cq).

Dimethyl(2-(methoxymethyl)phenyl)boronate

2-(methoxymethyl)phenylbromide (1.15 g, 5.7 mmol, 1 eq) was dissolved in dry THF (0.2 M), under nitrogen flux and kept at -78°C . At this solution *n*-BuLi (1.6 M in hexane, 5.56 ml, 8.58 mmol, 1.5 eq) was added dropwise and kept stirring at -78°C for 1 hour. Keeping the solution at the same temperature, trimethylborate (1.78 g, 17.2 mmol, 3 eq) was added dropwise and kept stirring for 1 hour. The reaction was kept stirring overnight at room temperature, then the 0.2 M solution was used for the next synthesis step without any further work up.

2-(2-(methoxymethyl)phenyl)-3-methylpyridine (9)

A mixture of 3-methyl-2-bromopyridine (0.11 ml, 1 mmol, 1 eq) and 2-methoxybenzyl-phenylboronic dimethyl ester (0.2 M in THF, 7.5 ml, 1.5 mmol, 1.5 eq), under nitrogen flux, were dissolved in dry (0.10 M). Then potassium carbonate (2 M, 0.69 g, 5 mmol, 5 eq) and the palladium catalyst Pd(PPh₃)₄. The stirred solution was kept at reflux for 2 hours. Water was then added and the solution was extracted three times with dichloromethane. The organic layer was dried (Na₂SO₄), filtered on silica gel and concentrated at reduced pressure. The crude was then purified by silica flash chromatography (7:3 petroleum ether/ethyl acetate), and by semi-preparative HPLC on Synergi 4u Hydro RP (80:20 v/v acetonitrile/H₂O). The clean product was obtained with a 48% yield.

¹H-NMR (600 MHz, CD₂Cl₂, 5.22 ppm, +25°C): δ 3.09 (s, 3H), 4.12 (s, 2 H), 7.08 (d, $J = 7.9$ Hz, 1 H), 7.11 (q, $J_1 = 4.8$ Hz, $J_2 = 7.57$ Hz, 1 H), 7.26

(t, $J = 7.5$ Hz, 1 H), 7.31 (dt, $J_1 = 1.24$ Hz, $J_2 = 7.5$ Hz), 7.44 (d, $J = 7.9$ Hz, 1 H), 7.51 (d, $J = 7.9$ Hz, 1 H), 8.36 (d, $J = 4.33$, 1 H).

^{13}C -NMR (150.8 MHz, CD_2Cl_2 , 53.40 ppm, +25°C): δ 18.19 (CH_3), 57.21 (CH_2), 71.08 (CH_3), 126.39 (CH), 127.11 (CH), 127.40 (CH), 127.88 (CH), 131.05 (Cq), 135.72 (CH), 136.95 (CH), 138.86 (Cq), 145.56 (CH), 157.81 (Cq).

Dimethyl(2-(fluoromethyl)phenyl)boronate

2-(fluoromethyl)phenylbromide (1.28 g, 6.8 mmol, 1 eq) was dissolved in dry THF (0.2 M), under nitrogen flux and kept at -78°C . At this solution *n*-BuLi (1.6M in hexane, 6.34 ml, 10.15 mmol, 1.5eq) was added dropwise and kept stirring at -78°C for 1 hour. Keeping the solution at the same temperature, trimethylborate (2.3 ml, 20.3mmol, 3eq) was added dropwise and kept stirring for 1 hour. The reaction was kept stirring overnight at room temperature, then the 0.2 M solution was used for the next synthesis step without any further work up.

2-(2-fluoromethyl)phenyl)-3-methylpyridine (10)

A mixture of 3-methyl-2-bromopyridine (0.11ml, 1 mmol, 1 eq) and dimethyl (2-fluoromethyl)phenyl)boronate (0.2 M in THF, 7.4 ml, 1.5 mmol, 1.5 eq), under nitrogen flux, were dissolved in dry (0.10 M). Then potassium carbonate (2 M, 0.691 g, 5 mmol, 5 eq) and the palladium catalyst $\text{Pd}(\text{PPh}_3)_4$. The stirred solution was kept at reflux for 2 hours. Water was then added and the solution was extracted three times with dichloromethane. The organic layer was dried (Na_2SO_4), filtered on silica gel and concentrated at reduced pressure. The crude was then purified by silica flash chromatography (7:3 petroleum ether/ethyl acetate), and the product was obtained with a 49% yield.

$^1\text{H-NMR}$ (600 MHz, CD_2Cl_2 , 5.22 ppm, $+25^\circ\text{C}$): δ 2.04 (s, 3 H), 5.11 (d, $J = 47.3$ Hz, 2 H), 7.15 (m, 2 H), 7.36 (m, 2 H), 7.48 (d, $J = 7.8$ Hz, 1 H), 7.53 (d, $J = 7.8$, 1 H), 8.37 (d, $J = 4.5$, 1 H).

$^{13}\text{C-NMR}$ (600 MHz, CD_2Cl_2 , 53.40 ppm, $+25^\circ\text{C}$): δ 18.99 (CH_3), 82.45 (d, $J=164.7$ Hz, CH_2), 131.83 (Cq), 134.36 (Cq), 134.49 (Cq), 122.55 (CH), 128.14 (CH), 128.35 (CH), 128.40 (CH), 128.99 (CH), 138.00 (CH), 146.44 (CH), 157.67 (Cq).

3,5-diethyl-2-(2-methylphenyl)pyridine (11)

$^1\text{H-NMR}$ (600 MHz, CD_3CN , 1.96 ppm, $+25^\circ\text{C}$): δ 1.03 (t, $J = 7.6$ Hz, 3 H), 1.30 (t, $J = 7.6$ Hz, 3H), 2.40 (bs, 2 H), 2.70 (q, $J = 7.7$ Hz, 2H), 7.15 (d, $J = 8.3$, 1H), 7.26 (m, 1H), 7.32 (m, 2H), 7.58 (d, $J=2.5$ Hz, 1H), 8.35 (d, $J=2.5$ Hz, 1H).

$^{13}\text{C-NMR}$ (600 MHz, CD_3CN , 118.69 ppm, $+25^\circ\text{C}$): δ 14.59 (CH_3), 15.28 (CH_3), 19.24 (CH_3), 25.47 (CH_2), 25.85 (CH_2), 125.81 (CH), 128.114 (CH), 129.25 (CH), 130.38 (CH), 136.07 (CH), 136.37 (Cq), 137.20 (Cq), 138.60 (Cq), 140.95 (Cq), 146.59 (CH), 156.80 (Cq).

3,5-diethyl-2-(2-ethylphenyl)pyridine (12)

$^1\text{H-NMR}$ (600 MHz, CD_2Cl_2 , 5.32 ppm, $+25^\circ\text{C}$): δ 0.98 (t, $J = 7.6$ Hz, 3 H), 1.02 (t, $J = 7.7$ Hz, 3 H), 1.26 (t, $J = 7.7$ Hz, 3 H), 2.34 (m, 4 H), 2.66 (q, $J = 8.3$ Hz, 2 H), 7.08 (dd, $J = 7.7$, 0.9 Hz, 1 H), 7.22 (dt, $J = 7.4$, 1.4 Hz, 1 H), 7.31 (t, $J = 7.0$ Hz, 1 H), 7.34 (t, $J = 7.7$ Hz, 1 H), 7.48 (s, 1 H), 8.28 (s, 1 H).

$^{13}\text{C-NMR}$ (150.8 MHz, CD_3CN , 118.69 ppm, $+25^\circ\text{C}$): δ 14.109 (CH_3), 14.497 (CH_3), 14.820 (CH_3), 25.078 (CH_2), 25.418 (CH_2), 25.814 (CH_2), 125.359 (CH), 127.980 (CH), 128.416 (CH), 128.998 (CH), 135.698 (CH),

136.928 (Cq), 138.272 (Cq), 139.821 (Cq), 142.065 (Cq), 145.872 (CH), 156.230 (Cq).

1-(2-(3,5-diethylpyridin-2-yl)phenyl)-*N,N*-dimethylmethanamine (13)

¹H-NMR (600 MHz, CD₂Cl₂, 5.32 ppm, +25°C): δ 1.08 (t, *J* = 7.6 Hz, 3 H), 1.32 (t, *J* = 7.6 Hz, 3 H), 2.06 (s, 6 H), 2.40 (bs, 2 H), 2.71 (q, *J* = 7.7 Hz, 2 H), 3.17 (bs, 2 H), 7.15 (dd, *J* = 7.5, 1.2 Hz, 1 H), 7.29 (dt, *J* = 7.2, 1.3 Hz, 1 H), 7.31 (dt, *J* = 7.7, 1.2 Hz, 1 H), 7.47 (d, *J* = 2.2 Hz, 1 H), 7.59 (dd, *J* = 8.2, 1.4 Hz, 1 H), 8.32 (d, *J* = 2.1 Hz, 1 H).

¹³C-NMR (150.8 MHz, CD₃CN, 118.69 ppm, +25°C): δ 15.386 (CH₃), 16.261 (CH₃), 26.399 (CH₂), 26.812 (CH₂), 46.187 (CH₃), 61.998 (CH₂), 127.621 (CH), 128.965 (CH), 130.363 (CH), 130.411 (CH), 136.701 (CH), 138.409 (Cq), 139.134 (Cq), 139.459 (Cq), 141.879 (Cq), 147.135 (CH), 157.135 (Cq).

3,5-diethyl-2-(2-(methoxymethyl)phenyl)pyridine (14)

¹H-NMR (600 MHz, CD₂Cl₂, 5.32 ppm, +25°C): δ 1.05 (t, *J* = 7.3 Hz, 3 H), 1.31 (t, *J* = 7.9 Hz, 3 H), 2.40 (q, *J* = 7.7 Hz, 3 H), 2.70 (q, *J* = 7.7 Hz, 2 H), 3.19 (s, 3 H), 4.19 (s, 2 H), 7.16 (dd, *J* = 7.5, 1.1 Hz, 1 H), 7.33 (dd, *J* = 7.5, 1.1 Hz, 1 H), 7.40 (dt, *J* = 7.7, 1.2 Hz, 1 H), 7.47 (d, *J* = 1.9 Hz, 1 H), 7.53 (d, *J* = 7.7 Hz, 1 H), 8.31 (d, *J* = 2.0 Hz, 1 H).

¹³C-NMR (150.8 MHz, CD₂Cl₂, 54 ppm, +25°C): δ -5.814 (CH₃), -5.642 (CH₃), 4.726 (CH₂), 5.806 (CH₂), 38.367 (CH₃), 52.598 (CH₂), 108.227 (CH), 109.267 (Cq), 109.637 (2CH), 111.017 (CH), 117.065 (CH), 117.164 (Cq), 122.205 (Cq), 122.476 (Cq), 124.354 (CH), 129.264 (Cq).

2-ethyl-2'-methoxy-1,1'-biphenyl (15)

A mixture of 2-bromoanisole (0.1 ml, 0.8 mmol, 1 eq) and 2-ethylphenylboronic acid (0.150 g, 1 mmol, 1.25 eq), under nitrogen flux,

were dissolved in a 8:3 mixture of toluene/ethanol (0.15M). Then potassium carbonate (1 M, 0.55 g, 4 mmol, 4 eq) and the palladium catalyst Pd(PPh₃)₄. The stirred solution was kept at reflux for 2.5 hours. Water was then added and the solution was extracted three times with dichloromethane. The organic layer was dried (Na₂SO₄), filtered on silica gel and concentrated at reduced pressure. The crude was then purified by semi-preparative HPLC on Luna C18 column (90:10 v/v acetonitrile/H₂O). Yield 57%.

¹H-NMR (600 MHz, CD₂Cl₂, 5.32 ppm, +25°C): δ 0.43 (t, *J* = 7.6 Hz, 3 H), 1.81 (bs, 2 H), 3.11 (s, 3 H), 6.33 (d, *J* = 8.1 Hz, 1 H), 6.37 (dt, *J* = 7.3, 0.8 Hz, 1 H), 6.51 (t, *J* = 8.7, 1.4 Hz, 1 H), 6.58 (m, 1 H), 6.67 (dd, *J* = 7.0, 0.8 Hz, 1 H), 6.71 (dt, *J* = 7.9, 1.7 Hz, 1 H).

¹³C-NMR (150.8 MHz, CD₂Cl₂, 54 ppm, +25°C): δ 4.939 (CH₃), 6.194 (CH₃), 35.559 (CH₂), 90.830 (CH), 100.496 (CH), 105.412 (CH), 107.360 (CH), 107.924 (CH), 108.638 (CH), 110.439 (CH), 110.648 (Cq), 111.351 (CH), 118.310 (Cq), 122.908 (Cq), 136.604 (Cq).

1-(2-bromophenyl)-*N,N*-dimethylmethanamine

A mixture of 2-bromobenzylbromide (1.35 g, 5.4 mmol, 1 eq) and a solution 33% (w/w) of dimethylamine (7.40 ml, 54 mmol, 10 eq) was dissolved in 2 ml of ethanol. The stirred solution was kept in agitation for two hours at 60°C. After this time, 10 ml of water were added and the aqueous phase was extracted with dichloromethane (3 x 20 ml). The collected organic layers were dried (Na₂SO₄), filtered and the crude mixture was then washed with *n*-pentane, collected and concentrated under reduced pressure, giving the clean product with 47% yield.

¹H-NMR (400 MHz, CDCl₃, 7.26 ppm, +25°C): δ 2.29 (s, 3 H), 3.51 (s, 2 H), 7.10 (dt, *J* = 7.8, 1.7 Hz, 1 H), 7.27 (dt, *J* = 7.5, 1.3 Hz, 1 H), 7.41 (dd, *J* = 7.7, 1.7 Hz, 1 H), 7.53 (dd, *J* = 8.0, 1.2 Hz, 1 H).

1-(2'-methoxy-[1,1'-biphenyl]-2-yl)-*N,N*-dimethylmethanamine (16)

A mixture of 1-(2-bromophenyl)-*N,N*-dimethylmethanamine (0.250 g, 1.04 mmol, 1 eq) and 2-methoxyphenylboronic acid (0.237 g, 1.56 mmol, 1.5 eq), under nitrogen flux, were dissolved in a 8:3 mixture of toluene/ethanol (0.10M). Then potassium carbonate (2 M, 0.55 g, 4 mmol, 4 eq) and the palladium catalyst Pd(OAc)₂. The stirred solution was kept at reflux for 2.5 hours. Water was then added and the solution was extracted three times with dichloromethane. The organic layer was dried (Na₂SO₄), filtered and concentrated at reduced pressure. The crude was then purified by a silica plug (dichloromethane + triethylamine 0.1 % - 0.5%). The eluted fraction contains the desired product in 49 % yield.

¹H-NMR (600 MHz, CD₃CN, 1.96 ppm, +25°C): δ 2.08 (s, 6 H), 3.27 (bs, 2 H), 3.73 (s, 3 H), 7.03 (dt, *J* = 7.4, 1.1 Hz, 1 H), 7.06 (dd, *J* = 8.4, 0.7 Hz, 1 H), 7.14 (m, 2 H), 7.30 (dt, *J* = 7.4, 1.3 Hz, 1 H), 7.37 (dt, *J* = 7.6, 1.4 Hz, 1 H), 7.40 (dt, *J* = 7.9, 1.7 Hz, 1 H), 7.62 (dd, *J* = 7.8, 0.7 Hz, 1 H).

¹³C-NMR (150.8 MHz, CD₃CN, 118.69 ppm, +25°C): δ 45.802 (CH₃), 56.303 (CH₃), 61.728 (CH₂), 112.190 (CH), 127.719 (CH), 127.969 (CH), 128.672 (CH), 130.195 (CH), 130.297 (CH), 131.352 (Cq), 131.495 (CH), 132.282 (CH), 138.659 (Cq), 140.204 (Cq), 157.975 (Cq).

2-methoxy-2'-(methoxymethyl)-1,1'-biphenyl (17)

A mixture of (2'-methoxy-[1,1'-biphenyl]-2-yl)methanol (0.098 g, 0.46 mmol, 1 eq), potassium *t*-butoxyde (0.057 g, 0.51 mmol, 1.1 eq) and iodomethane (0.126 ml, 2.02 mmol, 4 eq), under nitrogen flux, in dry THF.

The reaction was conducted at room temperature until complete conversion of the reagent. Then water was added and the aqueous phase was washed three times with dichloromethane. The organic phase was dried, filtered and concentrated under reduced pressure. The crude was then purified by semi-preparative HPLC on Luna C18 column (90:10 v/v acetonitrile/H₂O). Yield 50%.

¹H-NMR (600 MHz, C₂D₂Cl₄, 7.26 ppm, +25°C): δ 3.25 (s, 3H), 3.77 (s, 3 H), 4.27 (bs, 2 H), 6.97 (d, *J* = 8.4 Hz, 1 H), 7.03 (t, *J* = 7.5, 1H), 7.18 (dd, *J* = 7.4, 1.7 Hz, 1 H), 7.23 (d, *J* = 7.2 Hz, 1 H), 7.33 (t, *J* = 7.2 Hz, 1 H), 7.38 (t, *J* = 7.2 Hz, 1 H), 7.53 (d, *J* = 7.5 Hz, 1 H).

¹³C-NMR (150.8 MHz, CD₃CN, 118.69 ppm, +25°C): δ 56.357 (CH₃), 58.725 (CH₃), 73.143 (CH₂), 112.291 (CH), 121.777 (CH), 128.418 (CH), 128.697 (CH), 128.843 (CH), 130.450 (CH), 130.772 (Cq), 131.512 (CH), 132.204 (CH), 138.622 (Cq), 139.222 (Cq), 157.960 (Cq).

2-(fluoromethyl)-2'-methoxy-1,1'- biphenyl (18)

A mixture of 2-bromoanisole (0.12 ml, 1 mmol, 1 eq) and dimethyl (2-fluoromethyl)phenyl)boronate (0.2M in THF, 7.5 ml, 1.5 mmol, 1.5 eq), under nitrogen flux, were dissolved in dry (0.10M). Then potassium carbonate (2M, 0.69 g, 5 mmol, 5 eq) and the palladium catalyst Pd(PPh₃)₄. The stirred solution was kept at reflux for 2 hours. Water was then added and the solution was extracted three times with dichloromethane. The organic layer was dried (Na₂SO₄), filtered on silica gel and concentrated at reduced pressure. The crude was then purified by silica flash chromatography (7:3 petroleum ether/ethyl acetate), and the product was obtained with a 49 % yield.

¹H-NMR (600 MHz, C₂D₂Cl₄, 5.59 ppm, 0°C): δ 3.71 (s, 3 H), 5.18 (dq, *J*₁ = 11.03 Hz, *J*₂ = 48.60 Hz, 106.93 Hz, 2 H), 6.92 (d, *J* = 8.15 Hz, 1 H),

6.99 (t, $J = 7.58$ Hz, 1 H), 7.14 (dd, $J_1 = 1.49$ Hz, $J_2 = 7.46$ Hz, 1 H), 7.23 (m, 1 H), 7.53 (m, 3 H), 7.50 (m, 1 H).

^{13}C -NMR (150.8 MHz, $\text{C}_2\text{D}_2\text{Cl}_4$, 74.02 ppm, $+25^\circ\text{C}$): δ 55.63 (CH_3), 83.11 (d, $J = 163.87$ Hz, CH_2), 110.91 (CH), 120.82 (CH), 127.60 (CH), 127.67 (CH), 128.52 (CH), 129.44 (CH), 130.72 (CH), 131.48 (CH), 135.11 (Cq), 137.46 (Cq), 156.38 (Cq).